AN INVESTIGATION ON THE KNEE OF THE COSMIC RAY ENERGY SPECTRUM

A THESIS SUBMITTED TO THE

UNIVERSITY OF NORTH BENGAL

FOR THE AWARD OF

DOCTOR OF PHILOSOPHY [SCIENCE]

IN

PHYSICS

BY

Biplab Bijay

SUPERVISOR

Dr. Arunava Bhadra

High Energy & Cosmic Ray Research Centre

&

Department of Physics

University of North Bengal
Darjeeling-734013

February 2016

DECLARATION

I declare that this thesis entitled, **"AN INVESTIGATION ON THE KNEE OF THE COSMIC RAY ENERGY SPECTRUM"** has been prepared by me under the guidance of **Dr. Arunava Bhadra**, Senior Research Physicist of **High Energy & Cosmic Ray Research Centre**, **University of North Bengal**. No part of this thesis has formed the basis for the award of any degree or fellowship previously.

Biplab Bijay

Date: 8th **February 2016** **(Biplab Bijay)**

High Energy & Cosmic Ray Research Centre
&
Department of Physics
University of North Bengal
Darjeeling-734013

UNIVERSITY OF NORTH BENGAL

HIGH ENERGY & COSMIC RAY RESEARCH CENTRE

Dr. Arunava Bhadra
Sr. Research Physicist

ENLIGHTENMENT TO PERFECTION

P.O. NORTH BENGAL UNIVERSITY
Darjeeling, West Bengal
India, PIN 734013
Phone: (0353) 2776358 (O)
Fax: (0353) 2699001

CERTIFICATE FROM THE SUPERVISOR

I certify that **Sri Biplab Bijay** has prepared his thesis entitled **"AN INVESTIGATION ON THE KNEE OF THE COSMIC RAY ENERGY SPECTRUM"**, for the award of PhD degree of the **University of North Bengal**, under my guidance. He has carried out the work at the **High Energy & Cosmic Ray Research Centre** and **Department of Physics**, **University of North Bengal**.

Date: 8th February 2016

(Arunava Bhadra)

Dr. Arunava Bhadra
Sr. Research Physicist
High Energy & Cosmic Ray Research Centre
University of North Bengal, Siliguri 734013

IN MEMORY

OF

MY LATE FATHER

Acknowledgements

This work was carried out at ***High Energy & Cosmic Ray Research Centre, University of North Bengal*** *with the financial assistance from the* ***Department of Science and Technology, India****.*

I would like to express my warmest thanks to:

Supervisor of this thesis - ***Dr. Arunava Bhadra****, who fearlessly accepted me as PhD student for his project and was the main creator of the great ideas, techniques and whole background of this thesis. We experienced together all the ups and downs of routine work, the shared happiness of success and the depression of failure when (sometimes) everything went wrong. He managed to teach me how to work independently (which is very important), but at any time, his useful advice was available to me. In my opinion, this is how an ideal supervisor should be. It is a real pleasure to work and communicate with such a polite, honest and open-minded person. I would also like to acknowledge his language abilities which were extremely useful, particularly in the beginning of my work and life in HECRRC.*

My teacher - ***Dr. Govinda Mazumdar*** *from* ***TIFR****, who kindly allowed me to work in TIFR. He has helped me greatly during all these years (special appreciation for helping me to learn some simulation programs like GEANT4, HEED, MAGBOLTZ & GARFIELD) and has always been extremely supportive and nice to me. It was only his great help in science and "beyond science" life that I got the chance to initiate and complete this thesis. He is now working actively in the development of INO detectors.*

Collaborator - ***Dr. Partha Sarathi Joarder*** *from* ***Bose Institute****, who generously accommodated me and let me continue to work in Bose Institute. His great support, huge work experience and patience were necessary for finishing this thesis.*

Colleague and co-member of our small "HECRRC group" - ***Dr Samir Sarkar*** *&* ***Mr. Arindam Mukherjee****, for their enormous everyday help in work and life, wise advice and tolerance of me as their "office mate".*

All present and former colleagues, permanent and "visiting" members of the High Energy & Cosmic Ray Research Centre - ***Dr. R. K. Dey, Dr. Subhranshu Ghosh, Mr. Prabir Banik, Mr. Sadhan Paul*** *and all others, for their assistance and providing an excellent working atmosphere to me. Special thanks to my friends and family members who stand by me in my every ups and downs.*

Abstract

The present thesis reports, research works done by the author (in collaboration with a few others) on various aspects of the cosmic ray knee. The main objective of the works are

i) to review the present status of the knee in the energy spectrum,

ii) to examine whether different components of cosmic ray extensive air shower, consistently and unequivocally suggest the existence of the knee in the primary cosmic ray energy spectrum,

and

iii) to propose a new self-consistent theoretical model of the knee, which is devoid of any fine tuning problem.

Due to the rapidly falling intensity with increasing energy, higher energy cosmic rays can only be studied indirectly by observations of cosmic ray extensive air showers (EAS), which are cascades of secondary particles produced by interactions of cosmic ray particles with atmospheric nuclei, on ground based installations. To interpret the EAS results in terms of primary cosmic rays, one has to take the help of the Monte Carlo simulation that relies on the high energy particle interaction models. The knee feature has been inferred from size (total number of particles) spectrum of electrons in air showers. The Monte Carlo simulation requires particle interactions at high energies as input for constructing cosmic ray EAS events. Computation of hadron production, particularly at low transverse momenta, is not yet possible from first principles within quantum chromodynamics. One, therefore, relies on phenomenological models that are appropriately tuned to match with the prevailing experimental data. Even a parametrization of such models may be difficult as the accelerator data for the relevant target-projectile combinations covering the whole kinematic region are not available. Experimental data on hadron-hadron interactions in the forward kinematic region at high energies and the data on hadron-nucleus and nucleus-nucleus interactions at all energies covering the whole kinematic range are particularly scarce. One has to resort to theoretical models of particle interactions in such cases. Before generating EAS events to examine the knee feature, one has to make some tests of interaction models in order

to check the reliability of the interaction models and thereby to choose the proper model(s) for work.

We study the effect of particle interaction models at relatively lower energies (< 80 GeV) on the theoretical estimates of atmospheric proton and antiproton fluxes by comparing the BESS observations of proton, muon and antiproton spectra with the spectra obtained by means of a full three dimensional Monte Carlo simulation program. For such a purpose, we use two different microscopic interaction models, namely FLUKA and UrQMD to simulate proton, muon and antiproton spectra at multiple observation levels. We also compared the atmospheric proton, muon and antiproton fluxes predicted by a few popular microscopic high energy particle interaction models with each other to get an idea about the influence of such models at energies beyond the BESS upper cutoff up to about 100 GeV. We find that the FLUKA reproduces the results of BESS observations on the secondary proton spectrum reasonably well over the whole observed energy range, the model UrQMD works well at relatively higher energies. It is further noticed that the model-predicted proton fluxes at a lower altitude are quite closer to the observed proton fluxes in comparison with those at a higher altitude. The model UrQMD presents reasonable description of the BESS $\bar{p}$ data at mountain altitude and at sea level whereas FLUKA consistently yields a higher $\bar{p}$ flux than the measurements at all the observation levels. Overall both UrQMD and FLUKA work reasonably well but when both proton and anti-proton fluxes are considered, UrQMD has an edge over FLUKA. So we have selected UrQMD as the low energy interaction model for simulating EAS events. At higher energies there was no way to check the validity of hadronic interaction models untill the Large Hadron Collider data were available. The comparison of different interaction models behavior with the LHC data suggest that the QGSJET 01c has a close agreement with the data and hence we select the model as the high energy interaction model for the simulation study though a small sample of data are also generated using EPOS.

Next with the help of Monte Carlo simulation we examine whether a consistent primary energy spectrum of cosmic rays emerges from both the experimentally observed total charged particles and muon size spectra of cosmic ray extensive air showers considering primary composition may or may not change beyond the knee of the energy spectrum. It is found that EAS-TOP observations consistently infer a knee in the primary energy spectrum provided the primary is pure unchanging iron whereas no consistent primary spectrum emerges from simultaneous use of

the KASCADE observed total charged particle and muon spectra. However, it is also found that when primary composition changes across the knee the estimation of spectral index of total charged particle spectrum is quite tricky, depends on the choice of selection of points near the knee in the size spectrum.

Finally we propose a new model of cosmic ray knee based on mass distribution of progenitor of cosmic ray sources. The proposed model can account all the major observed features about cosmic rays without invoking any fine tuning to match flux or spectra at any energy point. The proposed model predicts that the mass composition should not be changed much across the knee which is found consistent to that obtained from simultaneous use of EAS-TOP observed electron and muon size spectra. The prediction of the proposed model regarding primary composition scenario beyond the knee is quite different from most of the prevailing models of the knee and thereby can be discriminated from precise experimental measurement of the primary composition.

The material/results reported in this thesis have been published in different journals/proceedings as shown below

1. Arunava Bhadra, Biplab Bijay, Sanjay K. Ghosh, Partha S. Joarder, Sibaji Raha, *"Influence of microscopic particle interaction models on the flux of atmospheric antiprotons"*, Astroparticle Physics, **35**, 277 (2012) (DOI: 10.1016/j.astropartphys.2011.09.002)

2. Partha S. Joarder, Arunava Bhadra, Biplab Bijay, Sanjay K. Ghosh,, Sibaji Raha, *"Dependence of Simulated Atmospheric Antiproton Flux on the Microscopic Models of Particle Interactions"*, Proc: 32nd Int: Cosmic Ray Conf:, Beijing, **1**, 129 (2011) DOI: 10.7529/ICRC2011/V01/1115

3. *"Does the knee in the primary cosmic ray energy spectrum exist?"*, B. Bijay and A. Bhadra, Exploring the Cosmos, (Ed. A. Bhadra, Lambert Academic Publishing (Germany), ISBN-13: 9783844391657) p 106, (2011)

4. *"The origin of the knee of the cosmic ray energy spectrum"*, Arunava Bhadra and Biplab Bijay, Proc: 32nd Int: Cosmic Ray Conf:, Beijing, **6**, 186 (2011) DOI: 10.7529/ICRC2011/V06/1023

5. Biplab Bijay, Prabir Banik, Arunava Bhadra, *"The knee in the cosmic ray energy spectrum from the simutaneous EAS charged particles and muon density spectra"*, communicated for publication (eprint arXiv:1511.05739)

6. Biplab Bijay, Arunava Bhadra, *"Progenitor model of cosmic ray knee"*, Research Astron. Astrophys **16**, 6 (2015) (DOI: 10.1088/16744527/16/1/006)

Preface

Cosmic Rays are relativistic particles coming somewhere from outer space and hitting on the top of the earth's atmosphere. The energy spectrum of these particles spreads over a wide range of energies, from a few hundred MeV to more than 10^{20} *eV, the flux of which can be described well by a single power law with negative spectral index. However, the spectral index of the spectrum changes at least two energies; one around 3 PeV where the magnitude of the spectral index changes from about 2.7 to 3.1 i.e. the spectrum becomes steeper above this energy which is known as the knee of the cosmic ray energy spectrum and again the spectral index takes it original value of 2.7 above about 5 EeV which is known as the ankle of the energy spectrum.*

The origin of the knee is not convincingly known yet. Several models have been proposed in the literature so far but none of them are free from problems. The existence of the knee in the spectrum is definitely an important imprint of the true model of origin of cosmic rays and hence a proper explanation of the knee is expected to throw light on the problem of cosmic ray origin. The present thesis presents theoretical and Monte Carlo simulation based study of the knee of the cosmic ray energy spectrum. Particularly we critically examine the existence of the knee in the cosmic ray energy spectrum through detailed Monte Carlo simulation studies of cosmic ray extensive air showers. We then propose a new model of the knee, based on the mass distribution of progenitor of cosmic ray sources, which is devoid of the lecunas of the existing models.

The organization of the thesis is the following:

In ***Chapter 1*** *of this present work a general introduction to the cosmic rays and some of its important features are summarized.*

Large number of experiments are going on in order to study cosmic radiations in different energy ranges with ground based installations, balloons and satellites through the detection of both primary & secondary cosmic ray particles. Several theoretical models have been proposed in order to explain the origin of the primary cosmic rays, their acceleration and origin of the knee in primary energy spectrum. In ***Chapter 2*** *the experimental results and theoretical models are discussed briefly. The present status of the knee problem is also summarised.*

In order to find out informations about primary particles from secondary particle informations, it is important to reconstruct the air shower, through monte-carlo simulation which includes various hadronic interaction models. For that, verification of these models at different energies and atmospheric depth is required. In ***Chapter 3*** *of this work , these air shower reconstruction methods and monte-carlo simulation programs are briefly described. Also the consistency of some of these simulation programs are checked by comparing the simulated results with other experiments.*

In ***Chapter 4****, using these above mentioned simulation methods, verification of low energy hadronic interaction models in use are done by cross checking the simulation results with experimental data. The material presented in this chapter has been published in Astroparticle Physics (Elsevier) (Arunava Bhadra, Biplab Bijay, Sanjay K. Ghosh, Partha S. Joarder, Sibaji Raha, "Influence of microscopic particle interaction models on the flux of atmospheric antiprotons", Astroparticle Physics,* ***35****, 277 (2012) (doi 10.1016/j.astropartphys.2011.09.002)) which is attached at the end of the thesis.*

In ***Chapter 5*** *, a critical examination of various relevant features of primary cosmic rays around the knee energy using Monte Carlo simulation (CORSIKA) and search for any new feature is done. The material presented in this chapter has been communicated (Biplab Bijay, Prabir Banik, Arunava Bhadra, "The knee in the cosmic ray energy spectrum from the simutaneous EAS charged particles and muon density spectra", eprint arXiv:1511.05739) which is attached at the end of the thesis.*

In ***Chapter 6*** *, a new model of cosmic ray knee is proposed based on mass distribution of progenitor of cosmic ray sources. The material presented in this chapter has been published in Research in Astronomy & Astrophysics (Biplab Bijay, Arunava Bhadra, "Progenitor model of cosmic ray knee", Research Astron. Astrophys* ***16****, 6 (2015) (doi: 10.1088/16744527/16/1/006)) which is attached at the end of the thesis.*

In ***Chapter 7****, the summary of this present work along with a brief discussion is presented.*

Contents

List of Tables

List of Figures

Chapter 1

Cosmic Rays and Extensive Air Showers

1.1 Introduction

Highly energetic charged (nuclei, electrons, positrons) and neutral (neutrinos, photons) particles coming from outer space and hitting earth's atmosphere are generally referred as cosmic rays. These were first discovered by Hess in 1912 [1] during several balloon flight experiments. The energy spectrum of these particles spreads over a wide range of energies, from a few hundred MeV to more than 10^{20} eV, the flux of which can be described well by a power law

$$\frac{dN}{dE} \propto E^{-\gamma} \tag{1.1}$$

whose main feature is the so called knee, a change in the spectral index , γ from 2.7 to 3.1, at about 3×10^{15} eV as shown in Fig. 1.1. The measurement techniques are different depending on the involved flux. In fact, over the entire energy range, the integral flux drops from 1 particle $m^{-2}\ s^{-1}$ at 10^{11} eV, to 1 particle $m^{-2}\ year^{-1}$ at 10^{15} eV, down to 1 particle $km^{-2}\ century^{-1}$ at 10^{19} eV. A further steepening of the spectrum (the second knee) has been claimed recently around 4×10^{17} eV, which is called as the *iron knee*. The spectrum gets flattened at about 4×10^{18} eV, giving rise to another interesting feature, the *ankle*.

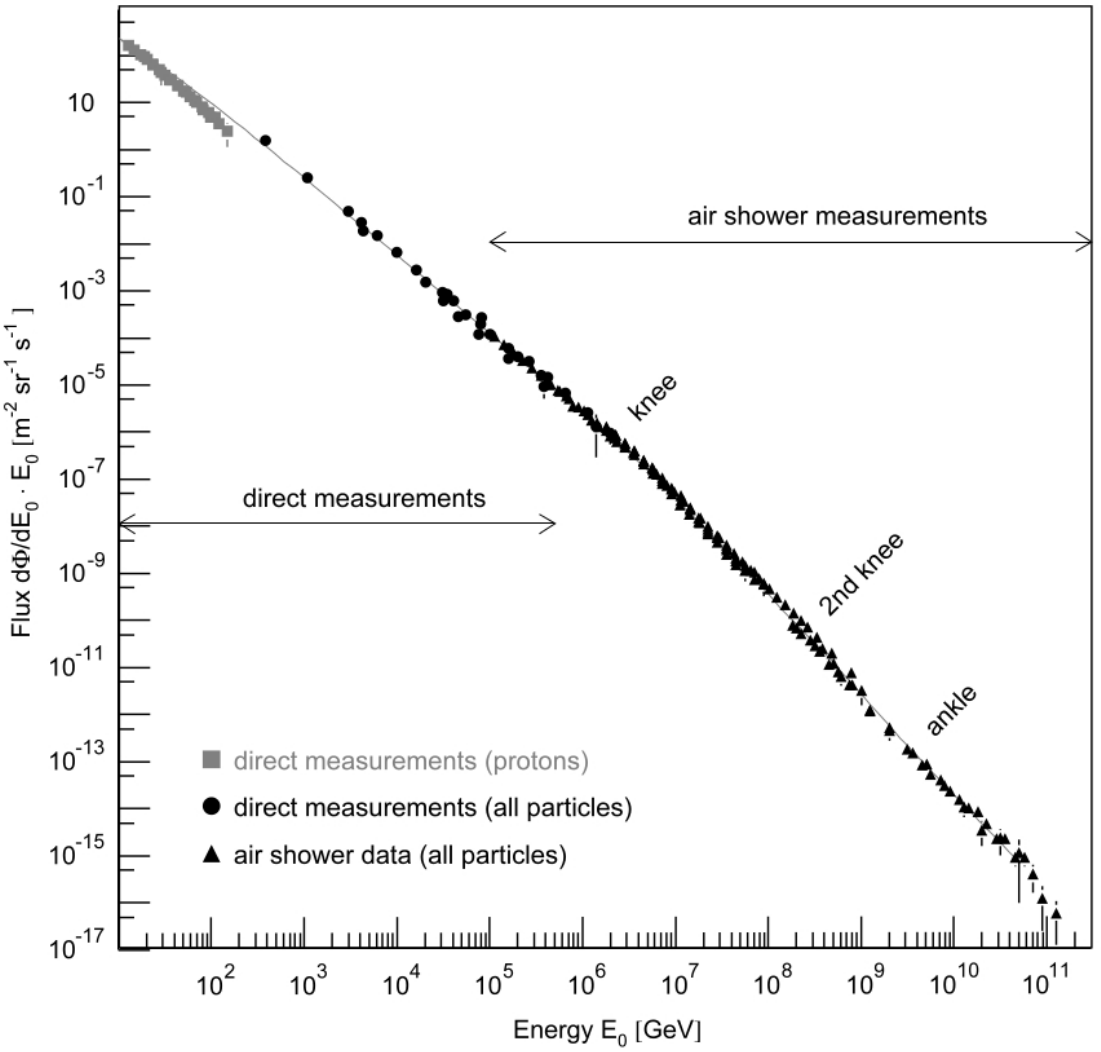

FIGURE 1.1: The differential energy spectrum of PCR and its various important features like the *1st knee*, the *2nd knee* and the *ankle* (figure taken from [2]).

The *knee*, a sharp turn in the energy spectrum of cosmic rays around 3 PeV , is an important characteristic feature of the spectrum which demonstrates a sudden decrease in spectral slope. The study of the knee has been an important topic of research both in experimental and theoretical astroparticle physics world wide since it was first detected in the studies of Moscow State University group in 1958 [3, 4]. For the following (fifty seven) years, quite a few experiments have been confirming the existence of this knee, displayed by various observable, mapping the primary CR spectrum. The existence of knee in the energy spectrum of the primary CR is an important imprint of the true model for origin of cosmic rays and hence proper understanding of this spectral feature is vital in connection with the problem for origin of cosmic rays.

Several mechanisms have been proposed to explain the knee which is discussed in detail in Chapter 2. In their first conclusion the discoverers argued that the knee in the spectrum is a consequence of the superposition of cosmic rays of galactic and extragalactic origin [5]. In subsequent years many new ideas have been proposed which vary from astrophysical reasons such as leakage from the galaxy due to reduced efficiency of galactic magnetic field to confine the cosmic ray particles within galaxy [6–14], rigidity cut-off at the acceleration [15], nuclear photo-disintegration at the sources [16, 17], or the single-source model in which dominance of the flux at the knee is coming from a nearby supernova [18–20] to a scenario adopting a new channel of the primaries interaction producing new unobserved particles carrying away some energy [21, 22]. Sveshnikova has ascribed the knee as the result of cosmic ray acceleration by a variety of supernovae [23–25]. On the other hand employing improved analysis techniques spectra for individual elements or mass group around the knee of the spectrum have been obtained from modern experiments through simultaneous measurements of many observables [85]. These results indicate rigidity dependent breaks; the knee is due to the steepening of proton/light elements spectra. But none of the existing models of the knee are free from problems. For instance, if the knee corresponds to break in proton spectrum then maximum energy of iron flux from the same sources should be around 10^{17} eV. Hence a special variety of supernovae or some other type of galactic source has to be invoked as generator of cosmic rays between 10^{17} eV and the ankle. The problem with such a fine-tuning is to match both the flux and the energy at the point of taking over. Moreover, it is already been noticed that rigidity dependent break scenario of composition does not consistently described the whole data set of the measurements over the whole energy region. Though single source model can avoid such criticisms but a problem with the proposal is that in normal circumstances the source should be observed in high energy gamma rays but no strong evidence for gamma ray emission from any nearby SNR exists. The change in interaction scenario at the knee energy has not received any support from the accelerator experiments against the expectations. In Chapter 6, we shall propose a new theoretical model for the knee.

The tail of the CR spectrum, above 10^{20} eV, is scarcely populated. A cut-off is predicted by Greisen, Zatsepin and Kuzmin (GZK cut-off) [26–28] at 5×10^{19} eV , due to the interaction of the primary particles with the photons of the cosmic microwave background (CMB) radiation. The highest energies of the cosmic ray spectrum are studied by the Pierre Auger Observatory [29, 30] with good statistics

which has observed a sharp decrease of flux around 5×10^{19} eV which could be the GZK cut-off.

1.2 Composition of cosmic rays

The chemical composition of cosmic rays is estimated from direct measurements up to energies below 10^{14} eV. The estimation of elemental distributions have been studied by satellite [34–48] and baloon flight experiments [49–65] up to energies of 1-2 TeV/nucleon. It is found about 98% of cosmic radiation are hadrons out of which 87% are protons,12% is Helium and 1% corresponds to charged nuclei of heavier element like Fe, C, N, O, B etc.

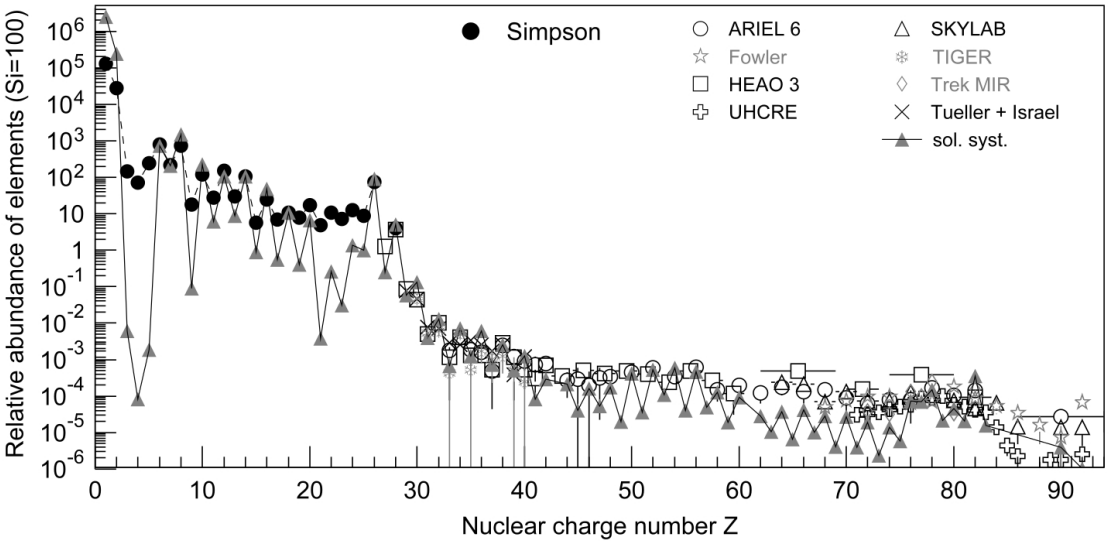

FIGURE 1.2: Comparison of the relative abundance of elements as a function of Z in the solar system and the primary cosmic radiation at source around 1 GeV/n, normalized to Si = 100 [31]. Data for $Z \leq 28$ is from [32] where as data for heavy nuclei are taken from ARIEL 6 [37, 38], HEAO 3 [39], SKYLAB [40], TIGER [41], TREK/MIR [42, 43] and UHCRE [44]. Data showing the abundance of elements in the solar system is taken from [33]. This figure is taken from [2].

As shown in Fig 1.2, the comparison of relative elemental abundances in the solar system with the derived abundance at the sources has similarities, suggesting that cosmic rays are accelerated out from a sample of well mixed interstellar matter. In cosmic rays, elements like Li, Be, and B are overabundant, as well as all the groups with atomic mass lower than Fe. No significant difference is found, instead, in the abundances of heavier elements. But in cosmic rays lighter elements like Li,

Be and B are abundant. So it is believed that while propagating through galaxy, lighter elements are generated by the process of spallation when heavier nuclei interact with interstellar medium. After that they got trapped into the galactic magnetic field with trapping time period about 10^7 years. As most of the primary particles are charged hadrons, their path is affected by the galactic magnetic field because of which it is impossible to locate the original source.

The composition scenario evolve from indirect observations involving air shower studies is not unequivocal. Recent results favour that the composition shifted towards heavier elements beyond the knee. At higher energies, an evolution from iron dominated composition at 10^{17} eV to a proton dominated composition above 10^{18} eV is reported by some experiments .

1.3 Extensive air showers(EAS)

The highest energies reached by cosmic rays are much larger than the ones produced in any of the present and forthcoming colliders (i.e. TeVatron and LHC). From Fig. 1.3 in which the cosmic ray energy spectrum is compared with the laboratory energies of the colliders, it can be understood how air shower phenomena can work as a great natural laboratory giving the opportunity to compare and considerably enlarge the field of view on particle physics.

Extensive air showers were first studied in 1938 by P. Auger et al. [66] and independently by W. Kohlhorster et al. [67], which is nothing but a stream of secondary particles generated in the Earth's atmosphere when highly energetic cosmic ray particles interact with air molecules multiple times (Fig. 1.3). The resulting secondaries while propagating in downward direction suffer repeated collisions with air molecules generating billions of particles (depending on the primary energy) that gain transverse momenta because of the repeated collisions. At the end, mostly electrons, muons and gammas are observed. Due to this fact, the EAS is usually spread over a large area with a thickness increasing with the distance from shower axis which is represented by the incident direction of the primary. Spread of an EAS depends on energy of the primary particles. Distribution of the arrival times of these particles also gives us some idea about the direction of primaries.

After the first interaction of a primary cosmic ray particle with Earth's atmosphere, its energy is dissipated by secondary interactions, resulting secondaries

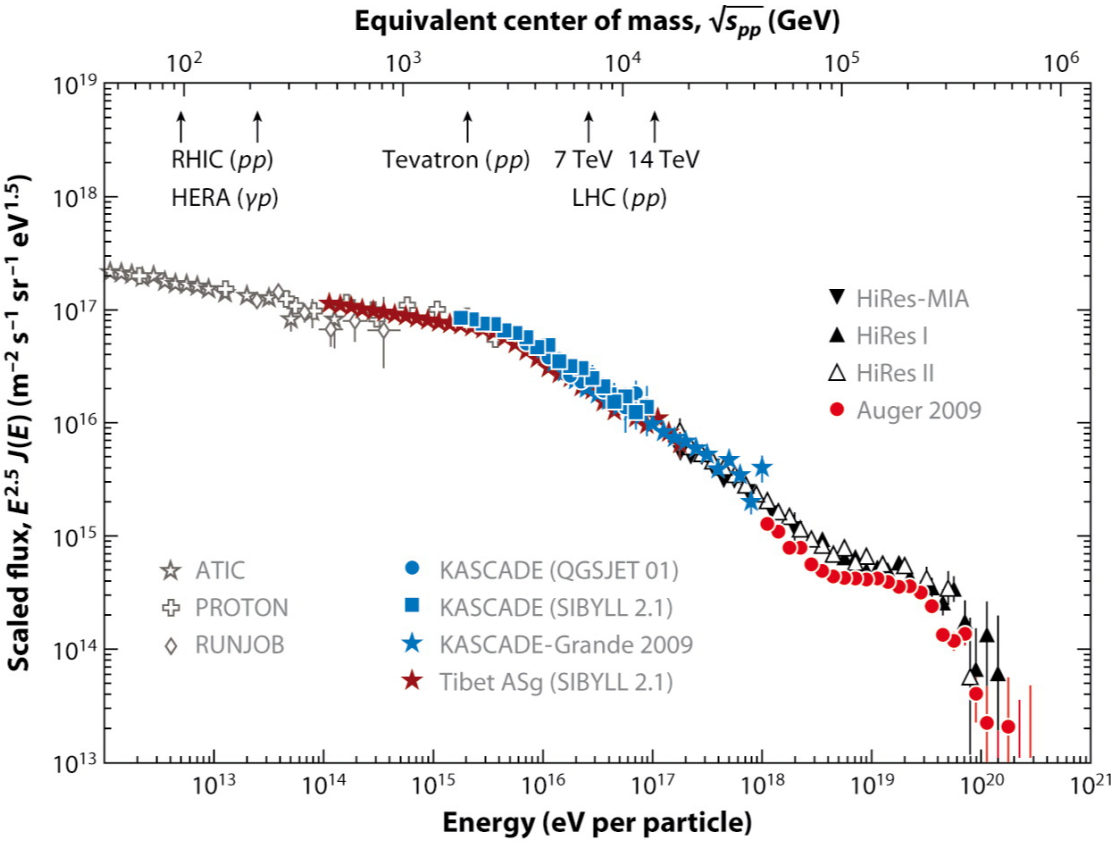

FIGURE 1.3: Primary cosmic ray energy spectrum and the equivalent beam energies of the RHIC, Tevatron and Large Hadron Collider (figure taken from [68]).

which again interacts with air while propagating in downward directions. So the number of secondaries increases as a shower propagates. Also the EAS particles suffer decay and absorption during its propagation. The dominating electromagnetic component (photons and electrons) is usually the one absorbed faster in both time and with distance to the point of first interaction and shower core. Other components are more penetrating like the muon component. At the earlier stages of a shower, the production process of secondaries dominates over the absorption and decay because of the energetic secondaries, resulting an important feature X_{max}, the altitude at which the number of secondaries are maximum. This plays an important role in the estimation of cross section of primary particles with air nuclei.

There are thee main components of EAS at the sea level, electromagnetic, muonic and hadronic.

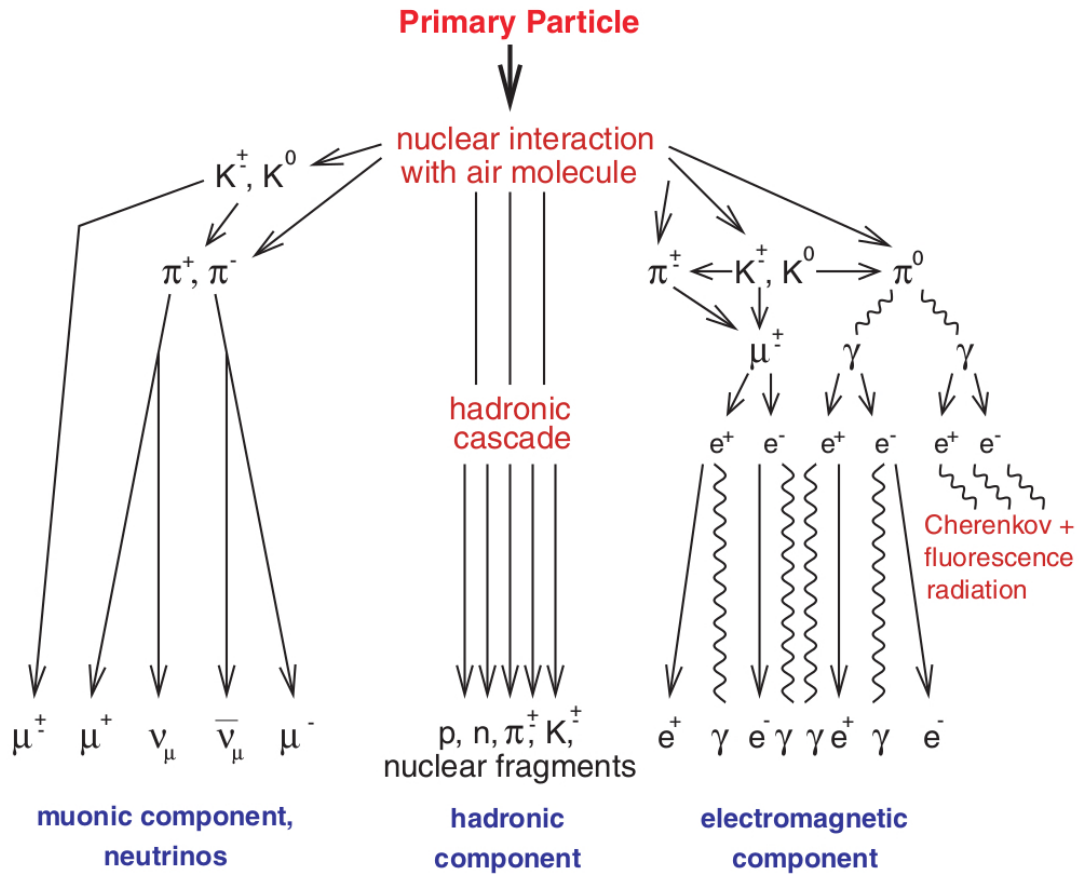

FIGURE 1.4: Schematic diagram of an EAS initiated by the interaction of a PCR particle with the Earth's atmosphere (figure taken from [69]).

The electro magnetic components constitute mainly electrons and photons. At sea level, 95% of particles are electromagnetic out of which about 85% of particles are γ rays and rest are electrons and positrons. When primary cosmic ray particles interact strongly with an air molecule of Earth's atmosphere, mostly mesons are produced which gives us an idea about multiplicity. Among these many produced particles, one particle carries great fraction of the incident primary energy, the fraction being called elasticity. The fraction of energy that is not given to that particle is called inelasticity. The inelastic part of energy is distributed among rest of the secondary particles.

Most of these produced mesons are pions and kaons. The neutral pions decays instantly into γ rays after its production.

$$\pi^0 \longrightarrow \gamma + \gamma$$

These γ rays start electromagnetic avalanches by pair production ($e^- + e^+$) and by bremsstrahlung processes. When electrons and positrons reach an energy level of about 100 MeV, energy loss by ionization starts to become important and the particles are stopped quickly. After reaching its maximum size, the particle number in the EAS decreases approximately in an exponential way. The charged mesons either interact with atoms of the atmosphere or decay into muons and neutrinos(anti-neutrinos).

$$\pi^{\pm} \longrightarrow \mu^{\pm} + \nu(\bar{\nu})$$

$$K^{\pm} \longrightarrow \mu^{\pm} + \bar{\nu}(\nu)$$

Muons form the penetrating EAS component since they get less absorbed and reach the ground with high probability (the higher energy muons can penetrate in the deep underground). This is also due to their comparatively long lifetime, which is enlarged by relativistic time dilatation. The decay of charged muons lead to the generation of decay electrons that add to the electromagnetic component. Together with electron, muon forms the charged particle component with the integrated intensity (shower size) N_{ch}. For not too inclined EAS, the shower size is sometimes considered more or less equivalent to the electron size.

$$N_e \approx N_{ch.} \tag{1.2}$$

Finally, the core of an air shower is situated around the shower axis and consists of the hadronic component containing mostly pions but also nucleons, antinucleons, K-mesons and more exotic particles.

In order to measure the sizes of the different components, a typical EAS experiment uses an array of detector stations covering a large area in the 10^3 m^2 range and records the lateral particle densities distributions by sampling the area of various kinds of detectors. Then, using an a-priori assumed form for the lateral distribution (lateral distribution function) of the particles, size is determined.

The three main EAS components, whose developments usually studied, are accompanied by Cerenkov, nitrogen fluorescence and radio emission in the atmosphere. Each component provides specific observables that carry information about the primary particles. Depending on the kind of observable one wants to record, different types of detector systems are used leading in many cases to the installation

of complex detector systems capable of detecting different components of the same EAS simultaneously. By such a detection system, correlated studies among different observables become possible.

EAS measurements are difficult because the primary energy and composition are unknown and have to be indirectly inferred from a precise determination of the EAS observables and deep theoretical assumptions on the shower interactions. Investigation of EAS which has been in former times directed to explore the inherent features, the development and structure of the phenomenon, is nowadays mainly focused to the understanding, in which way some features can be related to the energy and mass of the primary and can be used as signatures for these primary properties. Simulation studies have demonstrated that, on the average, heavy ion induced air showers develop differently from proton induced showers due to a smaller interaction length and due to a larger number of nucleons in the projectile. This is corroborated by the effect that the multiplicity of secondary particle production per nucleon varies only slowly with the energy. Thus the muon content of an iron induced EAS appears to be larger than for the proton induced one. Simultaneously the number of electromagnetic particles (e/γ) gets larger in the proton EAS because their energies reflect the energy of neutral pions they originate from. As electrons and positrons are rapidly absorbed when their energies drop below 100 MeV, an A-nucleon shower, with each nucleon carrying the energy E/A, reaches earlier the maximum of its longitudinal development, i.e. higher in atmospheric altitude. That means for the same primary energy E, the shower size (N_e) is different for different kind of primaries observed at the observation level. Since we neither know a-priori the energy nor mass of the primary, energy determination and mass discrimination is an entangled problem. Therefore many attempts are focused to minimize the influence of mass on the observable which serves as the energy estimator.

Chapter 2

Current status of the Cosmic Ray Knee

2.1 Introduction

At energies above 10^{14} eV, direct measurements of cosmic rays are not possible because of its very low flux following a power law spectrum. Therefore, while at energies below 10^{14} eV the large flux allows direct measurements by sending small detectors on balloon flights and artificial satellites, above 10^{14} eV, use of large arrays of ground based detectors for many years of exposure is the only way to study and extract informations about the primary cosmic rays. By acquiring information about the secondary particles produced by the interaction of primary cosmic rays with the atmospheric nuclei the results of such indirect way of measuring cosmic rays depend on the understanding of high energy interactions in the atmosphere. Different methods have been employed by several experimental groups on the basis of results obtained from Monte Carlo simulation codes for EAS, upgraded by their authors to extract information about the cosmic ray primary.

The experimental status of the cosmic ray knee and its theoretical explanations are discussed below.

2.2 Review of world wide experimental data

First the detection of the knee in the shower size spectrum was done by the MSU experiment [3, 4]. There after several cosmic ray air shower experiments detected the knee feature. Several studies have been performed over last six decades in the knee region to derive primary energy spectrum of cosmic rays and its composition. The past air shower experiments mostly derived all-particle energy spectra from their measurements. However, modern experiments obtained the energy spectra for groups of elements in the PeV region have from indirect measurements too. Systematic studies were done to compare the effect of hadronic interaction models used in simulations in order to reconstruct the primary energy spectrum from EAS.

As mentioned before, the cosmic ray energy spectrum extends up to 10^{20} eV with a knee at energy around 3 PeV. Below the knee region, the spectrum is obtained by satellite based experiments like PROTON [35, 36], SOKOL [45–47] and balloon flight based experiments like JACEE [57, 58] and RUNJOB [61, 62]. Fluctuations in these kind of experiments are very high because of the smaller detection area. Above the knee region, experiments like Haverah Park [70], Fly's Eye [71, 72] and HiRes–MIA [73] have been performed. These experiments are ground based with an objective of determining the energy spectrum above knee with primary composition. In the knee region, various ground based experiments at different altitudes, such as Akeno (1984, 1992) [74, 75], EAS-TOP (1999) [76, 77], CASA-MIA (1999) [78, 79], DICE (2000) [6], BLANCA (2001) [80], HEGRA (2000) [81], Yakutsk (2001) [82], GRAPES-3 (2001)[83], BASJE (2004) [84], KASCADE (2005) [85] and Tibet (2008) [86] have been performed with different methods. These experiments are summarized in the table 2.1.

Here, only the experiments in the knee region are discussed. Based on the type of detectors used, these experiments can broadly be divided into 3 categories which are briefly discussed below.

2.2.1 Experiments using particle detectors only

The energy spectrum of the cosmic rays between $10^{14.5}$ eV and 10^{18} eV was studied by Akeno air shower array [74, 75]. With 150 scintillation detectors and 9 stations

of proportional counters, electromagnetic and muon components of EAS were detected. The primary energy spectrum was derived form electron size spectrum using the longitudinal development curve observed at mount Chakalatya. A knee can be seen at energy $10^{15.67}$ eV at which the spectral index is 2.62 ± 0.12 below and 3.02 ± 0.05 above. No further significant change in the slope of electron and muon size spectrum is seen beyond $10^{15.67}$.

CASA-MIA [78, 79] detectors included 1089 surface particle detectors (CASA) , spaced 15 m apart over a square grid and 1024 underground muon detectors(MIA) at the Dugway Proving grounds, south-west of Salt Lake City, Utah at an altitude of 870g cm^{-2}. The goal of this experiment was to study the cosmic ray energy spectrum in th energy range 10^{14} eV to 10^{16} eV. The MOCCA [87] shower simulation program, using the SIBYLL [88–90] hadronic interaction model was used for the event generation purpose [78]. The differential shower size spectrum obtained from this experiment clearly shows a kink around $10^{5.8}$ particles. A change in the spectral index from 2.69 to 3.12 can be seen at energy $10^{15.5}$ eV which is shown in the table.

The BASJE-MAS [84] array is located at an altitude of 5200 m above seal level at Mt Chacaltaya. With its 68 unshielded scintillation detectors and one shielded detector, it measures the showers with energies around the knee region near their maximum development. Because of this the shower size at maximum, $N_{e_{max}}$, is independent of shower development fluctuations and/or different primary composition. The calculation of energy spectrum is done by comparing the equi-intensity curves for various zenith angle bins with the simulated ones with five primary components and using CORSIKA [91, 92], a 3-D air shower simulation program, with the QGSJET [93–95] model.

The KASCADE [85] experiment was situated at an altitude 110 m above sea level. With an array of electron and muon detectors, a central hadron calorimeter with substantial muon detection areas and a tunnel with streamer tube muon telescopes, it is claimed to be one of the most precise air shower experiments in the world. After the shower reconstruction, the all particle spectrum and spectra for elemental groups [96–100] derived from electromagnetic, muonic and hadronic components are compiled with CORSIKA [91, 92], using QGSJET [93–95] and SIBYLL [88–90] hadronic interaction models. A rigidity dependent cut-off was observed in the analysis of these spectra.

The GRAPES-3 [83] high density air shower array is designed for the studies of extensive air showers near the knee. It is located at Ooty at an altitude 2200 m above sea level. With its 721 scintillation detectors and 16 muon stations it performs multi information studies on electromagnetic and muon components of EAS. Two small muon telescopes are used below the scintillation detectors for calibration. The primary energy spectrum is derived by compiling CORSIKA simulation. The results are shown below in the table.

The Tibet air shower array [86] was designed to perform studies on EAS as well as high energy celestial gamma rays. It consists of 761 scintillation detectors which spreads over an area of 36, 900 m^2. The primary energy of each event is derived from the shower size N_e which is calculated by fitting the electron densities with NKG function. The all particle energy spectrum is derived comparing the experimental data with CORSIKA [91, 92] simulation with QGSJET01c [93–95] and SIBYLL2.1 [88–90] interaction models. Several kinds of mixed composition models were used, namely QI, QHD, QPD, QP and SHD [86] in order to analyze the data. A distinct knee can be observed in the all particle spectrum. However, the main uncertainty with the primary composition is not resolved because of the unavailability of muon data.

2.2.2 Experiments using photon detectors only

Each of the the two DICE [6] telescopes, located at the CASA-MIA [78, 79] site in Dugway, Utah as described before, consisted of a 2 m diameter f/1.16 spherical mirror with a focal plane detector of 256 close packed 40mm hexagonal PMTs which provided $\sim 1^o$ pixels in an overall field of view $16^o \times 13.5^o$, centered about the vertical and are separated by 100 m. The collected data were analyzed by comparing with simulated events from CORSIKA [91, 92]. A sharp knee was observed around 3 PeV in the all particle energy spectrum derived from this analysis.

The Yakutsk [82] array in Siberia is one of the most complex array which covers an area of 18 km^2. Along with 58 ground-based and 6 underground scintillation detectors, it was designed to study cosmic rays between energies 10^{16} eV to 10^{18} eV. Also 35 photomultiplier systems were installed to study Cerenkov radiation associated with air shower. Currently the array has been rearranged to cover an area of 10 km^2 so that detailed study of EAS can be made around 10^{19} eV. The change in spectral index from 2.7 to 3.12 can be observed around 3 PeV.

2.2.3 Experiments using both particle and photon detectors

The EAS-TOP [76, 77] experiment, located at 2000 m above sea level at Campo Imperatore, Italy performed multi-component studies of EAS in the energy range between 10^{14} eV and 10^{16} eV using electromagnetic, muon, hadron and Cerenkov detectors. The results are shown in the table. The proton spectrum obtained from hadrons agrees well with the extrapolation of the direct measurements [101]. The Cerenkov data combined with MACRO muon data is normalized to the proton + helium flux of direct measurements and the results obtained are compatible with the extrapolation of the direct measurements [102].

The AIROBICC Cerenkov array and the scintillation detector matrix of the HEGRA [81] air shower complex was located at a height of 2200 m above sea level and covers an area of $180 \times 180 m^2$. 243 plastic scintillation huts of the detector matrix and 49 open photo multiplier tubes(fitted with Winston cones) of the AIROBICC array were used to derive a spectrum for the proton and helium component together as well as an all-particle spectrum [103] between 0.3 PeV and 10 PeV. CORSIKA [91, 92] simulations were used for event reconstructions. A knee can be seen in the all particle spectrum(normalized to the extrapolation of direct measurements below 1 PeV) as well as in the combined spectrum of proton and helium.

CASA-BLANCA [78–80] detectors included 144 angle-integrating detectors (BLANCA [80]) with an average separation of 35 to 40 m which recorded the lateral distribution of air shower Cerenkov light along with 957 scintillation counters (CASA [80]) for the detection of particles. The Cerenkov measurements were compared with CORSIKA [91, 92] simulations with EGS4 [104] and GHEISHA [105] codes within the energy rage 0.3 to 30 PeV. Several hadronic interaction models like QGSJET [93–95], VENUS [106], SIBYLL [88–90], and HDPM [91] were used for the extrapolation of available particle data. The observed all particle spectrum shows a smooth knee around 2-3 PeV primary energy.

The results of these experiments are given below in the table 2.1.

TABLE 2.1: Status of the CR experiments and the knee. γ_1/γ_2 are the spectral indices for the energy spectrum below/above the estimated knee energy($\mathbf{E_{knee}}$).

Name of the Experiment	**Detector Type**	**Simulation Model/ Particle Type**	γ_1	$\mathbf{E_{knee}}$ **(PeV)**	γ_2	$\mathbf{E_{range}}$**/GZK (PeV)**
PROTON(1970)	Particle	–	2.62	–	–	0.001–0.1
Akeno(1984-1992)	Particle	–	2.62±0.12	5	3.02±0.03	1.0–630
SOKOL(1993)	Particle	Proton All	2.85±0.14 2.68±0.07	–	–	0.0025–0.005
Fly's eye(1994)	Photon	–	–	–	3.01±0.06	200–3200
JACEE(1995)	Particle	Proton Helium	2.86±0.07 2.72±0.09	–	–	0.002/n–0.04/n 0.002/n–0.06/n
EAS-TOP(1999)	Particle & Photon	–	2.76±0.03	2.7–4.1	3.19±0.06	0.9–10
CASA-MIA(1999)	Particle	MOCCA	2.66±0.02	1.0	3.00±0.05	0.1–10
DICE(2000)	Photon	–	–	3	–	0.2–15
HEGRA(2000)	Particle & Photon	–	2.72±0.02	3.98	3.22±0.47	0.3–10
CASA-BLANCA(2001)	Particle & Photon	–	2.72±0.02	2.0	2.95±0.02	0.5–10
Yakutsk(2001)	Photon	–	2.63±0.03	3.0	3.12±0.02	1.0–10
HiRes-MIA(2001)	Photon	–	–	–	3.07±0.11	100–2500
BASJE-MAS(2004)	Particle	QGSJET	2.66±0.00	3.16	3.19±0.02	0.1–10
RUNJOB(2005)	Particle	Proton Helium	2.74±0.08 2.78±0.20	–	–	0.01/n–0.5/n
KASCADE(2005)	Particle	QGSJET SIBYLL	2.70±0.01 2.70±0.06	4.0±0.8 5.7±1.6	3.10±0.07 3.14±0.06	1–100
GRAPES-3(2001–Present)	Particle	QGSJET SIBYLL	–	–	–	0.03–30
Tibbet(2008)	Particle	QI QHD QPD QP SHD	2.81±0.01 2.67±0.01 2.65±0.01 2.60±0.01 2.67±0.01	4.4±0.1 4.0±0.1 3.8±0.1 3.4±0.1 4.0±0.1	3.21±0.01 3.10±0.01 3.08±0.01 3.03±0.01 3.12±0.01	0.1–100 0.1–100 0.1–100 0.1–100 0.1–100

2.3 Theoretical models of the knee

There are several theoretical models modelling the knee in the cosmic ray spectrum. They can be broadly categorized into two groups. The first category of models consider the knee as an intrinsic property of the energy spectrum where as the authors of the second category of models consider new type of physics processes/interaction in the atmosphere as the source of the knee. In other words the first category of models consider the knee to be astrophysical in origin whereas the second category describes the knee as an effect of the extensive air showers in the atmosphere.

Some of the models of the first category relate the knee with the acceleration of cosmic rays by supernova explosions and its several extensions [5, 15, 23, 24, 108]. Recent studies show that magnetic field is amplified by SNR which confines cosmic rays more effectively to the shock region, thus resulting more efficient

acceleration [109]. Thus this amplification of magnetic field accelerates cosmic rays to PeV energies in supernova remnants. A source related model [18–20] is there which considers a nearby single source as a primary source of cosmic rays. Models like re-acceleration of cosmic rays by spiral shocks in the galactic wind [110] and acceleration of comic rays by the ejected matters in the galactic halo [111, 112] were advanced to explain the knee. Diffusive shock acceleration of the cosmic ray particles with energy dependent path length [6] and diffusive propagation of cosmic rays in the galaxy [7–10] are also proposed as the origin of the knee in the primary energy spectrum. Some other models consider interaction of the cosmic ray particles with background photons [11–14] or the neutrino background [113] as the cause of the knee. Diffusive propagation with photo-disintegration [16, 17] also proposed as the origin of the knee.

The models of the second category consider the knee as a result of creation of new particles during the development of air shower which is not seen in the modern day experiments. These models argue that the energy is transferred into techni-hadrons [21] or gravitons [22] which can not be observed by air shower experiments. Also since the energy threshold of these interactions is in the knee region which is above the collider experiments, it is not observed there too.

Some of these theoretical models are discussed below.

2.3.1 Acceleration in supernova remnants

Based on the diffusive propagation of cosmic rays in SNRs, Berezhko and Ksenofontov [15] in their work explained that the energy of cosmic ray particles is increased significantly because of their repeated crossings of the shock front which in turn modifies the planar nature of the shock front. This generates a power law spectrum of cosmic rays which is altered because of the modification in shock wave due to the hardness of spectrum. A minimum velocity is required to cross the shock wave front, that determines the injection rate of the particles. It is believed that the injection efficiency is related to the mass to charge ratio (A/Z) of the nucleus considered. So heavier elements are expected to accelerate more efficiently. Considering pre-acceleration in the wind of the predecessor star, the maximum energy achieved is $Z \times 10^{15}$ eV. The resulting all particle energy spectra is found to have a knee due to the charge dependence of the maximum energy achieved in the acceleration process.

2.3.2 Acceleration by supernova shocks

Stanev et al. [5], based on the concept of particle acceleration in the shocks where shock normal is perpendicular to the prevailing magnetic field, proposed that the energy spectrum of cosmic rays is consisted of three components. The first part is formed by protons with a spectral index of 2.75 which are accelerated up to the energy 10^5 GeV by the blast waves, generated from the explosions of supernovae into an approximately homogeneous interstellar medium. The second part of the spectrum is formed by the particles with energy up to 3×10^9 GeV (heavier elements and rigidity dependent) which are produced because of the explosions of stars into their former stellar wind. It has a spectral index 2.67 up to rigidity dependent bend in the spectrum and 2.97 up to rigidity dependent cut-off. The last and extragalactic part is formed by the particles with even higher energies, up to near 10^{11} GeV produced in the hot spots of $Fanaroff\ Riley\ class\ II$ radio galaxies with a spectral index -2 up to the pileup just below the cut-off due to the interaction with the cosmological microwave background.

This model argues that shocks that travel down a steady stellar wind with spiral magnetic field accelerate the main fraction of galactic cosmic rays above about 10 TeV. The shock normal is assumed to be perpendicular to the magnetic field except around the poles where direction of propagation of the shock is parallel to the magnetic field which results a harder spectra for the accelerated particles. Thus polar cap has a very little contribution towards the spectrum up to 10 TeV while from 10 TeV to the knee, polar cap contributes appreciably. At knee energies, polar cap begins to contribute significantly, almost equally in comparison with rest of the hemisphere, resulting a sharp bend in all particle spectrum. So the logical outcome from this model is the change in composition of the all particle spectrum around the knee region since the fluxes of nuclei are different according to their charge Z.

2.3.3 Acceleration by oblique shocks

In this model, Kobayakawa et al. [108] used slightly modified version of the diffusive acceleration of particles in supernova remnants where magnetic fields are at arbitrary angles to the velocity of shock front. The basic idea is based on the fact that particles are accelerated to higher energies in oblique shocks as compared

to parallel shocks. The shape of shock fronts, generated because of the ejected material from a supernova explosion that expands into the interstellar medium, are supposed to be almost spherically symmetric. The directions of the interstellar magnetic field lines is considered to be random rather than well aligned. It is assumed that the field lines meet the shock front at random angles and the cosines of these angles are distributed uniformly. The injection efficiency into the acceleration regime is believed to be a function of the angle between the magnetic fields and the normal of the shock front. It also makes the spectrum harder. The spectra generated by this model shows a rigidity dependent knee.

2.3.4 Acceleration by a variety of supernovae

Based on the recent astronomical observations of supernovae, Sveshnikova [23, 24] proposed a new approach which is a slightly revised version of the standard approach of cosmic rays acceleration in shock fronts of supernovae. This new approach gives us a scenario in which the maximum energy reached in SNR acceleration is the knee energy and depends on three factors, the charge Z of the nucleus, strength of the magnetic field B and density of protons in the interstellar medium and on the energy of explosion as well as the velocity of shock.

2.3.5 The single-source model

Erlykin and Wolfendale [18–20] in their model considered a single nearby source as an additional source of cosmic rays because of which a two-kink structure related to the cut-offs of oxygen and iron nuclei from the single source is supposed to be seen in the cosmic ray energy spectrum. They used shower size spectra (normalized to the knee position) to show the two fold structure. After re-binning the normalized shower size spectra a twofold structure in the all-particle spectrum at 3×10^6 GeV and 10^7 GeV was seen. But the structure at 10^7 GeV is yet to be observed in the all particle spectrum obtained from the present day experiments.

2.3.6 Re-acceleration in the galactic wind

Volk and Zirakashvili [110] proposed that galactic wind, mainly driven by cosmic rays and hot gas generated in the disk, reaches supersonic speeds at about 20 kpc

above the disk, and is assumed to be very extended (several 100 kpc) before it ends in a termination shock. Also the galactic rotation leads to strong internal wind compressions, bounded by cosmic ray shocks that re-accelerate the most energetic particles from the disk by about two orders of magnitude in rigidity which ensures a continuation of the energy spectrum beyond the knee up to the ankle. The maximum energy achieved by this process is

$$E_{max} = Z \times 10^{17} eV \tag{2.1}$$

which concludes that the knee in the all-particle spectrum is intrinsic in nature , i.e. a feature of the source spectrum itself.

2.3.7 The cannonball model

Based on the model discussed by Dar and De Rujula [114] to explain the gamma ray bursts, Plaga [111, 112] proposed a mechanism for the acceleration of the cosmic ray hadrons in which he investigated that masses of baryonic plasma (cannonballs), ejected in bipolar supernova explosions, could be the universal sources of the hadronic galactic cosmic rays. It is assumed that the total cannonball energy is converted to the energy of the cosmic ray particles in order to match the observed cosmic ray flux. The two scenarios for the acceleration are ultra-relativistic shocks in the interstellar medium which can accelerate the cosmic rays up to the knee energies and second-order Fermi acceleration inside the cannonballs. Energy spectra for groups of elements, derived from this model show a knee which is proportional to the charge with a soft change in the spectral index. The obtained all particle spectrum which is dominated by light particles in the whole energy range is in reasonable agreement with the average measured flux.

2.3.8 The minimum-pathlength model

Swordy [6], based on Leaky Box model for the cosmic ray propagation, proposed that the knee is a consequence of leakage of particles from the galaxy. It is assumed that the spectra of particles accelerated by diffusive shocks have the same spectral slope for all elements at the source with a rigidity dependent cut-off above which the spectra decreases. The path-length for escape from the galaxy which

is a function of the galactic radius is assumed to decrease with rigidity but has some minimum value. The energy spectra is calculated by taking the fractional abundances and using the average all particle spectrum as obtained from many experiments. A smooth change in the spectral index can be seen in the individual spectra calculated from this model.

2.3.9 Anomalous diffusion in the Galaxy

Lagutin et al. [7, 8], using fractal geometry as a description of interstellar medium and the magnetic field, proposed that the knee structure is due to the anomalous diffusion of the cosmic rays in the magnetic fields of the galaxy. The large free paths of the cosmic ray particles in the magnetic field domain are considered to be the results of this anomaly and can not be explained with normal diffusion process for their propagation. The spectrum is considered to be formed of two parts. The first part between energies 0.1 Gev to 10 GeV is considered to be formed by the numerous distant sources where as the higher energies region are formed by the contribution from near by sources, including 16 supernova remnants. The energy spectra for individual elements obtained from this model show a very smooth behaviour in the knee region, no kink in the spectra is visible and no distinct energy for the knee can be specified. The all particle spectra, derived from this model, shows a very smooth change of the spectral slopes.

2.3.10 Photo-disintegration and diffusion

Several authors have considered that the knee is due to the interactions of cosmic rays with various background particles. Based on the idea of Hillas [115, 116], photo-disintegration of nuclei in a dense field of photon is considered one major process which results the knee. Cosmic rays are considered to be accumulated near the source because of the magnetic field and therefore interacts with photons on their pass across the photon field. Photo-disintegration process along with the leakage of cosmic rays from the galaxy by diffusion process in the galactic magnetic field are considered for the explanation of the knee. Authors like Karakula [16] and Tkaczyk [17] considered that the cosmic ray particles, following a power law spectrum with a spectral index of 2.75 for protons and 2.55 for all other nuclei up to iron, interact with the photon background having a Planck type distribution.

The energy loss processes, like pair production, pion photo-production on nucleons, and photo-disintegration of nuclei were taken into consideration. Assuming the galactic magnetic field to be dominated by its turbulent component, trajectories of particles were calculated starting at random positions inside the galactic disk. The leakage of cosmic rays from the galaxy is also taken into account. The knee, in the region between 1 and 30 PeV in the all particle spectrum is explained by the photo-disintegration of nuclei and due to leakage.

2.3.11 Neutrino interactions in the galactic halo

Dova et al. [113] considered that the knee is due to the interaction of cosmic rays with massive neutrinos in the galactic halo. Significant increase in the average number density of standard model neutrinos with mass m $<$ 1 MeV due to gravitational clustering in galaxies and a magnetic dipole moment of massive neutrinos are considered to explain the increase in the cross-section for the inelastic scattering of nucleons on the neutrino background. Considering a cosmic ray spectrum with a spectral index 2.8 and having 60% protons and 40% iron, the propagation is described by a diffusion model, taking into account the galactic magnetic field. The calculated spectra for the proton and iron are found to be in agreement with the measurements. But this model overestimates the flux of light elements above the knee.

2.3.12 Nucleophysical Process in atmosphere

The basic idea behind this model is that a new type of interaction transfers energy to particles which are not yet observed in air shower experiments. These interactions start at the knee region which is above the energy of today's collider experiments. Kazanas and Nicolaidis, in this model proposed that the energy is transferred into techni-hadrons [21], the lightest super symmetric particles, and gravitons [22]. A single power law primary spectrum with spectral index 2.75 is assumed. It is considered that at energies above knee, a fraction of protons interact with this new type of interaction whose cross-section increases with increase in energy and particles like techni-hadrons and gravitons were formed which can not be observed by the modern day experiments. The spectrum calculated by this model shows some deviation from observed spectrum.

Chapter 3

EAS Simulation Techniques

3.1 Introduction

Many quantitative problems in astrophysics are nowadays solved via statistical sampling on a computer. Such Monte Carlo(MC) methods can be used in three different ways:

(1) to generate random objects and processes in order to observe their behavior,

(2) to estimate numerical quantities by repeated sampling, and

(3) to solve complicated optimization problems through randomized algorithms.

This part of the present manuscript describes the importance of Monte Carlo programs used for both estimation and optimization purposes in Astrophysical problems as in the case of cosmic ray air shower simulation programs. A range of established MC programs as well as some of the latest adaptive techniques are also discussed in later part of this chapter.

3.2 Importance of MC programs and high energy interaction models

As mentioned before, direct measurement of primary cosmic rays are not possible above few hundred TeV as its flux decreases with increase in energy, following a

power law spectrum. That is why above this energy, ground based detector arrays are used to study various observables of EAS produced by the interaction of primary cosmic ray particles with air nuclei. Few such important observables are cross-section of the interactions (that determines the shower depth), particle multiplicity (that determines the number secondary particles produced), pseudo-rapidity (that determines the longitudinal momentum of the secondary particles) and transverse momentum (p_T) distribution (which is related to lateral development of the shower). After that, various Monte Carlo simulation programs like MOCCA [87], COSMOS [117], GEANT4 [118, 119], CORSIKA [91, 92] and AIRES [125] containing high energy hadronic interaction models like QCDJET [126], QGSJET [93–95], VENUS [106], NEXUS [127, 128], DPMJET [129–132], SIBYLL [88–90], HDPM [91], EPOS [107] and low energy hadronic interaction models like GHEISHA [105], UrQMD [133, 134] and FLUKA [135, 136], are used to study the hadron production processes in EAS and informations related to them so that the primary particles can be traced back. But computation of hadron production, particularly at low transverse momenta, is not yet possible from first principles within QCD framework. One, therefore, relies on phenomenological models that are appropriately turned to match with the prevailing experimental data. Even a parametrization of such models may be difficult as the accelerator data for the relevant target-projectile combinations covering the whole kinematic region are not available. Experimental data on hadron-hadron interactions in the forward kinematic region at high energies and the data on hadron-nucleus and nucleus-nucleus interactions at all energies covering the whole kinematic range are particularly scarce. One has to resort to theoretical models of particle interactions in such cases. Microscopic models are preferred over the parametrized inclusive models in view of the preservation of correlations such that the basic conservation laws are maintained at every single interaction level. Moreover, such microscopic models have predictive power in the regions in which experimental data are not available.

Hadronic interactions are well described by resonance production and subsequent resonance decay near the particle production threshold; whereas, such particle production scenario becomes too complex at higher ($E_{lab} > 5$GeV) energies. In the latter situation, most of the particles are produced with low transverse momenta and, therefore, along the projectile direction so that a very large number of resonances of very short lifetimes have to be considered to describe particle

production that may not be possible in practice. Such a difficulty gives rise to a number of attempts to develop various hadronic interaction models.

Most of the high energy hadronic interaction models are based on parton interactions or Gribov-Regge theory where particle productions are explained using fragmentation of strings with other effects taken into account differently. So the largest uncertainty in the results of air shower simulation comes from the use of different hadronic interaction models which interpret hadronic interactions differently at high energies. Therefore, testing of these high energy interaction models at the highest energies is very important for the understanding of hadronic interactions and interpretation of air shower data. This testing is done by comparing the model predictions with various LHC data.

A brief description of these codes with models and comparison of these model predictions with LHC data is given below.

3.2.1 MOCCA

MOCCA [87] is Monte Carlo simulation program that simulates the cascade generated when a Cosmic Ray particle enters into Earth's atmosphere and detectors. It also uses thinning techniques to make the simulation faster at higher energies up to 10^{20} eV. It can be used to study secondary particles including Cerenkov radiation. Because of its special feature it was used widely in various shower experiments. Some special features of this program is outlined here. The height of the atmosphere is considered to be 100 km at which a cosmic ray particle (nucleus, nucleon, electron or gammas) enters into Earth's atmosphere. The secondary particles are traced down to 50 KeV and they can be traced into the scintillation detectors and absorbers Monte Carlo techniques are directly used for generating particles instead of looking for interaction libraries. The Thinning process is done by following all particles down to a fixed energy E_1 and beyond that only certain particles are followed with a given weight > 1 which is inverse of the probability of the particle with the energy E_2 ($probability = E_1/E_2$) to compensate for this incompleteness. Because of this the accuracy is reduced in the results. An "energy-splitting' basis simple but accurate high energy hadronic interaction model is employed to study high energy hadron interactions. Due to the non-inclusion of low energy nucleon cascading of nucleons, this program is inadequate to study the large flux of slow neutrons. The Nishimura-Kamata analytic treatment for electron-photon cascades

becomes inadequate at high energies because of the inclusion of the process which describes production of Pions by photons. The Landau-Pomeranchuk-Midgal effect in air and neutral Pion non-decay at very high energies is also included. This program allows to calculate detector signals along with the complete Monte Carlo Simulation of air showers. It also allows to study parentage of particles arriving at the detector level. The longitudinal and lateral development of the shower can also be studied by this program. Other hadronic interaction models can also be called form this program in order to study hadronic interactions. This program is in Pascal language. The upgraded version of this model is called ARIES [125] which is in FORTRAN language.

3.2.2 COSMOS

The program COSMOS [117] was first written in assembly language. It was changed to Fortran language in late 1970's. Gradually, improvements were made by adding heavy iron and their breaking processes, QCD jet production process, Lund Monte Carlo code Jetset, Fritiof, Nucrin, Hadrin and an improved multiple production model at high energies etc. In 1995, the main version was re-written. In 2001, a new interaction model DPMJET3 [132] was introduced in COSMOS. Also low energy phenomena such as atmospheric neutrino problems taking the muon polarization into account, or very high energy air showers in the GZK cuto region with magnetic bremsstrahlung and pair creation effects or the LPM effects are included into the code. The DPMJET3 [132] model will be discussed later.

3.2.3 GEANT4

GEANT4 [118, 119] is a 3-D detector simulation program written in the C++ language. It is used widely to simulate various types of particle detectors. It can also be used for the simulation of extensive air-shower [120–122]. Its a completely new detector simulation toolkit for which the reader is assumed to have a basic knowledge of object-oriented programming using C++. Although GEANT4 is a fairly complicated software system, only a relatively small part of it needs to be understood in order to begin developing detector simulation and air shower applications.

It is a free software package composed of tools which can be used to accurately simulate the passage of particles through any matter. The aspects of simulation process which have been included in it are given below :

• the geometry of the system, in which the user can define the geometry of the medium in which the particle will pass. It can be the atmosphere, a detector or any other material. User can use Detector Construction class to define and construct all these geometry related things.

• the materials involved, in which the user can define the material through which the particle pass through. It can be the air with its composition, or a detector with materials. The user can select the materials of the medium.

• the fundamental particles of interest, in which the user can select a primary particle which has to pass through the medium.

• the generation of primary events, in which the user can select the no. of primary events, their energy and flux.

• the tracking of particles through materials and electromagnetic fields, in which the user can track a particle up to certain energy and can define the electromagnetic field.

• the physics processes governing particle interactions, in which a user can select different hadronic interaction models and electromagnetic processes.

• the response of sensitive detector components, in which a user can select a particular portion of the detector as sensitive.

• the generation of event data, in which a user can select number events, the type of data to be generated etc.

• the storage of events and tracks, in which the user can select the tracks and data and store them in different formats.

• the visualization of the detector and particle trajectories, in which the user can generate the image of a detector, particles and their trajectories.

• the capture and analysis of simulation data at different levels of detail and refinement which can be done also in GEANT4.

The user may creates its own application based on the GEANT4 framework too. GEANT4 contains lots of different interaction models which can be used to handle the interactions of particles with matter across a wide range of energies. Because of the inclusion of data and expertise from various sources around the globe, GEANT4 can be considered as a scientific repository that incorporates most of the known particle interaction processes. Since it is written in C++ language and has advanced software engineering features, the user can build its own application by choosing different options and implementing it in user action class. Also new interaction models from outside can be added in GEANT4 by the user. Some of the hadronic interaction models, present in GEANT4 are discussed below.

All the hadronic interaction models used in GEANT4 can be classified into the following 3 categories.

3.2.3.1 Data driven models

When sufficient data like cross-section, angular distribution, multiplicity etc are available the data driven approach is the ultimate way to explain hadronic interactions. These models simply interpolate the available data in order to calculate interaction length and final state of a hadronic interaction. Usually linear interpolation of cross-section and Legendre's polynomials are used for these purposes in these models. Examples of interactions in which this data driven approach is used are coherent elastic scattering (pp, np, nn), radioactive decays and neutron decay (E $<$ 20 MeV). The classes G4LEpp and G4LEnp provide data-driven models for coherent elastic scattering over the range 10-1200 MeV. At high and inter mediate energy, an alternative model (The Glauber model [124]) is used for elastic and quasi-elastic hadron-nucleus scattering. Corrections for inelastic screening and the excitation of a discrete level or a state in the continuum for quasi-elastic scattering is considered at high energies. The Binary Cascade model is one such model which is described below.

The Binary Cascade model [123] : The Binary Cascade is a data driven intranuclear cascade model which explains the propagation of primary and secondary particles inside a nucleus. cross-section data are used to select collisions between primary and the nucleus and subsequent interactions. Equation of motions are solved numerically in order to explain the propagation of particles is the nuclear field. A threshold is set beyond which the cascade stops. It is designed for incident

energy between 100 MeV to 5 GeV. The modeling sequence is similar to the Bertni cascade model except that

• Nucleus is considered to be consists of nucleons.

• Hadron-nucleon reactions are handled by resonance formations which then decay according to their quantum numbers. Elastic scattering on nucleons are also taken into consideration.

• The secondary particles follow curved trajectories in nuclear potential.

• De-excitation is handled by Pre-compound model [123].

3.2.3.2 Parametrization driven models

The models of these category depends both on data and theory. Large amount of data is used to parametrized cross-sections, multiplicities and angular distributions of hadronic interactions. The final state of every hadronic interaction is determined by theory with data sampling in which conservation laws were used to get charge, energy etc. The interactions which are used by such approach is nuclear fission, nuclear capture etc. In GEANT4 mainly 2 sets of parametrized models are given in order to explain these hadronic interactions.

The low energy models [123] : These models work in the energy range of 1 GeV to 25 GeV.

The high energy models [123] : These models work in the energy range of 25 GeV to 10 TeV.

Both of these type of models are based on GHEISHA package of GEANT3 (a previous version of GEANT4). In these models, the final state of a collision of an incident particle with a nucleon inside the nucleus consists of a recoil nucleon, the scattered incident particle, and possibly many hadronic secondaries. Formation of real particles are approximated by the quark-parton interactions over some time. These newly formed hadrons are able to form intra nuclear cascades inside the nucleus because of their interactions with each other. That is why in these models only the parent hadron-nucleon collision is simulated in detail. The simulation of the intra nuclear cascade is done by by generating additional secondary hadrons from the initial collision. The distribution, multiplicity and their type is

determined by theory (functions) which were fitted to experimental data or which reproduce general trends in hadron-nucleus collisions. It is difficult to explain the physical significance of the parameters that are used through out these models to obtain reasonable physical behavior. Because of this the use of these models as generators of hadron-nucleus interaction is restricted. On the other hand these models are fast and precise with significant predictive power. Two such parametrization driven model are given below.

The LEP model [123] : This is a low energy parametrized model derived from GHEISHA . The model is designed to work up to incident energy below 20 GeV.

The HEP model [123] : This is a high energy parametrized model derived from GHEISHA . The model is designed to work up to incident energy above 25 GeV.

3.2.3.3 Theory driven models

These models are based on various theories (QCD, strings, chiral perturbation theory) in order to explain hadronic interactions of different energy ranges. Here experimental data are used for normalization of the result and validation of the model. In these models, the final state of a hadronic interaction is determined sampling of theoretical distributions. Based on energy range, these models can be classified into three categories :

The low energy models (< 5 GeV) [123] : intra-nuclear cascade models at medium to low energies.

The high energy models (> 5 GeV) [123] : diffractive string model, dual parton model, quark gluon string model, parton string models at medium to high energies.

The very low energy models (MeV range) : nuclear evaporation model [123], fission models [123] in MeV ranges.

Few such theory driven models used in GEANT4 are described below.

The CHIPS model [123] : It is a theory driven, quark level, non-perturbative and three-dimensional event generator for the fragmentation of hadronic system into hadrons which is based on the Chiral Invariant Phase Space model [123] that uses a 3D quark-level SU(3) approach. Here only light (u, d, s) quarks are considered which in turn can create other (c, b, t) quarks by the gluon-gluon or photo-gluon

fusion. The most important parameter of this model is the critical temperature T_c (≈200 M eV) which defines the number of 3D partons with a fixed energy W. Since the probability of finding a quark with energy E decreases exponentially with increase in temperature, heavier quarks are suppressed. So it can be said that the critical temperature in CHIPS model defines the mass of the hadron. Isgur quark-exchange diagrams are used to explain the hadron-hadron interactions where as the fusion of quark-antiquark or quark-diquark partons treat the decay of excited hadronic systems in vacuum. The CHIPS model may be considered as a generalization of the hadronic phase space distribution since it considers the homogeneous distribution of asymptotically free quark-partons over the invariant phase space, as applied to the fragmentation of various types of excited hadronic systems. It generates angular momentum distributions as well as multiplicity distributions for a given set of hadrons, defined by multi-step energy dissipation process like decay.

It handles a hadronic or nuclear interaction above few hundred MeV by considering the creation of an intermediate state of excited hadronic matter (quasmon) which dissipates energy by radiating particles in vacuum or by quark exchange with surrounding nucleons or clusters of nucleons in addition to the vacuum quark fusion mechanism inside a material. It can be applied to to nucleon excitations, hadronic systems produced in e^+e^- and $p\bar{p}$ annihilation, and high energy nuclear excitations. Exclusive modelling of hadron cascades in materials is possible by CHIPS model, since it validates photon and hadron projectiles for hadron and nuclear targets.

The PreCompound model [123] : The GEANT4 precompound model gives a possibility to extend the low energy range of the intra nuclear transport model for nucleon-nucleus inelastic collision and it provides a “smooth” transition from kinetic stage of reaction described by the hadron kinetic model to the equilibrium stage of reaction described by the equilibrium de-excitation models. The energy range of this 0 to 100 MeV.

The Bertini cascade model [123] : This model is a collection of theory driven models with parametrization feature. It includes the Bertini intra-nuclear cascade model which is a solution of Boltzmann equation on average with excitons, a pre-equilibrium model, a nucleus explosion model, a fission model, and an evaporation model. It is intended to treat nuclear reactions initiated by long-lived hadrons such as p, n,π,K, Λ, Σ, Ξ, Ω and γ with energies between 0 to 10 GeV. The target

nucleus is considered to be made up of six concentric shells of constant density in order to explain the continuously changing density distribution of nuclear matter within nuclei. The cascade starts when an incident particle interacts with a nucleon in the target nucleus followed by production of secondaries. The secondaries are also allowed to interact with other nucleons or get absorbed. When all the secondaries escape the nucleus, the cascade ends. Energy conservation is checked at that point. The calculations are done by relativistic kinematics throughout the cascade.

3.2.4 CORSIKA

CORSIKA (COsmic Ray Simulations for Kascade) [91, 92] is a 3-dimensional simulation program which is used widely to study the evolution and properties of air shower. It was developed to simulate interactions and decays of nuclei, hadrons, muons, electrons, and photons in the atmosphere up to energies of some 10^{20} eV. The out put contains informations such as type, energy, location, direction and arrival times of all secondary particles of an air shower at a selected observation level. CORSIKA is a complete set of standard FORTRAN routines that consists basically of 4 parts. The first part is a general program frame that handles the in and output, decay of unstable particles and particle tracking considering ionization energy loss, multiple scattering and the Earth's magnetic field. The second part treats high energy hadronic interactions where as the third part simulates low energy hadronic interactions. The fourth part simulates particle transport and interaction of electrons, positrons, and photons.

For later three parts., CORSIKA uses several interaction models, which may be activated optionally depending on the precision of the simulation. High energy hadronic interactions are handled by one of the following models : The Dual Parton Model DPMJET [129, 132], the HDPM [91], the quark-gluon-string model QGSJET [93–95], the mini-jet model SIBYLL [88–90], VENUS [106], the NEXUS model [127, 128] and the EPOS [107] model. The low energy hadronic interactions are simulated using models like GHEISHA [105], UrQMD [133, 134] and FLUKA [135, 136]. The electromagnetic showers are treated using EGS4 [104] code which tracks each particle and its reactions. Also the analytic NKG [137, 138] code is used in order to simulate electromagnetic simulations to obtain electron densities at selected observation level. Few of these models are described below.

3.2.4.1 The VENUS model

The VENUS (Very Energetic Nuclear Scattering) [106] model is based on the Gribov-Regge theory [139], in which single or multiple Pomeron exchange is considered as the basis of high energy hadron-hadron interaction. Particle production in inelastic collision is explained by cutting Pomerons (which are essentially cylinders of gluons and quark loops), that give rise to colored strings which in turn forms neutral hadrons after fragmentation. Also, formation of massive quark droplets in collisions of heavy nuclei at high densities are considered. Same formalism is used for the explanation of diffractive and non-diffractive collisions as well as mesonic projectiles. In all these case, the final state interactions are taken into account. Because of this the VENUS model can treat all types of hadronic interactions involved in an air shower cascade. Because of the absence of jets, this model is not recommended at energies above 20 PeV.

3.2.4.2 The DPMJET model

The DPMJET (Dual Parton Model with JETs) [129, 132] is based on Gribov-Regge theory [139] with interactions described by multiple pomeron exchange that contains and contains multiple soft chains as well as multiple mini-jets. Here a supercritical Pomeron is introduced to explain soft processes where as hard processes are explained by introducing hard Pomerons. Triple Pomerons and Pomeron loops are used in order to describe high mass diffractive events where as low mass diffractive events are simulated outside Gribov-Regge theory. Two strings are produced by cutting a Pomeron, which are again fragmented by the JET-SET routines [140] on the basis of the Lund algorithm [141, 142]. Glauber theory is used in order to calculate the number of nuclei involved in a collision as well as the number of interactions. Intranuclear cascade model [143] is used for the of treatment of the residual nuclei with the nuclear excitation energy, models nuclear evaporation, high energy fission and break-up of light nuclei, and emission of de-excitation photons for projectile and target nuclei being taken into consideration.

DPMJET ensures the decay of short living secondaries. Since CORSIKA can not treat charmed hadrons, the produced charmed hadrons are replaced by strange hadrons In DPMJET which are tracked and undergoes decay or interactions within CORSIKA.

3.2.4.3 The QGSJET model

In QGSJET (Quark Gluon String model with JETs) [93–95] hadronic interactions are described on the basis of exchanging supercritical Pomerons which are divided into two strings each according the Abramovski-Gribov-Kancheli rule. After that fragmentation of these strings are done with an algorithm like Lund algorithm but with deviating treatment of the momenta at the string ends. Also mini-jets are included in QGSJET in order to describe the hard interactions at the highest energies. Glauber calculations are used to determine participants in a nucleus-nucleus collisions by assuming a Gaussian distribution of the nuclear density for light nuclei with $A \leq 10$ and a Woods-Saxon distribution for the heavier nuclei. The peripheral collisions are considered to be spallation like reaction where as central collisions are considered to be more or less like fragmentation. After that various fragmentation options available in CORSIKA can be applied.

3.2.4.4 The SIBYLL model

Contrary to the VENUS model, SIBYLL [88–90] is a mini-jet model designed to handle hadronic interactions in EAS Monte Carlo programs. Here it is considered that triplets and anti-triplets of colour are formed from the fragmentation of of both projectile and target hadrons in a hadronic soft collision. After that combination of the opposite colour of the two hadrons leads to the formation of two colour strings , the fragmentation of which leads to particle production. This fragmentation of the two colour strings is done by modified Lund algorithm [141, 142]. Hard collisions are explained with minijet production having high transverse momenta. The number of mini-jets are increased with energy which explains the increase in inelastic scattering cross-section with energy where as the contribution of the soft component is assumed to be energy independent. This model explains diffractive events independently of soft or hard collisions. The hadron-nucleus collisions are explained by the formation and fragmentation of string pairs of opposite colour while nucleus-nucleus collisions are treated with Glauber theory [144, 145] and thermal model [88]. In SIBYLL , the shot lived seconadry particles are decayed into known particles that are known to CORSIKA . If the secondary particles are nucleons and anti-nucleons, charged pions, and all four species of kaons, they are be treated as projectiles by SIBYLL and further collisions are considered. Decay of strange baryons after tracking and substitution of photon with a charged

pion in photo-nuclear reactions are two other important aspects of SIBYLL. The SIBYLL model contains its own nucleus-nucleus cross-section table including an interpolation routine.

3.2.4.5 The HDPM model

The HDPM [91] is a phenomenological generators which describes the hadronic interactions between hadrons and nuclei at high energies. It is inspired by the Dual Parton Model which is based on the assumption that in an hadronic interaction, interacting quarks of two hadrons form two dominant colour strings which after separation and fragmentation produce jets of many colour neutral secondaries around the primary quark directions. These jets are observed in many high energy physics experiments. Since the particles emitted in extreme forward directions are important in understanding the EAS, this model is built to reproduce collider data by correlating many quantities, such as the number and type of secondaries, the longitudinal and transverse momentum distributions and the spatial energy flow with the available energy. This model is valid up to 100 PeV.

3.2.4.6 The NEXUS model

While non of the above mentioned models violates important theoretical principles, NEXUS [127, 128] model is the first model in which the theoretically predicted energy-momentum sharing between the hadron constituents is consistently implemented in construction of scattering amplitudes. Being based on Gribov-Regge theory with soft, semi-hard and hard pomerons, this model for the first time employs the multiple scattering approach through a "three object picture"- a parton-ladder between a interacting parton and a diquark, one of which is from the projectile and the other is from the target, along with two excited colorless remnants formed by the spectator parton and diquark of the projectile and the target nucleons. The parton-ladder describes successive parton emission through the soft and the hard interactions with the soft interaction being described by the traditional soft pomeron exchange; where as, the hard interaction is realized through perturbative QCD within the concept of the semi-hard pomeron. According to the number of quarks and anti-quarks, to the phase space and to an excitation probability, a remnant may decay into mesons, baryons and anti-baryons [146]. The remnant produce particles mostly at large rapidities whereas the parton-ladders

emit particles at central rapidities. Such "three object picture" of the parton-ladder and the two remnants solve the multi strange problem of conventional high energy problems [147].

To implement energy conserving multiple scattering, this model consider both the open parton-ladders as well as closed parton-ladders, the latter being an important player in the calculation of partial cross-sections through interfering contributions. The NEXUS model uses relativistic string approach to obtain observable hadrons from partons *via.* two steps, namely, the formation of strings from the partons and then the string fragmentation into hadrons.

3.2.4.7 The EPOS model

The EPOS [148, 149] model, being the successor to NEXUS, is also based on parton based Gribov-Regge theory with special emphasis given on high parton densities for proton-nucleus or nucleus-nucleus collisions which are taken care of by the fragmentation of Pomerons in Pomeron-Pomeron interactions. This new multiple scattering approach, EPOS, stands for [148]

• Energy conserving quantum mechanical multiple scattering approach, on the basis of

• Partons (Pomerons)

• Off-shell remnants

• Splitting of Pomerons.

The outline of this model is given below :

1. In parton models it is considered that in case of a proton-proton collision, two partons, one from the projectile and one from the target interacts with each other leaving behind colored remnants (the diquarks) at the string ends. Just like NEXUS, in EPOS model, it is considered that in the case of a hadronic interaction, two fold objects like quark-diquark or quark-antiquark take part directly leaving behind colorless excited (off-shell) remnants. So finally three colorless objects will remain, the two off-shell remnants and one parton-ladder (also called as Pomerons : the whole structure of the dynamical process of successive emission of partons in case of hadronic interactions).

2. Just like NEXUS, the energy independent contribution from the remnants is responsible for the production of particles at large rapidities where as the parton-ladders mainly contribute at central rapidities which grows with energy. An energy conserving multiple scattering treatment [127] is applied to this scenario considering both open parton-ladders (representing inelastic scattering) as well as closed parton-ladders (representing elastic scattering) in order to calculate the partial cross-sections.

3. Finally the relativistic string approach is employed in order to explain the formation of colorless "strings" and its fragmentation into hadrons.

The EPOS model has adopted some additional aspects such as the nuclear effects related to Cronin transverse momentum broadening, parton saturation and screening. The particle production scenario is also expected to be very different depending on whether the interaction is with a peripheral nucleon or with a nucleon from the high density central part. This aspect has been accomplished in EPOS by allowing splitting (as well as merging) of parton-ladders based on an effective treatment of lowest order Pomeron-Pomeron interaction graphs with the corresponding parameters being adjusted from the comparision with accelerator data. In the case of meson projectile, the EPOS model leads to an increase of baryon and anti baryon production in the forward direction in agreement with the low energy pion-nucleus data [150].

3.2.4.8 The GHEISHA model

The GHEISHA [105] model is a data driven model, that treats hadronic interactions up to 80 GeV. This can handle all the baryonic projectiles with strangeness ± 1, ± 2, and ± 3 except nuclear evaporation products like deuteron, tritium and alpha particles. This package contains cross-sections for elastic and inelastic interactions obtained from interpolation and extrapolation of. tabulated experimental data. Nuclear fission routines are removed too. The interaction cross-section of projectiles with air (which contains elements like N, O, Ar) is derived from interpolation of cross-section data because of which some accuracy is lost. That is why validity of this model must be checked before simulation.

3.2.4.9 The FLUKA model

The interaction model FLUKA [135, 136] employs resonance superposition from threshold to about 5 GeV but incorporates the two string interaction model(DPM) at higher energies. In this model, the resonance energies, widths, cross-sections and the branching ratios are extracted from data and from the conservation laws by making explicit use of the spin and isospin relations. For high energy hadron-nucleus interactions, the model exploits the Glauber-Gribov cascade [151, 152]; whereas, it uses the pre-equilibrium-cascade model PEANUT [153, 154] below about 5 GeV. The nucleus-nucleus interactions above a few GeV/n are treated in FLUKA (version 2008.3b) by interfacing with the DPMJET-III [132] model. It may be added here that FLUKA describes the fixed target data reasonably well.

3.2.4.10 The UrQMD model

The UrQMD (Ultra-relativistic Quantum Molecular Dynamics) [133, 134] model was originally designed for simulating the relativistic heavy ion collisions in the *cms* (center of mass) energy range from around 1 AGeV to a few hundred AGeV for the RHIC experiment. This particular model inherits the basic treatment of the baryonic equation of motion in quantum molecular dynamic approach and describes the phenomenology of hadronic interactions at low to intermediate energies in terms of the interactions between known hadrons and their resonances. The model does not use an intrinsic cross-section calculation. Instead, the projectile is allowed to hit a sufficiently large disk involving maximum collision parameters as a result of which the program consumes rather a long CPU time. Like FLUKA, UrQMD also explains the fixed-target data reasonably well.

3.3 Comparison between predictions of high energy hadronic interaction models of CORSIKA with LHC data

The cross-section is a very important observable which is strongly correlated with shower depth of individual EAS. In all hadronic interaction models p-p scattering cross-section is used as the basis for understanding hadronic interactions. All

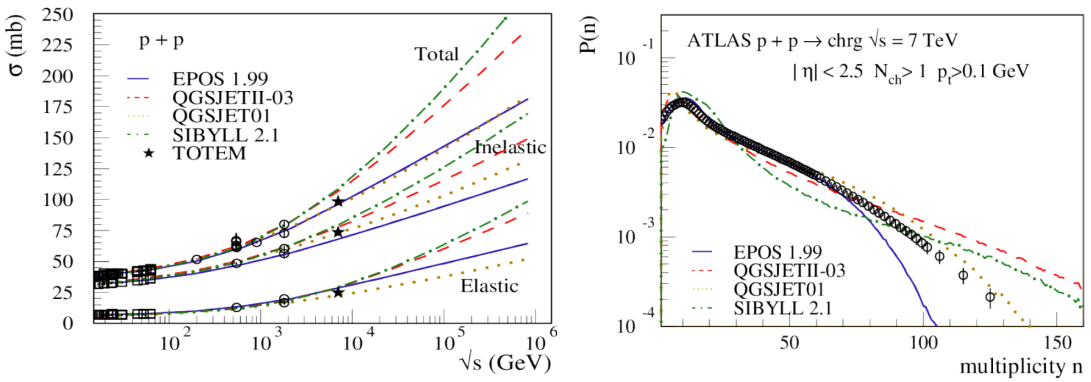

FIGURE 3.1: Comparison of model predicted cross-section (σ) and multiplicity (n) with LHC Data (figure taken from [160, 161]).

the models agrees well with experimental cross-section data at lower energies and start diverging at around 2 TeV cms energy. The TOTEM experiment [158] at 7 TeV cms reduces the differences between the models by 10-50 mb. Comparison [160, 161] of cross-sections predicted by the models with ALICE [155, 156], ATLAS [157] and TOTEM [158] data shows that QGSJET 01c agrees better with the data than EPOS 1.99, QGSJET-II-03 and SIBYLL 2.1 for inelastic and elastic scattering cross-section. Both EPOS 1.99 and QGSJET 01c are in good agreement with data for total scattering cross-section.

Just like the cross-section, the multiplicity is also an important observable in EAS which has a logarithmic dependence on particle production. Comparison of model predictions with ATLAS data [160, 161] for multiplicity distribution of charged particles at 7 TeV cms shows that EPOS 1.99 starts deviating sharply after multiplicity but it agrees well at lower multiplicities. SIBYLL 2.1 does not agree well with the entire data set whereas QGSJET-II-03 has better agreement at multiplicities below 80 than SIBYLL 2.1. The prediction by QGSJET 01c agrees better with the entire data set than prdeictions of other models, though it shows slight deviation above multiplicity 60.

The transverse momentum plays an important role in the development of the EAS. It is associated with the spread of hadronic and muonic showers in an EAS. Comparision of model predictions with CMS data [162] for transverse momentum (p_T) distribution of charged particles at 7 TeV shows a significant deviation of EPOS 1.99 predictions with the data after 5 GeV/c whereas predictions by QGSJET 01c and QGSJET-II matches well with the entire data set. Significant deviation can

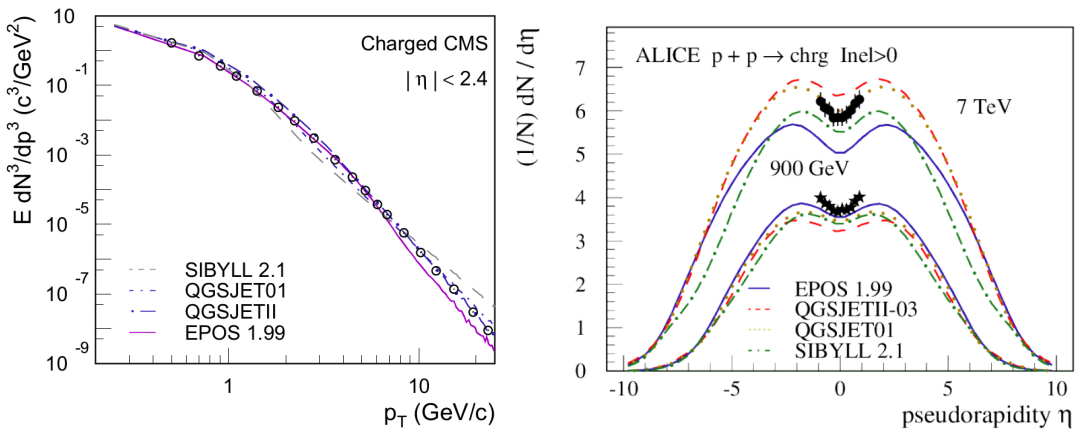

FIGURE 3.2: Comparison of model predicted transverse momentum (p_T) and pseudorapidity (η) with LHC Data (figure taken from [159–161]).

also be seen in the predicted values of p_T by SIBYLL 2.1 with the data set above 1 GeV/c.

The EAS observable pseudorapidity is strongly related with the longitudinal momentum distribution of secondary particles. Comparison of model predictions with ALICE data [163] for pseudorapidity distribution of charged particles at 7 TeV cms shows a complete mismatch of EPOS 1.99 predictions with the entire data set. Predictions by SIBYLL 2.1 as well as QGSJET-II-03 does not agree well with the entire data set whereas QGSJET 01c has a very close agreement with the data.

3.4 Comparison between predictions of high energy hadronic interaction models of CORSIKA with GEANT4

Accurate reproduction of EAS is an essential part of the air shower experiments. Most of the experiments have relied simulations from CORSIKA which is an EAS simulation program with low and high energy interaction models. Because of the limited understanding of hadronic interactions at high energy, uncertainty in muon number is expected from the model predictions. In fact, most of the CORSIKA interaction models predict lower muon number than expected. It also can not simulate low energy particles. On the other hand, GEANT4 is a detector simulation program having different high and low energy interaction models. Recently

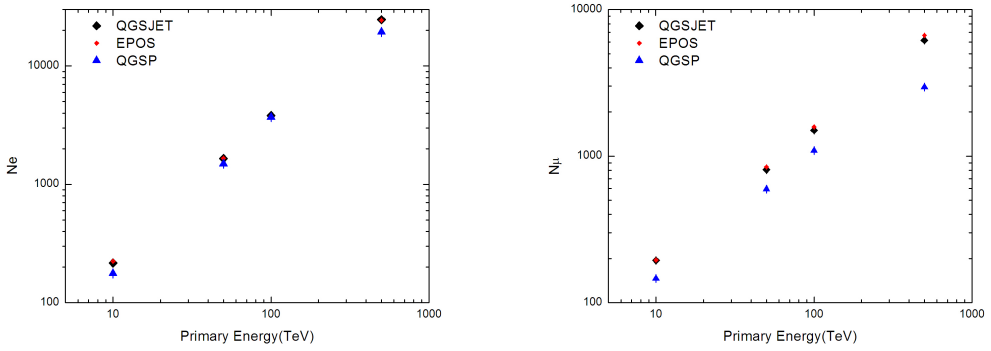

FIGURE 3.3: Shower size (N_e) and muon size (N_μ) predicted by models of CORSIKA and GEANT4.

GEANT4 has also been used for simulation of air shower. So comparison of interaction models of GEANT4 and CORSIKA may throw some light towards the shortcomings of hadronic interaction models and hence can give some idea about this uncertainty of muon numbers.

In GEANT4, the atmosphere was realized by constructing a volume of 1000 km length, 1000 km width and 100 km altitude. The altitude was divided into 1000 layers, each with thickness 0.1 km. Each layer was made up of air with density and composition varying with altitude as per US Standard atmospheric model. Observation level is set at 4300 m which was the altitude of EAS-TOP experiment and magnetic field was set accordingly. QGS model was selected to simulate high energy hadronic interactions < 500 GeV where as BiC model was used to handle low energy hadronic interactions. Electromagnetic interactions were simulated by STANDARD electromagnetic model of GEANT4 and cut off energy was set to 300 MeV.

In CORSIKA, observation level, magnetic field and cut off energy were set to the same values as GEANT4. Also QGSJET 1c and EPOS model were choosen to simulate high energy hadronic interactions, where as low energy interactions were handled by GHEISHA. EGS4 routine was used to simulate the electromagnetic interaction.

Both in GEANT4 and CORSIKA, proton is chosen as primary particle at energies 10 TeV, 50 TeV, 100 TeV and 1000 TeV. In case of GEANT4, 1000 showers were considered at each energy where as in CORSIKA, 50000 showers were considered at

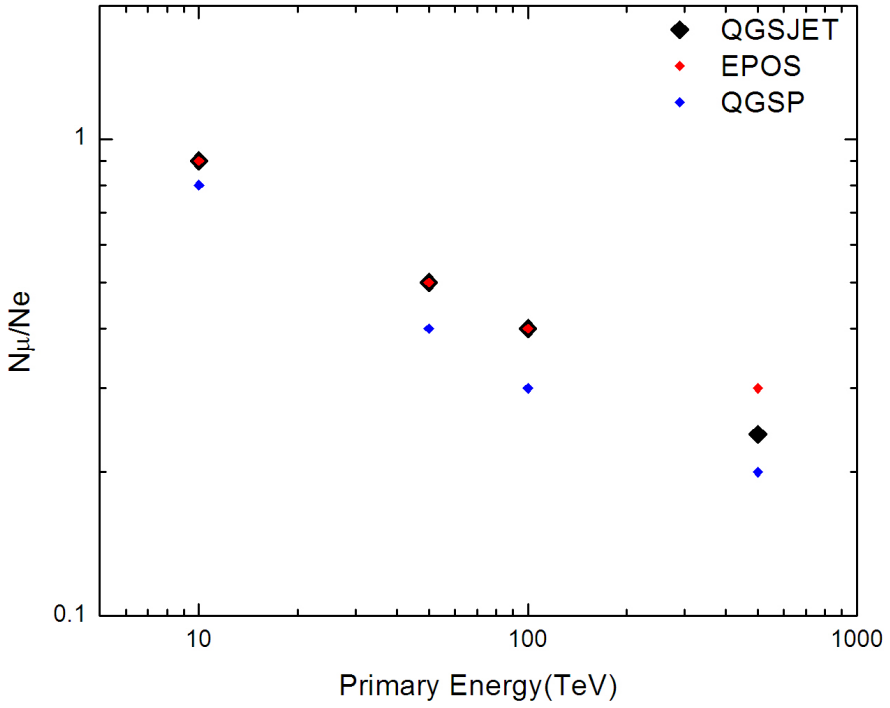

FIGURE 3.4: Ratio of shower size (N_e) and muon size (N_μ) predicted by models of CORSIKA and GEANT4.

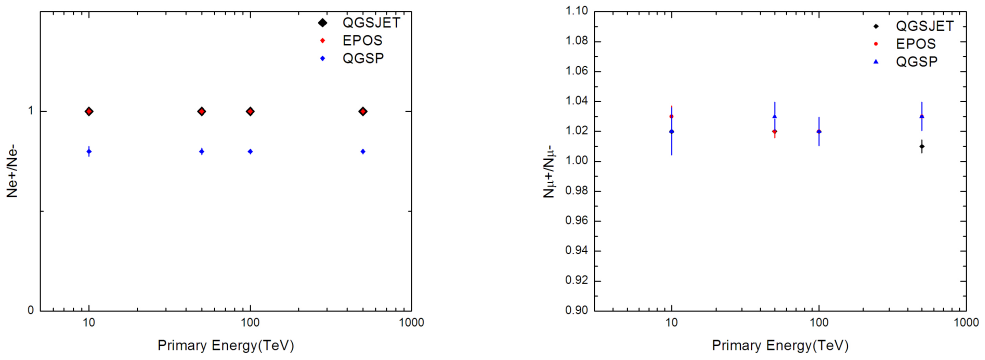

FIGURE 3.5: Comparison between shower size (N_e) and muon size (N_μ) predicted by models of CORSIKA and GEANT4.

each energies. Average number of electrons and muons, produced at each primary energy were studied.

The results were discussed below:

It can be seen from figure 3.3 that GEANT4 produces less number of electrons and muons compared to those in CORSIKA even for the same hadronic interaction(QGS) model.

The GEANT4 gives persistently smaller muon size to electron size ratio than that given by CORSIKA. The positron to electron ratio is substantial lower in GEANT4 than in CORSIKA. The reasons for such discrepancies are not clear at all.

Chapter 4

Influence of microscopic particle interaction models on the flux of atmospheric protons & antiprotons

4.1 Introduction

A proton flux deep in the atmosphere results from the production of protons in the interactions of primary/secondary cosmic rays with air nuclei as well as the absorption of such protons during their propagation through the Earth's atmosphere. Secondary proton spectrum at very high altitude is likely to contain cleaner information on proton production alone. As the major fraction of such secondary protons arises from hadronic interactions in the forward kinematic region, a study of such proton spectra at very high altitude is likely to provide us with an opportunity to investigate particle production in the forward region.

Antiprotons ($\bar{p}$) in cosmic rays, on the other hand, are supposed to provide information on the sources of cosmic rays and their propagation in the galaxy as well as the matter-antimatter asymmetry of the local universe [164]. They are also believed to play crucial role in indirect dark matter search [165–167]. Primary $\bar{p}$ may as well be produced from the evaporation of primordial black holes (PBH)

[168, 169]. Observations of $\bar{p}$ spectrum with appropriate features may, therefore, be considered for probing into the possible signatures of the PBH.

Recently, the PAMELA instruments attached to the Russian Resurs-DK1 satellite have made a precise measurement of $\bar{p}$ spectrum in the energy range from 60 MeV to 180 GeV [170, 171]. Comparison with several theoretical estimates [195, 214, 217] seems to support the view that the PAMELA $\bar{p}$ spectrum is consistent with a scenario of pure secondary production of $\bar{p}$ *via.* cosmic ray interactions in the interstellar medium (ISM) [170, 171].

An accurate estimation of the secondary proton/antiproton flux is, however, a difficult task. This is because of the fact that such an estimate requires precise knowledge of three factors, namely, the detailed features of cosmic ray propagation in the Galaxy, the characteristics of high energy particle interactions and the effect of solar modulation on the cosmic rays. While there have been a reasonable understanding of the solar modulation effect, major uncertainties in the predicted flux still arise from our incomplete knowledge of cosmic ray propagation and the high energy particle interactions.

Over the past few years, the BESS experiments have reported the results of the precise measurements of atmospheric $\bar{p}$ spectra in an energy range $0.2-3.4$ GeV at three observation levels, namely, the balloon altitude, mountain altitude and the sea level [51, 224]. It is interesting to note that the cosmic rays traverse a depth $(5-6$ g cm$^{-2})$ of matter in the Galaxy that is close to the average atmospheric depth (10.7 g cm^{-2}) of the BESS-2001 balloon observation at the location of Ft. Sumner, USA [224]. As the $\bar{p}$ production mechanism in the atmosphere is likely to be similar to that in the Galaxy, a study of such atmospheric $\bar{p}$ at balloon altitude would possibly provide us with an opportunity to quantify the uncertainty in the theoretical estimate of interstellar $\bar{p}$ flux that may be caused by our limited knowledge of high energy particle interactions.

A good knowledge of particle interactions in the energy range from sub-GeV to about 100 GeV is required to understand the production and transport of the BESS-detected atmospheric $\bar{p}$s with their energies in the range between 0.2 GeV to a few GeV. Due to the steeply falling energy spectra of the primary cosmic rays, the contribution of primary particles with energies above 80 GeV/n to such BESS-observed atmospheric $\bar{p}$ spectrum has been recently found to be insignificant [189]. GHEISHA (version 2002d) [105], UrQMD (version 1.3) [133, 134] and

FLUKA (version 2008.3b) [135, 136] are among the most popular models for describing particle interactions in the relevant energy range. Such models are useful for the study of the development of cosmic ray cascades in the atmosphere. Among the three models mentioned above, GHEISHA is based on the parametrization of accelerator data, while UrQMD and FLUKA describe particle interactions microscopically.

In this present work, the dependence of atmospheric proton flux at balloon altitude on various hadronic interaction models is examined apart from the study of such a dependence on the atmospheric $\bar{p}$ spectrum through the three dimensional Monte Carlo (MC) simulation methods. For such a purpose, first the atmospheric $\bar{p}$ spectra at multiple observation levels are simulated by using FLUKA and UrQMD models and then compare such simulated spectra with the BESS observations. The interaction model GHEISHA is not considered here (except in Figure 4.2(b) (right)) as the model is known to have shortcoming in describing fixed target accelerator data as well as the atmospheric cosmic ray data [189, 196, 203]. The present study is also prompted by the recently reported fact [189] that the BESS-measured atmospheric $\bar{p}$ flux at mountain altitude [51] is substantially less than the simulated flux obtained from FLUKA, while the flux obtained from UrQMD is consistent with experimental measurements. It is important to know whether such a discrepancy between the simulated and the experimental fluxes persists even at a very high (balloon) altitude or at the sea level. Such a study may have important bearing on our understanding of the reasons behind the disagreement between the FLUKA-derived results and the BESS measurements.

It can be noted that several MC simulations [187, 198, 205, 219, 220], relying mostly on phenomenological description of high energy particle interactions, have been carried out in the past to study the atmospheric $\bar{p}$ spectra. Such an approach does not usually satisfy many of the conservation laws in a single hadronic interaction and also suffers from various other inconsistencies (see, for instance, [190]). Besides, an understanding of the atmospheric $\bar{p}$ production also requires a good estimation of cosmic ray secondaries (mostly protons) in the atmosphere that was not considered in many of such earlier studies. In the present study, the residual effect of the galactic $\bar{p}$ flux at the observation level is further taken into consideration that was mostly ignored in the calculations mentioned above.

The BESS-measured $\bar{p}$ spectra are limited to 3.4 GeV that corresponds to the mean

vertical geomagnetic rigidity cutoff at the location of Ft. Sumner, USA. A simulation study of atmospheric $\bar{p}$ at very high altitude, that corresponds with the BESS observations at Ft. Sumner, is therefore relevant only for the low energy end of the galactic $\bar{p}$ spectrum measured by the PAMELA experiment [170, 171]. To simulate the atmospheric $\bar{p}$ flux up to about 100 GeV, a good understanding of particle interactions up to at least a few hundred GeV is necessary. Due to the paucity of experimental data [197] on the inclusive $\bar{p}$ production and annihilation cross-sections over the whole kinematic region in hadron-hadron, hadron-nucleus and nucleus-nucleus collisions in the stated energy range, one has to strongly rely on various theoretical models of particle interactions. In the absence of experimental data, It is here compare the predictions of the well known high energy interaction models QGSJET (version 01c) [94], VENUS (version 4.12) [106], NEXUS (version 3.97) [127, 128] and EPOS (version 1.6) [107], each in combination with FLUKA (version 2008.3b) for the description of hadronic interactions below 80 GeV/n, to get some idea about the theoretical uncertainties in the predicted $\bar{p}$ flux at energies beyond the upper cutoff for the BESS-2001 balloon experiment, i.e., over an energy range of about $3 - 100$ GeV.

Apart from the ambiguity in high energy particle interactions, a dominant systematic error in evaluating the flux of cosmic ray secondaries arises from the uncertainties involved in the estimation of input fluxes of primary cosmic rays. To minimize such uncertainties, spectra of different primary particles measured by the BESS-98 experiment [50] are used as the inputs in our simulations such that the systematic errors in the calculation of atmospheric fluxes are nearly eliminated as the BESS experimental fluxes of atmospheric protons/antiprotons at different altitudes are compared with.

The plan of this work is outlined as in the following. In the next section, the production mechanisms of $\bar{p}$ in high energy collisions and the ways in which different models implement such mechanisms are described briefly. In Sec. 4.3, a brief description of the adapted simulation technique is given. In Sec. 4.4, the results of our MC simulations are presented. Summary and discussion are presented in Sec. 4.5.

4.2 Production and transport of antiprotons in the atmosphere

4.2.1 General aspects

Antiproton flux in the atmosphere relies mainly on two factors, namely, the inclusive $\bar{p}$ production cross-section in cosmic ray-air nuclei collisions and the propagation of $\bar{p}$ in the atmosphere. The latter factor also includes ionization energy loss, loss of $\bar{p}$ due to annihilation and other interactions.

Antiprotons are produced in the atmosphere in high energy interactions of primary and secondary cosmic ray hadrons/nuclei with air nuclei. A typical example could be the interaction $p + N \rightarrow \bar{p} + p + p + N$ with N representing a nucleon. The threshold proton energy for such interaction is about 6.6 GeV in the rest frame of the target nucleon. In addition to the above interactions, meson-nucleon interactions may also lead to the excitation of color flux tubes and their subsequent decay into baryon-antibaryon pairs.

The final state in high energy hadron-nucleon collisions often consists of many particles. Basic reaction for the production of $\bar{p}$ is, therefore, the inclusive $N + N \rightarrow \bar{p}$ + anything process and the inclusive $\bar{p}$ production cross-section is one of the main ingredients for the calculation of atmospheric $\bar{p}$ flux. Such $\bar{p}$ production is likely to take place in the central kinematic region rather than the fragmentation region. Antibaryon absorption can also be important in the case of massive nuclear collisions. The $\bar{p}$ mean multiplicity is the other main input for the $\bar{p}$ production spectrum. For propagation of $\bar{p}$ through the atmosphere, the annihilation cross-section of $\bar{p}$ due to its collisions on light nuclei (N and O) are of primary importance.

In the instant case, several $\bar{p}$ production cross-section data on the collisions of proton with various fixed target nuclei in the (laboratory) energy range of a few GeV to about 400 GeV are available. A complete data set is, however, available for p, π, and K projectiles at 100 GeV (lab) energy on p, C, Cu, Sn and Pb targets where the momenta of the secondary antiprotons are measured [150]. Apart from such data, some measurements on the $\bar{p}p$ and $\bar{p}C$ collisions in the sub-GeV to hundreds of GeV energy range are also available [172, 193, 206, 221, 275]. A semi-phenomenological fit to such data can, therefore, be employed for the calculation

of atmospheric $\bar{p}$ flux with some level of accuracy and this has been a popular approach [186, 191, 218–220] for more than twenty five years.

A precise estimation of the atmospheric $\bar{p}$ flux additionally requires reliable estimates for the secondary cosmic ray flux that may, in turn, produce further $\bar{p}$ by colliding with air nuclei. Tertiary $\bar{p}$s (arising from inelastically scattered secondaries) also contribute at low energies. One needs to further consider the residual galactic component of $\bar{p}$ in the case of very high (balloon) altitude.

4.2.2 Brief outline of various particle interaction models

In the string-based models, the high energy nucleonic interactions lead to the excitation of color flux tubes. Antiprotons are produced *via.* the decay of such color flux tubes and also in antiresonance decays; whereas, the $\bar{p}$ annihilation is modelled *via.* the annihilation of quark-antiquark pairs and the formation and subsequent decay of two color flux tubes with baryon number zero. The annihilation of baryon-antibaryon pairs proceeds in UrQMD according to rearrangement diagrams. Here, the formation of two $\bar{q}q$-strings of equal energies in the c.m. system is assumed, while the remaining constituent quarks are rearranged into newly produced hadrons.

At higher energies, the interactions of nucleons and nuclei are calculated on the basis of the Gribov-Regge theory [139] that describes the observed rise of cross-sections at high energies as a consequence of the exchange of multiple supercritical Pomerons [185]. All observed scattering processes are successfully described with the Reggeon-Pomeron scattering scheme [185]. Presently, the Gribov-Regge theory-based interaction models used for cosmic rays include the QGSJET 01c [94], VENUS 4.12 [106], DPMJET-III [132], NEXUS 3.97 [127, 128] and the EPOS 1.6 [107] models. Such different models in this class differ from each other in the details concerning the precise formulation of string formation and decay, treatment of the remnants etc. Apart from these a mini-jet model SIBYLL [88–90] is also available in CORSIKA. Some of these models are described briefly in *Chapter 3.*

4.3 Implementation of the simulations

In the present work, atmospheric cosmic ray proton and antiproton spectra are generated by employing the interaction models FLUKA 2008.3b and UrQMD 1.3 in the framework of the cosmic ray EAS simulation code CORSIKA (version 6.735) [202]. Following the default settings of the CORSIKA code, FLUKA and UrQMD have been used up to 80 GeV/n, while the model QGSJET 01c has been used above such energy threshold. As mentioned in Sec. 4.1, also use the high energy interaction models VENUS 4.12, NEXUS 3.97 and EPOS 1.6 is used, each in combination with the FLUKA model, to compare various theoretical estimates of the atmospheric $\bar{p}$ flux at energies beyond the BESS upper cutoff up to about 100 GeV. Other considerations/settings used in this work are briefly described in the following.

4.3.1 The primary spectra

Uncertainties in the determination of primary cosmic ray flux have been substantially reduced in recent years due to the precise measurements of such flux by the BESS-98 [50], BESS-TeV [201] and the AMS [179, 180] experiments. The observed total primary nucleon flux below 100 GeV/n is found to agree within an accuracy of 4.0% in the above three experiments [52, 199]. For such a reason, and considering the fact that our results would be compared with the BESS observations, the BESS-98 spectra is chosen as the input primary spectra in our simulations while extending the maximum (kinetic + rest-mass) energy of the primary particles up to 1 PeV/n. For reproducing the BESS-observed primary spectra in CORSIKA, the effect of solar modulation on the spectra has been handled by using the *force field approximation* [200, 210] in which the primary particle flux is expressed in terms of a time dependent *solar modulation potential* $\phi(t)$ that takes on different values for different epochs of solar activity [222]. For the BESS balloon-borne measurements of the atmospheric proton and antiproton fluxes in September 2001 at Ft. Sumner, USA [174, 175, 224], the primary cosmic ray spectra are generated by taking a solar modulation potential $\phi = 891$ MV [222] into account. Again, for the BESS sea-level measurements of the antiproton fluxes [224] at Tsukuba, Japan during 6th-11th May and 7th-13th December 1997, $\phi = 410$ MV [222] is considered as the mean value of the solar modulation potential.

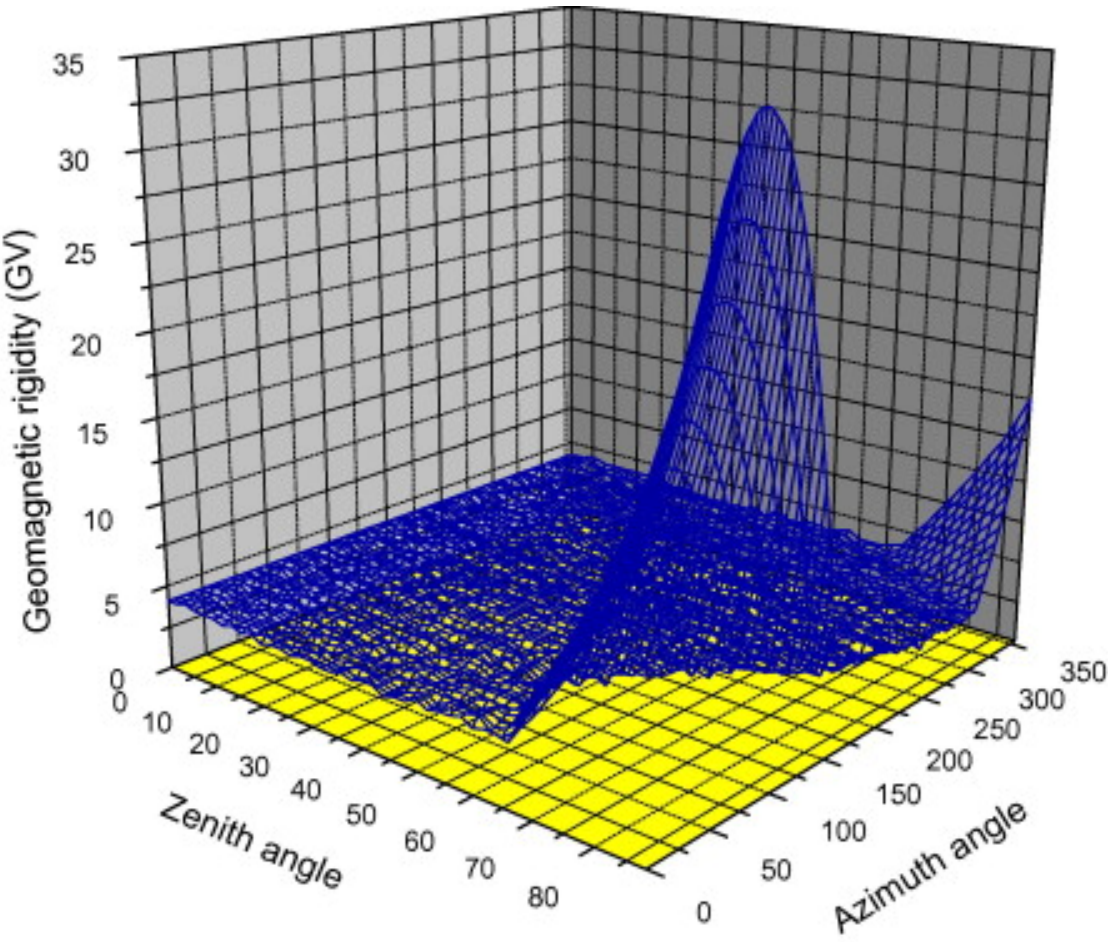

FIGURE 4.1: Directional dependence of the mean geomagnetic rigidity cutoff for primary cosmic rays at the location of Ft. Sumner, USA.

4.3.2 The geomagnetic rigidity cutoff

The geomagnetic rigidity cutoff calculations have been performed by using the (back) trajectory-tracing technique [216]. The quiescent International Geomagnetic Reference Field (IGRF) model of 1995 [215] for the Earth's magnetic field has been used for such calculations. Both the umbra and the penumbra regions in the rigidity range of a primary particle in any particular direction have been taken into consideration [189] in our treatment of the rigidity cutoff. In Figure 4.1, the values of the mean geomagnetic rigidity cutoff are displayed for the primary cosmic ray particles entering the atmosphere at the location of Ft. Sumner from various directions as an example of our rigidity calculations. Such cutoff calculations are used in the simulations to modify the primary cosmic ray spectra obtained from CORSIKA, although the calculation of the re-entrant albedo cosmic ray flux is not incorporated in the present simulations; see Section 4.5 below.

4.3.3 Other settings

The fluxes of cosmic ray particles also depend on the atmospheric density profile. Such a density profile, in turn, has latitudinal and seasonal variations. The effect of such variations on the atmospheric cosmic ray spectra is, however, expected to be small, particularly in the case of very high altitude observations. Therefore, the US-standard atmospheric model [209] with a planar approximationis considered in the present work.

Proton, helium and the heavier nuclei up to iron are considered here as the primary cosmic ray particles. Instead of taking each of the elements individually, the primary nuclei heavier than helium are taken in three separate groups, namely, medium ($5 < Z < 10, < A > \approx 14$), heavy ($11 < Z < 20, < A > \approx 24$) and very heavy ($21 < Z < 30, < A > \approx 56$) nuclei respectively [189]. The spectra for such groups are taken from the compilation of Reference [223]. The sum of the fluxes of individual elements in a group is taken as the flux of that particular group and the weighted average value of the power indices of such individual elements is taken as the power index of the group [189].

Particular care should, however, be taken for the simulation of atmospheric antiproton flux at a very high altitude. Such atmospheric antiprotons may, in fact, have significant contribution from the residual galactic $\bar{p}$s arriving at the observation level. In this work, a secondary $\bar{p}$ spectrum is generated by combining the simulation-generated (and normalized to the BESS-98 spectrum) primary proton spectrum with the recent measurement of antiproton to proton flux ratio obtained in the PAMELA experiment [170]. The resultant secondary $\bar{p}$ spectrum, adjusted for the location of Ft. Sumner and for a solar modulation potential appropriate for the BESS-2001 experiment, is considered along with the usual primary cosmic ray particles as the inputs in the simulations. However, the integrated secondary $\bar{p}$ flux is found to be only about $1.4 - 1.5\ 10^{-4}$ times the integrated primary proton flux in our simulations. It has been checked that such interstellar $\bar{p}$ flux, in fact, have negligible effects on the generated atmospheric antiprotons within the energy range considered by the BESS experiments and even beyond.

Note that the fluxes of atmospheric shower particles obtained by using CORSIKA have statistical as well as systematic errors. In the present work, nearly $4 - 20 \times 10^7$ events have been generated in each of our simulations for the estimation of the

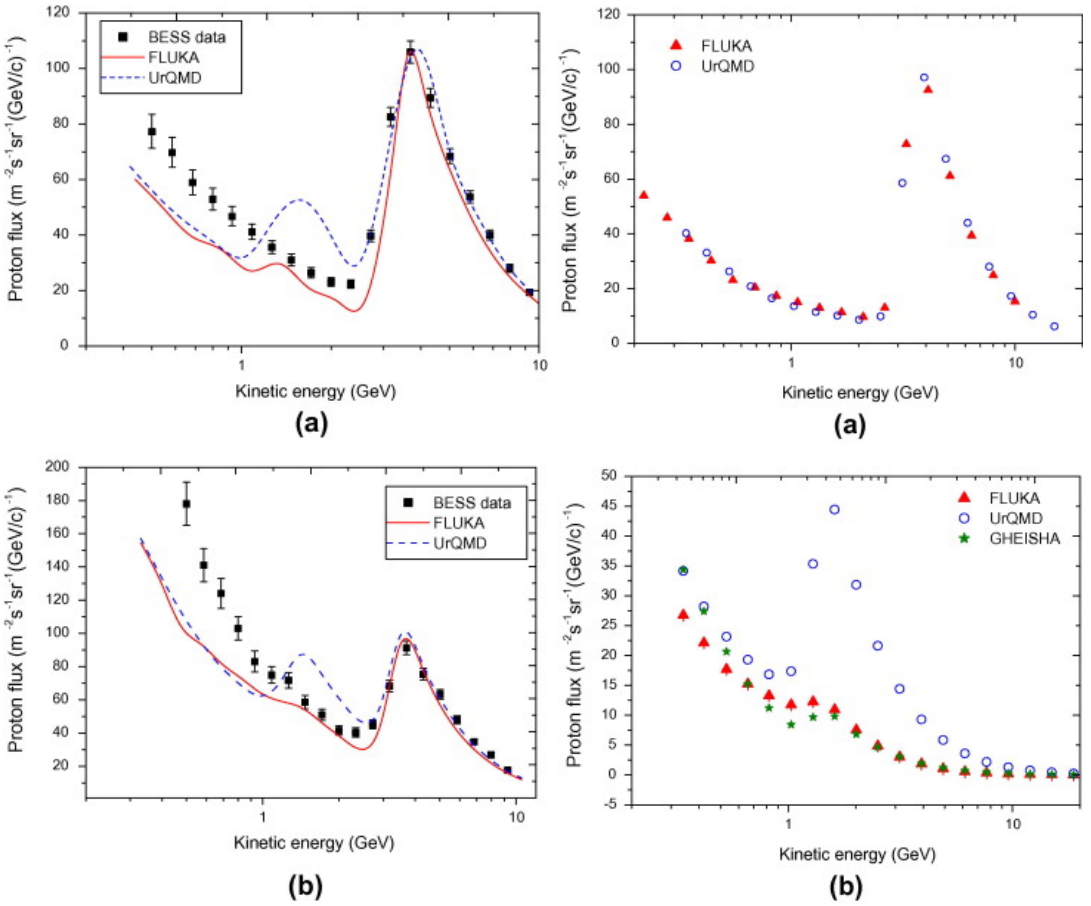

FIGURE 4.2: Left: Differential spectra of vertical atmospheric proton flux at the location of Ft. Sumner, USA that are obtained by using two hadronic interaction models at the atmospheric depths (a) 10.5 g cm^{-2} and (b) 26.4 g cm^{-2}. The results of the BESS-2001 observations at such depths [174, 175] are also given for comparison. Right: Contributions from (a) primary protons and (b) primary α particles to the simulated vertical secondary proton flux at an atmospheric depth 10.5 g cm^{-2} at the location of Ft. Sumner. The proton fluxes are generated by using various hadronic interaction models as indicated in the diagram.

fluxes of atmospheric shower particles, the results of which are presented in the following.

4.4 Simulated results and comparison with observations

The BESS-2001 experiment [174] is a balloon-borne experiment that was carried out in September 2001 at Ft. Sumner, USA. It consisted of a high resolution

spectrometer with a large acceptance capable of performing precise measurements of absolute fluxes of various cosmic rays and their dependence on the atmospheric depth. The secondary proton and helium spectra in an energy range $0.5 - 10.0$ GeV/n and the atmospheric muon spectra in a momentum range $0.5 - 10.0$ GeV/c were measured at atmospheric depths ranging from 4.5 to 28.0 g cm^{-2} during the slow descending period of the balloon flight [174, 175]. Atmospheric antiproton flux was also measured in the energy range $0.2 - 3.4$ GeV and, reportedly, at a mean atmospheric depth 10.7 g cm^{-2} [224]. The zenith angle θ_z of the BESS-2001 measurements was limited to $\cos\theta_z \geq 0.9$ to obtain nearly vertical fluxes of atmospheric particles [174].

The BESS experiment also measured the sea-level antiproton flux at KEK, Tsukuba during 6th-11th May and 7th-13th December 1997 at a mean atmospheric depth 994.0 g cm^{-2} in the energy range $0.2 - 3.4$ GeV [224].

Fig. 4.2 (left) depicts the simulated atmospheric proton flux at the location of Ft. Sumner at the atmospheric depths (a) 10.5 g cm^{-2} and (b) 26.4 g cm^{-2}. Corresponding BESS-measurements [174, 175] are also shown in the figure. It is noted that the statistical errors in the simulated spectra are quite small and fall within the widths of the representing lines in Fig. 4.2.

The BESS-2001-observed proton spectra in Fig. 4.2 (left) shows the following characteristic features. With the increase of energy from about 0.3 GeV, the differential flux initially decreases thus attaining a minimum value at about 2.5 GeV. Such a minimum is followed by an increase in flux up to a maximum at around 3.4 GeV above which the flux decreases again. Above about 2.5 GeV, bulk of the contribution to the observed flux is from primary protons with the peak being due to the geomagnetic cutoff effect. Below 2.5 GeV, the observed spectrum is due to secondary protons produced by the interaction of primary cosmic rays with atmospheric nuclei.

In Fig. 4.2 (left), it is found that the spectra derived from FLUKA and UrQMD models have features similar to those in the measured spectra. Both the models, however, yield fluxes that are lower than the measured values particularly at energies below 1.0 GeV. It is also noted that the simulated results match better with the measurements at 26.4 g cm^{-2} than at 10.5 g cm^{-2} in Fig. 4.2(left).

Fig. 4.2 (left) shows an additional peak in the UrQMD-derived spectrum at about 1.4 GeV. In this context, it is noted that the kinetic energy corresponding to the

mean vertical geomagnetic rigidity cutoff at Ft. Sumner [224] is also about 1.4 GeV/n for the threshold primary helium nuclei. To investigate if the anomalous peak in the UrQMD-derived flux in Fig. 4.2 (left) is due to such primary α particles, the separate contributions of (a) primary proton and (b) primary α components to the secondary proton flux are ploted in Fig. 4.2 (right) at an atmospheric depth 10.5 g cm^{-2} at the location of Ft. Sumner. It is clear from this figure that the additional peak in UrQMD in Fig. 4.2 (left) is indeed contributed by the primary helium nuclei. To check if there is any error in our simulations, the secondary proton flux from primary α particles is also computed in Fig. 4.2(b) (right) by using the GHEISHA model. It is found that no additional peak in the GHEISHA model, the result of which is consistent with the FLUKA result. Fig. 4.2 (right) thus seems to suggest that the fragmentation channel for quasi-elastic interactions between helium and air nuclei is overestimated in the UrQMD model. Such a finding is somewhat unexpected as the UrQMD model was primarily developed to address the nucleus-nucleus interactions and the model is known to well-reproduce the accelerator data. Further study on the stated feature in UrQMD seems, therefore, to be necessary. In Fig. 4.2, It is also noted that the results simulated with FLUKA and UrQMD models show very close agreement with each other at low energies, below about 1.0 GeV.

Fig. 4.3 shows the simulated atmospheric $\bar{p}$ fluxes in comparison with the BESS-measurements at balloon altitude, at mountain altitude and at the sea-level. The bandwidth of each of the bands displayed in this diagram represents the magnitude of statistical error in the simulations. At mountain altitude and at the sea-level, the $\bar{p}$ fluxes generated by UrQMD are found to be consistent with the BESS measurements within error bars. Such UrQMD-derived fluxes are, however, higher than the measured values at very high altitude. On the other hand, the FLUKA-generated fluxes are consistently higher than the measured values at all the atmospheric depths. The disagreement between the FLUKA-derived $\bar{p}$ spectra and the BESS observations is maximum at very high altitude and minimum at the sea level.

The results of our simulation for antiproton flux up to about 100 GeV at an atmospheric depth 10.7 g cm^{-2} is displayed in Fig. 4.4. To minimize statistical fluctuations, 40$-$50 million events are generated to obtain the flux from each model in this figure. The BESS measurements at Ft. Sumner [224] are also compared in Fig. 4.4. The fluxes generated by UrQMD + QGSJET and FLUKA + QGSJET

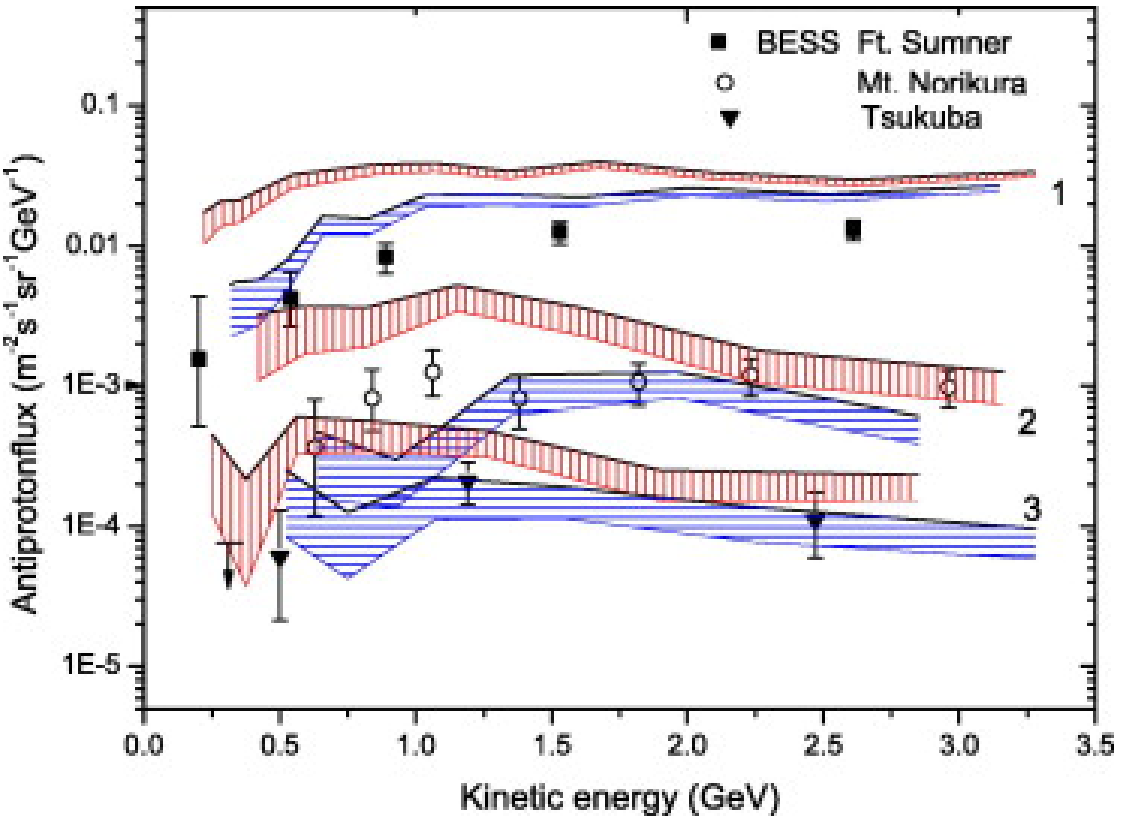

FIGURE 4.3: A diagram depicting the simulated differential spectra of vertical atmospheric antiprotons at multiple atmospheric depths. In this figure, the red (vertically striped) bands and the blue (horizontally striped) bands represent the results simulated with FLUKA and UrQMD models; whereas, the uppermost (marked by the numeral 1), middle (marked by the numeral 2) and the lowermost (marked by the numeral 3) pair of bands represent $\bar{p}$ fluxes at balloon altitude (at the location of Ft. Sumner, USA), at mountain altitude (Mt. Norikura, Japan) and at the sea-level (Tsukuba, Japan) respectively. Corresponding measurements by BESS-2001 [224], BESS-1999 [51] and BESS-1997 [224] experiments are also given for comparison. Note that the bands marked by the numeral 2 are obtained from our previous simulations [189].

combinations are found to differ significantly at the lower energy end; whereas, they predict nearly the same flux at higher (above about 5.0 GeV) energies. As we move to higher energies, the simulated $\bar{p}$ flux is increasingly influenced by the particle interaction characteristics at higher energies. It has been, so far, considered just a single model (QGSJET) for describing particle interactions above 80 GeV/n. It is, therefore, expected that the stated combinations of models will give nearly the same flux at such higher energies.

To probe further into the situations at energies ranging roughly from about 10 GeV to 100 GeV, additional sets of data are simulated by replacing QGSJET by

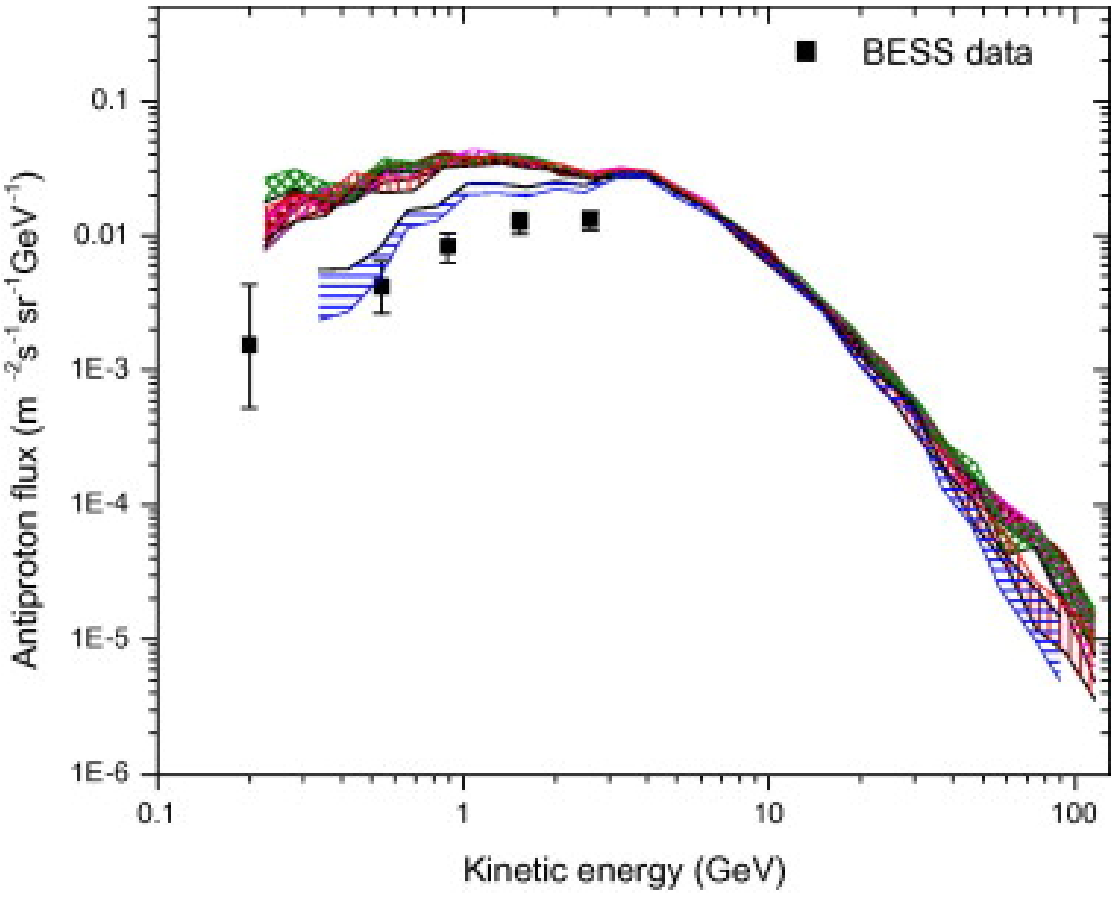

FIGURE 4.4: Atmospheric vertical antiproton flux simulated with UrQMD + QGSJET, FLUKA + QGSJET, FLUKA + VENUS, FLUKA + NEXUS and FLUKA + EPOS models at an atmospheric depth 10.7 g cm^{-2} at the location of Ft. Sumner, USA for the kinetic energy of antiprotons within a range $0.2 - 100$ GeV. Here, the blue (horizontally striped) band depicts the UrQMD + QGSJET combination, the red (vertically striped) band depicts the FLUKA + QGSJET combination, the magenta band (shaded by right-tilted lines) represents the FLUKA + NEXUS combination, the green (cross-hatched) band represents the FLUKA + VENUS combination and the brown (square-hatched) band represents the FLUKA + EPOS combination. Fluxes obtained by the BESS-2001 observation are also given for comparison.

VENUS, NEXUS and EPOS interaction models to describe particle interactions above 80 GeV/n, while continuing with FLUKA below 80 GeV/n. The spectra obtained from such combinations are also shown in Fig. 4.4. In the absence of any experimental data, the merit of the VENUS, NEXUS or the EPOS model could not be judged over the QGSJET model as far as the $\bar{p}$ production in the atmosphere is concerned. It is, however, clear from the comparison of $\bar{p}$ fluxes in Fig. 4.4 that the theoretically predicted antiproton flux has strong dependence on

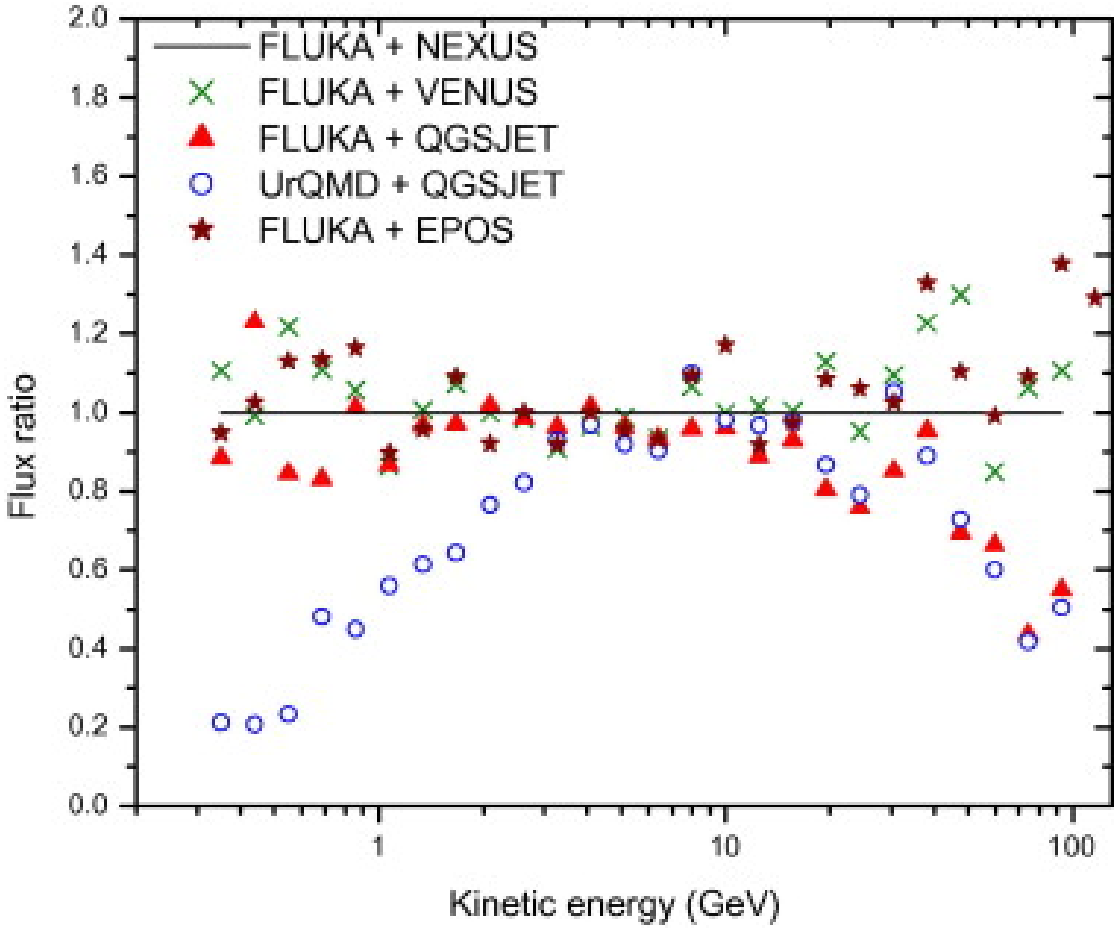

FIGURE 4.5: Ratios of the mean atmospheric antiproton fluxes simulated with each of the FLUKA + QGSJET, FLUKA + VENUS, FLUKA + EPOS and the UrQMD + QGSJET combinations to the ones simulated with the FLUKA + NEXUS model for various values of kinetic energy of the antiprotons at a mean atmospheric depth 10.7 g cm^{-2} at the location of Ft. Sumner, USA.

high energy interaction models over the energy range considered here.A characteristic feature of the atmospheric antiproton spectrum is that it peaks at around 2 GeV, decreasing rapidly towards lower energies, that is reflected in the simulated spectra as displayed in Fig. 4.4. Such a feature is not clearly visible in the BESS atmospheric observations because of the limited energy range of the experimental spectra.

To quantify the uncertainties in the theoretical $\bar{p}$ fluxes to a certain extent, the ratios of average $\bar{p}$ fluxes predicted by each of the FLUKA + QGSJET, UrQMD + QGSJET, FLUKA + VENUS and the FLUKA + EPOS combinations to the average fluxes obtained from the FLUKA + NEXUS combination (arbitrarily chosen as reference for the comparison) is plotted that are displayed in Fig. 4.5. While

such ratios are found to be close to unity in the energy range around $3 - 10$ GeV for all the models, they significantly deviate from each other at higher energies. The flux-ratios even show more than 60% variation for different models at energies around 100 GeV. In Fig. 4.5, it is found that the QGSJET-predicted mean flux at kinetic energies above about 10 GeV is substantially lower than those predicted by the NEXUS or the VENUS model. The EPOS 1.6 model follows a trend similar to that shown by VENUS at such high energies. Below about 3 GeV, the UrQMD model gives appreciably lower fluxes than those obtained by the FLUKA model as was already noted in Fig. 4.4. Possibilities of statistical fluctuations are, of course, present in such results, but such systematic deviations as depicted in Fig. 4.5 can not be accommodated in terms of statistical fluctuations.

Since all the interaction models used here are appropriately tuned to the results obtained from the known collider and other experiments, the difference between the predictions of such models are mainly due to our limited understanding of high energy particle interactions.

4.5 Summary and Discussion

Atmospheric proton and antiproton fluxes at different atmospheric levels are calculated in this article by using MC simulations with different particle interaction models and compared to the BESS experimental results. For spectra below about 10 GeV, corresponding to the experimental measurements, only the interaction models FLUKA and UrQMD are relevant. Here, it is further extend our study of the atmospheric $\bar{p}$ flux up to 100 GeV where the high energy particle interaction models QGSJET 01c , VENUS 4.12, NEXUS 3.97 and EPOS 1.6 start to influence the simulated flux. As a consequence, it can be examined the effect of such interaction models on the calculated $\bar{p}$ spectra in this article. The results of such study lead to the following observations.

1. It is interesting to note that the predictions of $\bar{p}$ fluxes obtained from FLUKA and UrQMD show significant deviations from each other, particularly at energies below about 3 GeV.

The model UrQMD presents reasonable description of the BESS $\bar{p}$ data at mountain altitude and at sea level; whereas, it overestimates the antiproton flux at very high altitude thus possibly indicating that there is an enhanced production of $\bar{p}$ followed by an enhanced annihilation in this particular model. Such an enhanced production of $\bar{p}$ in UrQMD may not be entirely unexpected as the model yields a higher multiplicity in comparison with the fixed target experiments.

The fact that FLUKA consistently yields a higher $\bar{p}$ flux than the measurements at all the observation levels possibly indicates a strongly enhanced $\bar{p}$ production in this model unless It is assumed that the BESS experiments have missed a sizable $\bar{p}$ events. The latter possibility is, however, thin as the fluxes obtained from UrQMD is consistent with the measured fluxes at sea-level and at mountain altitude. Atmospheric $\bar{p}$ annihilation also appears to be slightly enhanced in the FLUKA model as the disagreement between the FLUKA-generated $\bar{p}$ spectra and the ones obtained from the BESS measurements is found to decrease with increasing atmospheric depth.

As mentioned in Sec. 4.2, FLUKA mainly exploits the DPMJET-III model in describing high energy nucleon-nucleus interactions. DPMJET-III is known to moderately reproduce the energy dependence of antiproton to proton ratio at $y_{cm} = 0$ in proton-proton collisions as measured in the accelerator experiments [190]. It also reproduces the BRAHMS findings (from the RHIC experiment) regarding the dependence of antiproton to proton ratio on cms rapidity practically within experimental errors [188]. Although the consistency of the model parameters can not be checked in the energy range relevant for the present study as there is no direct experimental data on antiproton rapidity distribution in collisions with air or similar targets, the disagreement between the FLUKA-based fluxes and the measured fluxes on such a scale as noticed in the present study is, nevertheless, not an expected one.

It is worthwhile to note that the $\bar{p}$ flux obtained by Stephens [220] through a three dimensional MC simulation within a phenomenological framework was also found to be substantially higher in comparison with the BESS-observed flux at balloon altitude and in comparison with the theoretical unidirectional flux. Stephens [220] ascribed such a discrepancy to the use of the global spectra of primary cosmic ray particles instead of those observed by the BESS experiments. Such a possibility seems to be unlikely as the difference

between the measured flux and the theoretically predicted flux is rather large in this particular case. As mentioned earlier, the balloon in the BESS-2001 experiment at Ft. Sumner was initially floated at an atmospheric depth 4.5 g cm^{-2} from where it started to descend slowly to an atmospheric depth of around 30.0 g cm^{-2} before the termination of the experiment [224]. In the absence of any knowledge regarding the effective observation time at each atmospheric depth, the $\bar{p}$ flux at balloon altitude is computed in the present investigation (and in [220]) at 10.7 g cm^{-2} that was the mean atmospheric depth for the BESS-2001 experiment. As the $\bar{p}$ flux in the atmosphere does not vary linearly with the atmospheric depth, such an inability to precisely determine the atmospheric depth could be at least one of the possible reasons for the difference between the simulated and the measured fluxes at the balloon altitude.

It is here noted that a few phenomenological MC simulations yield $\bar{p}$ fluxes that are consistent with the BESS observation at balloon altitude except below 1.0 GeV unless it is assumed that the tertiary antiprotons do not loose their energy in collisions with atmospheric nuclei [224]. Notwithstanding such assumptions, none of the above simulations consistently describe the BESS measurements of $\bar{p}$ spectra at all the observation levels. The present study, on the other hand, seems to suggest that the BESS observations of $\bar{p}$ spectra are relatively well described by the UrQMD model.

2. The results presented in this article show a significant discrepancy between the BESS-observed secondary proton spectra at very high altitude below the geomagnetic rigidity cutoff and the ones obtained from the interaction models FLUKA and UrQMD, particularly at the low energy part of the observed spectra. It is worth noting here that the re-entrant albedo particles, a consideration of which has been left out of the present investigation, are unlikely to be the cause of such a difference between the measured and the simulated flux of the secondary protons. This is because of the fact that the flux of such re-entrant albedo protons, as measured by the AMS experiment [182], is smaller by more than an order in comparison with the BESS-observed secondary proton flux below the geomagnetic cutoff till down to at least 0.3 GeV. It is also noted that the BESS collaboration (see the footnote in Ref. [174]) found no such re-entrant albedo proton flux in their observation at the balloon altitude.

The difference that is found between the simulated and the observed proton spectra at very high altitude is in apparent contradiction with the results of our earlier simulations [189] that display reasonable agreement with the BESS-observed proton flux at mountain altitude. Fig. 4.2 in Sec. 4.4, however, demonstrate that the model-predicted proton fluxes at a lower altitude are indeed closer to the observed proton fluxes in comparison with those at a higher altitude. It may be thus inferred from the above results that the BESS observations seem to favour a higher production rate of protons in the nucleon-air collisions than the ones implemented in the FLUKA and the UrQMD models. It is, however, noted that the results of a single experimental measurement may contain uncertainties so that further observations of cosmic ray proton fluxes at multiple altitudes, along with the corresponding MC simulations, may be required to arrive at a definite conclusion on this particular issue.

3. The recent findings of the PAMELA experiment on positron excess [171, 177] but no antiproton excess [170] in the energy range from sub-GeV to about 180 GeV lead to a nontrivial constraint on dark-matter models that try to account for the positron excess [194, 204, 208]. In the stated findings, the excess is determined by comparing with the background predictions from cosmic ray propagation models. The background $\bar{p}$ spectrum, that originates from the hadronic production induced by cosmic rays on the ISM, is generally calculated with the GALPROP numerical propagation code either by applying the parametrization of the invariant $\bar{p}$ production cross-section [211] or by implementing the DTUNUC MC code [217]. Uncertainties in $\bar{p}$ flux due to the uncertainties in nuclear parameters, that are estimated from the parametrization of the maxima and the minima of the measured inclusive $\bar{p}$ cross-sections in hadron-hadron and hadron-nucleus collisions, were found earlier to be about $22 - 25\%$ [195]; whereas, the uncertainties in the nuclear parameters of the DTUNUC program, that essentially rests on the DPM model, were estimated to be about 40% [217].

   The present study also indicates, albeit indirectly, that the theoretical galactic $\bar{p}$ spectrum may contain large uncertainties due to the uncertainties in our knowledge of the particle interaction characteristics. Our investigation shows that at energies below about 3 GeV, the BESS observed atmospheric antiproton fluxes, at an atmospheric depth roughly comparable to the depth traversed by the cosmic rays in the Galaxy, are substantially lower than

those obtained with the model FLUKA that may be regarded as a DPM class of model. At energies above about 10 GeV, the model predictions cannot be tested experimentally but, importantly, the predictions from different popular microscopic high energy interaction models tend to differ appreciably. In this context, it can be noted that the model EPOS is known to produce more baryons/antibaryons in comparison with most of the other models including QGSJET that seems to be reflected in our results; see Figs. 5 and 6 in Sec. 4.4. Our investigation in Fig. 4.5, in fact, suggests that the amount of uncertainty between different model predictions is not the same at all energies. Around 300 MeV, such uncertainity is as large as 80% that reduces substantially towards higher energies, particularly above about 3 GeV. Above 10 GeV, the uncertainity, however, increases again with energy and even becomes more than 60% at about 100 GeV. In the near future, to take up a further investigation on the secondary antiproton spectrum is planned by extending the maximum kinetic energy of such antiprotons to about 180 GeV or even beyond and by exploiting the updated versions of high energy interaction models, such as the QGSJET-II [212, 213] and the EPOS 1.99 [149] models, in the framework of CORSIKA 6.980 (along with FLUKA 2011.2 to simulate below 80 GeV/n) for a better understanding of the recent PAMELA observations [171]. It may also be important here to note that the proposed measurements of $p + C \rightarrow \bar{p}$ and $\pi + C \rightarrow \bar{p}$ by the NA61/SHINE fixed-target experiments [176, 183] at a few hundred GeV (lab) energy is expected to assist us in improving our understanding on the production of antiprotons thereby resolving the noted discrepancies between the interaction models in near future.

Finally, it may be argued that the magnitude of uncertainties quoted in the theoretical calculations of $\bar{p}$ flux, that are obtained by employing semi-phenomenological fit to the experimental data, should perhaps be taken with some caution. This is because of the fact that the errors in the experimental results, based on which the model parameters are fitted or parametrized, are often underestimated or overlooked that may, in turn, affect the entire theoretical prediction. Well known examples are the inelastic $p - \bar{p}$ cross-sections that were measured by three different experiments at FERMILAB and the values at $\sqrt{s} = 1800$ GeV were found to vary from 80.03 ± 2.24 mb to 71.71 ± 2.02 mb [173, 181, 184]. Therefore, it is obvious that the model parameters that were tuned in accordance with the earlier quoted

experimental $p - \bar{p}$ cross-sections would suffer from additional uncertainties. Thus, the consistencies of the predictions of a model in different circumstances may alone provide the validity of its inputs. In view of the results of the present analysis, a detailed study of the galactic $\bar{p}$ flux by exploiting different microscopic interaction models seems to be worth pursuing in the context of the PAMELA observation and its interpretation in terms of the standard/non-standard (dark matter etc.) sources.

Chapter 5

The knee in the cosmic ray energy spectrum from the simultaneous EAS charged particles and muon density spectra

5.1 Introduction

The primary energy spectrum of all particle cosmic rays is known to exhibit a power law behavior with few features including a slight bend of the spectrum at about 3 PeV, the so called knee of the spectrum, where the power law spectral index changes from about -2.7 to nearly -3.0. The knee is generally believed to be of astrophysical origin. The common explanations of the knee include rigidity-dependent upper limit on the energy that cosmic ray protons can attain at supernova remnants [225], leakage of cosmic rays from the galaxy [226], a nearby single source [227], mass distribution of progenitors of cosmic ray sources [228] etc.

The primary cosmic ray particles after entering into the Earth's atmosphere interact with the atmospheric nuclei and produce secondary particles. The detection of cosmic rays above the atmosphere is thus the only way to obtain direct measurements of the characteristics of primary cosmic ray particles including their energy spectra and mass composition. The energy spectrum of primary cosmic rays has

been measured directly through satellite or balloon borne detectors up to few hundreds TeV. Above such energy direct methods for studying primary cosmic rays become inefficient due to sharp decrease in the flux of primary particles and the study of primary cosmic rays has to perform indirectly, through the observation of cosmic ray extensive air shower (EAS) which are cascades of secondary particles produced by interactions of cosmic ray particles with atmospheric nuclei. From their experimental results the Moscow State University group first noticed that the EAS electron size (total electron content) spectrum had a pronounced increase of slope (β increases suddenly) at a size corresponding to a primary energy of about 3 PeV [4] which was inferred as due to a break or the knee in the cosmic ray primary energy spectrum. Since then many EAS experiments covering this energy range confirm such a break in the spectral index of electron size spectrum and the existence of the knee in the cosmic ray energy spectrum is now considered as a well- established fact.

Some authors, however, cast doubt on the astrophysical origin of the knee. In particular a new type of interaction that transfers energy to a not yet observed component with interaction threshold in the knee region was proposed as the cause of the observed knee feature in the shower size spectrum [229, 230]. However, such a proposal has not received any support from the LHC experiment against the expectations. On the other hand Stenkin [231, 232] refuted the reality of the knee in the primary cosmic ray energy spectrum on the ground that the knee has been noticed observationally only in the electromagnetic component of EAS but not in the muonic and the hadronic components of EAS. In other words the knee feature in the primary cosmic ray energy spectrum is not consistently revealed from electromagnetic, muonic and hadronic components of EAS. Stenkin proposed an alternative explanation of the break in shower size spectrum in terms of coreless EAS [231, 232]. Further a new experiment PRISMA has been proposed to investigate the situation [233].

While arguing against the astrophysical knee, Stenkin did not consider any effect of change in primary mass composition in the knee region on air shower muon and electron spectra [231]. Here it is worthwhile to mention that the almost all the well known models of the knee generally predict for a change in the mass composition of cosmic rays across the knee energy. For instances, the scenarios like rigidity dependent acceleration mechanism in the source or leakage from the Galaxy (which is also a rigidity dependent effect) predict for a heavier cosmic

ray mass composition beyond the knee while the models based on nuclear photo-disintegration processes in the presence of a background of optical and soft UV photons in the source region predict for a lighter composition above the knee. The modern precise EAS experiments estimated primary energy spectra of different mass groups or even of various elements based on the deconvolution of either measured electron size distribution along with the information of muon content (as a function of electron size) or from a measured two-dimensional electron muon number distribution. Though conclusions of different experiments on primary mass composition in the knee region are not unequivocal, majority conclude that the knee represents the energy at which proton component exhibits cut-off [228] i.e. the knee of the spectrum has been ascribed as the proton knee.

It is thus imperative to examine whether the primary knee feature is consistently revealed in electron and muon components of EAS when primary composition changes from lighter primaries to heavier primaries beyond the knee energy. This is precisely the objective of the present work. Our main emphasis will be to check whether the different EAS observables suggest for consistent spectral indices in the primary cosmic ray energy spectrum before and after the knee considering the fact that primary composition may or may not change across the knee. For this purpose perform a detailed Monte Carlo simulation study of EAS shall be performed using CORSIKA [234] in the concerned energy range and different experimental data on size spectrum of various EAS observables will be analyzed to check the mutual consistency. Also the spectral indices of electron and muon size spectra for different primary composition scenario will be estimated assuming primary cosmic ray energy spectrum has a knee. The hadronic component is not considered in this work as only few data in this regard are available and more importantly the uncertainties are quite large.

The organization of the paper is as follows. In the next section the principle of deriving the cosmic ray energy spectrum from the EAS observables is outlined briefly in the framework of Bhabha-Heitler theory of electromagnetic cascade . In section 5.3 analysis of cosmic ray EAS size spectra is described based on the Monte Carlo simulation study. The procedure adapted for the Monte Carlo simulation of cosmic ray EAS is discussed in the subsection 5.3.1. In the subsection 5.3.2 spectral index of primary energy spectrum is evaluated from the measured electron and muon size spectra considering different primary composition scenario. The expected shower size and muon size spectra for different mass composition scenario

assuming the primary energy spectrum has a knee are obtained in the subsection 5.3.3. Finally the findings and their probable explanations is discussed in the section 5.4.

5.2 Primary energy spectrum from EAS observations and the knee

Usually, cosmic ray EAS arrays employ scintillation detectors for detection of electrons, which is the dominating component among the charged particles in EAS. However, such detectors also detect other charged particles including muons. So essentially EAS observations give information about total charged particle spectrum instead of electron size spectrum. The observational charged particle size (often known as shower size) spectrum in EAS is found to exhibit power law behavior i.e.

$$\frac{dN}{dN_{ch}} \propto N_{ch}^{-\beta_{ch}} \tag{5.1}$$

Though the development of EAS is a very complicated process that can be properly addressed only via Monte Carlo simulation technique but an idea of how electron and other secondary particle sizes are related to primary energy can be obtained based on the Bhabha - Heitler analytical approach of electromagnetic cascade [235, 236]. A cosmic ray particle interacts with the atmospheric nuclei while moving through the atmosphere and produced dominantly charged and neutral pions. There will be also secondary hadrons (leading particles). Neutral pions quickly decay to photons which subsequently initiate electromagnetic cascades. The charged pions may interact with atmospheric nuclei (thereby further produce secondary particles) or decay depending on their energy. The decay of charged pions yields muons and neutrinos. The energy dependence of total number electrons, muons and hadrons at shower maximum (at which the number of particles in a shower reaches its maximum) in EAS initiated by a nucleus with atomic mass number A and energy E_o can be expressed as [235, 236]

$$N_i^{max} = N_i^o E_o^{\alpha_i} \tag{5.2}$$

where i stands for e (electron), μ (muon) and h (hadron). For pure electromagnetic cascade and under few simple approximations such as the all electrons have the same energy E_e^c (which is the critical energy (85 MeV in air), at which ionization losses and radiative losses are equal) α_e is nearly equal to 1. Similarly when all muons are considered to have the same energy E_π^c (which is the energy at which the probability for a charged pion to decay and to interact are equal) and taking the charged pion production multiplicity is 10 (constant), $\alpha_\mu \sim 0.85$ [236]. When the effect of inelasticity is taken into consideration, α_μ will be slightly higher, ~ 0.90 [236]. If one considers that total primary cosmic ray energy is distributed between electron and muon component, α_e will be slightly higher, about 1.05 [236].

Two important points to be noted are (i) the total number of electrons increases with energy slightly faster than exactly linear whereas the total number of muons grows with energy slightly less than exactly linear. (ii) The electron number decreases with increasing mass number whereas muon number grows with mass number.

After shower maximum, electron (and hadron) size decreases due to attenuation whereas muon size almost remain constant because of its large attenuation length. Hence at a observational level well passed the shower maximum, the equation (5.2) is not strictly valid, particularly for electrons and hadrons.

Assuming that the electron size spectrum and total charged particle size spectrum are more or less the same, from equations (5.1) and (5.2) one can infer the primary cosmic ray spectrum as follows

$$\frac{dN}{dE_o} = \frac{dN}{dN_e^{max}} \frac{dN_e^{max}}{dE_o} \propto E_o^{-\gamma} \tag{5.3}$$

where

$$\gamma \equiv 1 + \alpha_e(\beta_e - 1) \tag{5.4}$$

will be the slope of primary cosmic ray differential energy spectrum. Since a sudden change in β_e at a size corresponding to a primary energy of about 3 PeV is observed, consequently a change in γ at 3 PeV is inferred which is the so called knee of the cosmic ray energy spectrum.

Equations (5.2) and (5.3) imply that muon and hadron size spectra also should exhibit power law behavior with $\beta_i = 1 + (\gamma - 1)/\alpha_i$. Since $\alpha_\mu < \alpha_e$, change in β_μ

should be larger than β_e for a change in γ. Observationally, however, no significant change in β_μ is found. This is why Stenkin objected the existence of a knee in the primary energy spectrum [231, 232].

Note that the semi-analytical expressions described above, though match reasonably well with the simulation results, are approximated description of cosmic ray cascade in the atmosphere. Moreover, the relation between electron size and energy (Eq. 2) is valid only at shower maximum. So a detailed Monte Carlo simulation study needs to be done to draw any concrete conclusion in this regard.

5.3 Monte Carlo simulation study of size spectrum

In the present work EAS for three different mass composition scenario: proton as primary over the whole energy range, secondly proton and Fe respectively as primary below and above the knee energy and finally Fe as primary over the whole energy range have been simulated. Subsequently it is explored that whether a consistent mass composition scenario evolve from simultaneous study of electron and muon size spectra in the knee region. α_i is evaluated from simulation data for proton and iron primaries both below and above the knee and using the observed β_i from experiments, subsequently γ is estimated following the equation (5.4) and is checked whether electron, muon and hadron observations give a consistent primary energy spectrum when primary composition is allowed to change across the knee.

5.3.1 Simulation procedure adopted

The air shower simulation program CORSIKA (COsmic Ray SImulation for KAscade) (version 6.690) [234] is employed here for generating EAS events. The high energy (above 80GeV/n) hadronic interaction model QGSJET 01 (version 1c) [237] has been used in combination with the low energy (below 80GeV/n) hadronic interaction model UrQMD [238]. A relatively smaller sample has also been generated using the high-energy interaction model EPOS (version 2.1) [239] and low energy interaction model GHEISHA (version 2002d) [240] to judge the influence of the hadronic interaction models on the results. Note that GHEISHA exhibits a few

shortcomings [241, 242] but the low energy interaction models has no significant effect on the total number of secondary particles for primaries in the PeV energy range.

The US-standard atmospheric model with planar approximation which works only for the zenith angle of the primary particles being less than 70^o is adopted. The EAS events have been generated for proton and iron nuclei as primaries at several fixed energy points spreaded between 3×10^{14} to 3×10^{16} eV as well as over a continuous energy spectrum between 3×10^{14} to 3×10^{16} eV with differential energy spectrum slop -2.7and -3.1 below and above the knee (3×10^{15} eV) respectively. The EAS events have been simulated at geographical positions correspond to experimental sites of KASCADE [243] and EAS-TOP [76]. The magnetic fields, observation levels, threshold energies of particle detection and zenith angles are provided accordingly.

5.3.2 Inferring Primary cosmic ray spectrum from measured EAS size spectra

Only a few EAS experiments so far measured both β_{ch} and β_{μ} before and after the knee. Here the results of two experiments are considered, the KASCADE [244, 245] and EAS-TOP [246]. The KASCADE experiment was considered as one of the most precise air shower experiments in the world which was situated in the site of Forschungszentrum Karlsruhe (Germeny) at an altitude 110 m above sea level at 49.1^o N, 8.4^o E, covering an energy range from about 100 TeV to nearly 100 PeV and was in operation during October 1996 to 2003. The experiment consisted an array of electron and muon detectors, spread over 700 m^2 $\times$ 700 m^2, a central hadron calorimeter with substantial muon detection areas and a tunnel with streamer tube muon telescopes. This multi-detector system was used for the study of electromagnetic, muonic and hadronic components of EAS. The experiment was later extended to KASCADE-GRANDE in 2003 to study primary cosmic rays at higher energies. On the other hand the EAS-TOP array was located at Campo Imperatore, National Gran Sasso Laboratories in Italy, 2005 m a.s.l.,(820 $g\ cm^2$) atmospheric depth. This multi-component experiment consisted of detectors of the electromagnetic, muon, hadron and atmospheric Cherenkov light components for the study of EAS over the energy range 100 TeV to about 10 PeV. Two layers

of streamer tubes with total surface area $12 \times 12\ m^2$ was used for detection of EAS muons having threshold energy of 1 GeV.

The results of these two experiments on β_{ch} and β_{μ} are shown in Table 5.1. Note that the shower size (N_e) and muon size are generally evaluated from the experimental measured particle (electron/muon) densities by fitting with the lateral density distribution function. To minimize the bias by the functional form of the muon lateral distribution function, KASCADE experiment introduced the quantity truncated muon number which is essentially the muon size within 40 m and 200 m core distance.

TABLE 5.1: The measured spectral indices of primary energy spectrum below and above the knee from the electron and the muon size spectra of KASCADE and EAS-TOP observations

Experiment	Component	$\beta_{<knee}$	$\beta_{>knee}$
KASCADE	charged particles	2.45 ± 0.06	2.94 ± 0.12
KASCADE	muon ($>$ 490 MeV)	3.05 ± 0.006	3.27 ± 0.01
EAS-TOP	charged particles	2.61 ± 0.01	3.01 ± 0.06
EAS-TOP	muon ($>$ 1 GeV)	3.12 ± 0.03	3.67 ± 0.07

Using the public data of KASCADE experiment provided through KCDC [247] β was estimated. For vertical air showers ($\theta < 18^o$), it is found that β equals to 2.54 ± 0.06 and 2.97 ± 0.05 below and above the knee are respectively for total charged particles and 2.96 ± 0.08 and 3.24 ± 0.06 for muons below and above the knee respectively which are closed to the KASCADE reported β.

To estimate α Monte Carlo simulation method is exploited. The figure 5.1(a) displays the variation of total charged particle number in EAS obtained with Monte Carlo simulation as a function of energy at KASCADE location for proton primary whereas the variation of muon content with primary energy in proton induced EAS is shown in figure 5.1(b). Power law fits to the data points are also shown in both the figures. It is found that find that the dependence of shower size on primary energy can be described by a power law with constant spectral index as given in equation (5.2). It has also been checked whether the data suggest different spectral slops at lower and higher energies by fitting the data below and above the knee separately. But the so fitted slops are found only to differ within the error limits of the single constant spectral index. The estimated power law indices (α_{ch} and α_{μ}) are displayed in table 5.1 for proton primary. In figure 5.2 the electron and muon sizes in Fe initiated EAS as a function of primary energy

has been plotted. The α_{ch} and α_{μ} for Fe primary are also evaluated from power law fitting and are shown in table 5.2.

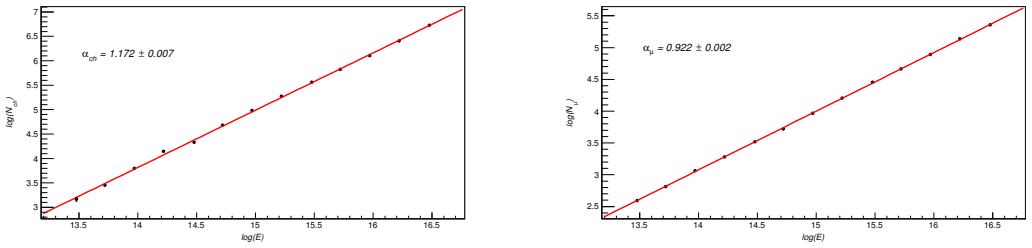

FIGURE 5.1: Energy dependence of (a) (left) total charged particles and (b) (right) muon content in proton induced EAS at KASCADE location from the Monte Carlo simulation data.

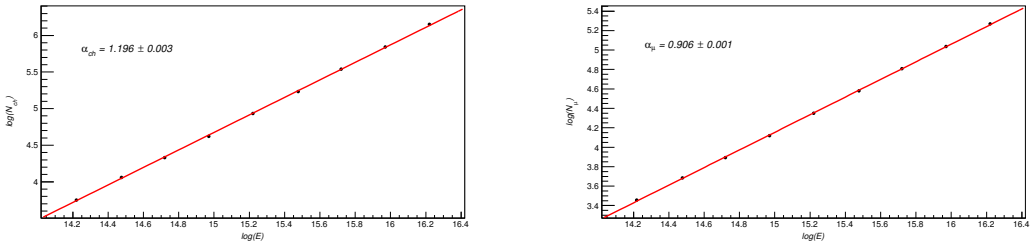

FIGURE 5.2: Same as Figure 5.1 but in Fe initiated EAS.

Since β_is are known from observations, it has been estimated γ straightway using the expression (5.4). Both proton and Fe were considered as primaries below the knee as well as above the knee and γ was evaluated. Subsequently $\delta\gamma$ is evaluated across the knee. The results are given in Table 5.1 for the KASCADE measurements. It is noticed that no consistent γs below and above the knee emerge from the KASCADE measured electron and muon spectra irrespective of the primary composition. The $\delta\gamma$s from the observed electron and muon spectra also differ significantly.

TABLE 5.2: Spectral indices of primary energy spectrum below and above the knee from the electron and the muon size spectra of KASCADE observations

Primary before the knee	Primary after the knee	Secondary	$\alpha_{<knee}$	$\alpha_{>knee}$	$\gamma_{<knee}$	$\gamma_{>knee}$	$\Delta\gamma$
Proton	Proton	electron	1.172 ± 0.007	1.172 ± 0.007	2.70 ± 0.08	3.27 ± 0.16	0.57 ± 0.24
		Muon (> 490 MeV)	0.922 ± 0.002	0.922 ± 0.002	2.89 ± 0.01	3.09 ± 0.02	0.20 ± 0.04
Proton	Fe	charged particles	1.172 ± 0.007	1.196 ± 0.003	2.70 ± 0.08	3.32 ± 0.14	0.62 ± 0.22
		Muon (> 490 MeV)	0.922 ± 0.002	0.906 ± 0.001	2.89 ± 0.01	3.05 ± 0.02	0.16 ± 0.03
Fe	Fe	charged particles	1.196 ± 0.003	1.196 ± 0.003	2.73 ± 0.08	3.32 ± 0.14	0.59 ± 0.22
		Muon (> 490 MeV)	0.906 ± 0.001	0.906 ± 0.001	2.86 ± 0.01	3.05 ± 0.02	0.19 ± 0.03

Results of a similar analysis for the EAS-TOP electron and muon spectra are displayed in figures 5.3 nad 5.4 from simulation data and in Table 5.3. In EAS-TOP

location the α of charged particles for proton primary is found quite small than that for the KASCADE location which suggests that α changes with atmospheric depth and approaches to one at shower maximum as predicted by the cascade theory. For Fe primary, however, no significant difference in α of charged particles noticed in two stated locations. This is probably due to the fact that air showers reaches to its maximum development much earlier for heavier primaries, so even at EAS-TOP altitude, PeV energy Fe initiated showers are quite old. The spectral index (of primary cosmic ray energy spectrum) derived separately from the EAS-TOP observed electron and muon size spectra is found somewhat mutually consistent when cosmic ray primary is dominantly Fe, both before and after the knee. The $\delta\gamma$s from the observed electron and muon spectra also found mutually consistent for unchanging Fe dominated primary.

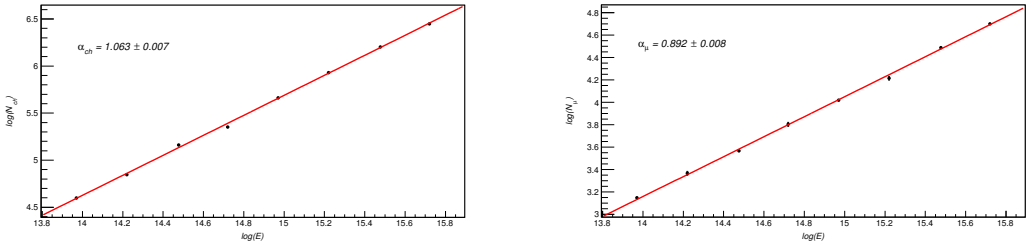

FIGURE 5.3: Energy dependence of (a) (left) total charged particles and (b) (left) muon content in proton induced EAS at EASTOP location.

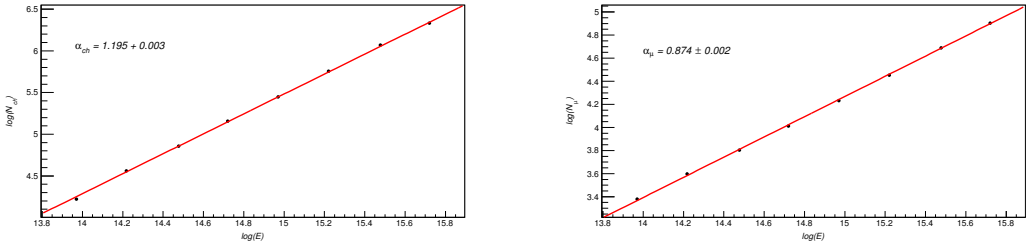

FIGURE 5.4: Same as Figure 5.3 but in Fe initiated EAS .

TABLE 5.3: Spectral indices of primary energy spectrum below and above the knee from the electron and the muon size spectra of EAS-TOP observations

Primary before the knee	Primary after the knee	Secondary	$\alpha_{<knee}$	$\alpha_{>knee}$	$\gamma_{<knee}$	$\gamma_{>knee}$	$\Delta\gamma$
Proton	Proton	charged particles	1.063 ± 0.007	1.063 ± 0.007	2.71 ± 0.02	3.14 ± 0.07	0.43 ± 0.09
		Muon	0.892 ± 0.008	0.892 ± 0.008	2.89 ± 0.04	3.38 ± 0.09	0.49 ± 0.13
Proton	Iron	charged particles	1.063 ± 0.007	1.195 ± 0.003	2.71 ± 0.02	3.40 ± 0.08	0.69 ± 0.10
		Muon	0.892 ± 0.02	0.874 ± 0.002	2.89 ± 0.04	3.33 ± 0.07	0.44 ± 0.11
Iron	Iron	charged particles	1.195 ± 0.003	1.195 ± 0.003	2.92 ± 0.02	3.40 ± 0.08	0.48 ± 0.10
		Muon	0.874 ± 0.002	0.874 ± 0.002	2.85 ± 0.03	3.33 ± 0.07	0.48 ± 0.10

5.3.3 Electron and muon spectra for astrophysical knee

It appears that the main difficulty of arriving a consistent knee from simultaneous charged particles and muon spectra in EAS from the KASCADE experiment is the very small spectral slope difference in muon spectrum ($\Delta\beta_{mu}$) across the knee relative to the spectral slope difference in charged particle spectrum ($\Delta\beta_{ch}$). Here a reverse process shall be followed, the expected spectral slopes shall be estimated in charged particle and muon spectra for different primary composition scenario assuming that the primary energy spectrum has a knee. The spectral index of the primary energy spectrum below the energy 3 PeV is taken as -2.7 whereas above 3 PeV it is assumed as -3.1. The EAS are generated from the minimum energy of 100 TeV and only vertical showers ($Z < 18^o$) are generated.

The charged particle and muon size spectra at KASCADE location from the simulation results are displayed in figures 5.5. Unchanged proton and Fe mass compositiona over the entire energy range as well as a change in mass composition after the knee from pure proton to pure iron was considered. The knee structure is found present in both electron and muon size spectra for all the mass composition scenario considered. The β value obtained from the simulation results are displayed in Table 5.4 for the different composition scenario. To estimate the β values in electron and muon size spectra the differential total charged particle (muon) numbers is multiplied by some suitable power (selected by varying the power index slowly) of total charges particles (muons) to emphasize the small difference in slope and plot it against the total charged particles (muons) in log-log scale. It is found that the points below and above a certain total charged particle number have distinct slopes. The best fitted slopes give the β below and above the size knee whereas the crossing point of the two straight lines (in log-log scale) give the position of the knee in the size spectra.

The spectral index of total charged particle spectrum above the knee obtained from the simulation results is found slightly lower than the observational result whereas for muon spectrum the spectral index below the knee from the simulation data is found slightly larger than the observations which is of not much importance as spectral index of primary spectrum is assumed arbitrarily. The spectral indices for proton and iron primaries are found close. When composition changes across the knee it is noticed that the spectral index below (or above) the knee depends

not only primary composition below (above) the knee of the primary energy spectrum but also the composition above (below) the knee of the energy spectrum, unless points close to the knee in the size spectra are excluded to determine the spectral index. There are few other noteworthy points :

i) the position of the knee in the charged particles and muon spectra also influence by the primary composition both below and above the knee of the cosmic ray energy spectrum,

ii) the knee in the muon spectrum is slightly more revealing in comparison to that in the electron spectrum for pure proton or Fe primaries over the entire energy range but the same may not be true when primary composition changes across the knee,

and iii) for proton primary before the knee and Fe primary after the knee the muon spectrum exhibits a break not only in the spectral index but also in the flux. The later feature is due to larger muon size in Fe initiated EAS in comparison to proton induced EAS.

TABLE 5.4: Spectral indices of the simulated charged particles and the muon size spectra for cosmic ray energy spectrum with the knee

Primary before the knee	Primary after the knee	Secondary	$\beta_{<knee}$	$\beta_{>knee}$	$\Delta\beta$
Proton	Proton	charged particles	2.39 ± 0.01	2.70 ± 0.01	0.31 ± 0.02
		Muon	2.80 ± 0.03	3.30 ± 0.02	0.50 ± 0.05
Proton	Iron	charged particles	2.16 ± 0.01	3.03 ± 0.01	0.87 ± 0.02
		Muon	2.86 ± 0.03	3.28 ± 0.02	0.42 ± 0.05
Iron	Iron	charged particles	2.40 ± 0.01	2.70 ± 0.01	0.30 ± 0.02
		Muon	2.88 ± 0.02	3.30 ± 0.02	0.42 ± 0.04

The modern EAS experiment usually employ two-dimensinal plots of total charged particle and muon size spectra to evaluate primary energy spectrum and composition. From simulation data two-dimensional plots of total charged particles and muon size spectra for different composition scenario are also obtained and depicted in figures 5.6 at KASCADE location. An interesting observation is that the knee is not clearly visualized from the two-dimensional plots. Since Fe induced EAS contains lower electrons and higher muons in compare to proton induced EAS, the two dimensional figure exhibits some mismatch in shower and muon sizes around the knee for a sharp change in composition from proton to Fe across the knee which is not observed experimentally.

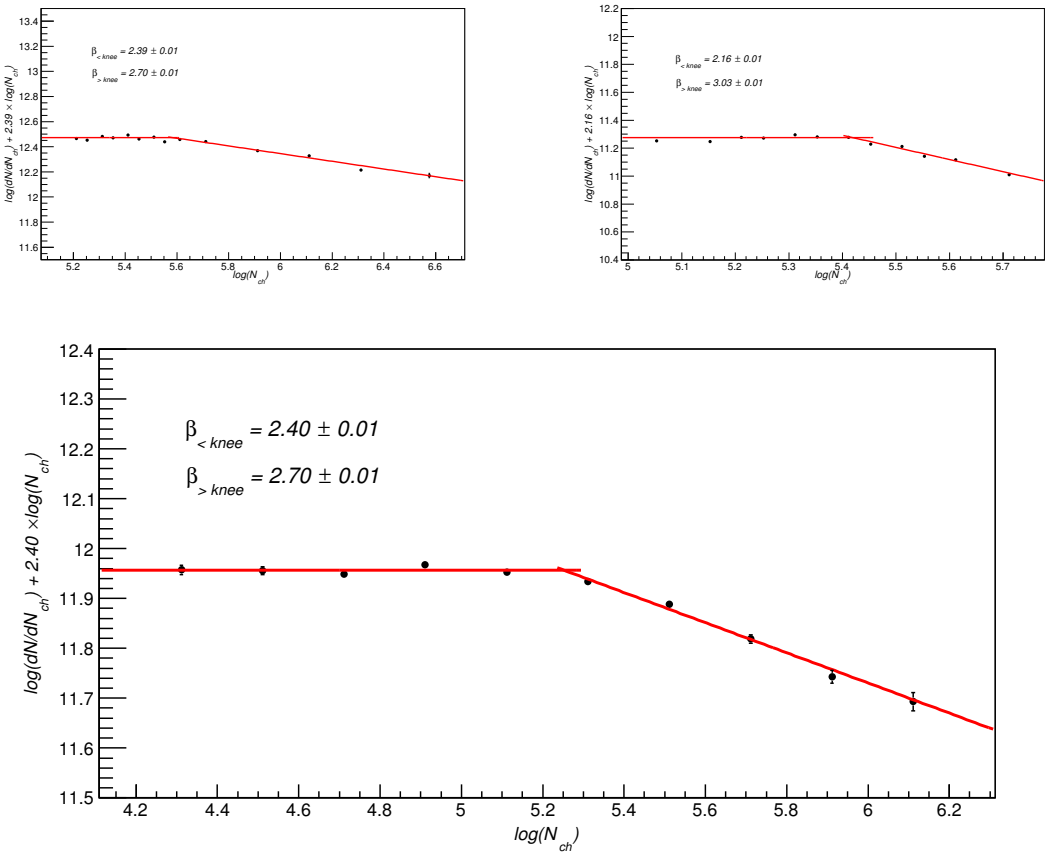

FIGURE 5.5: Expected total charged particle size spectrum for different mass composition scenario across the knee (a) (left) unchanged proton primary (b) (right) proton below the knee and Fe above the knee and (c) (below) unchanged Fe primary.

5.4 Discussion and Conclusion

The knee of the primary energy spectrum has long been inferred from the break in shower size spectrum of cosmic ray EAS at certain shower size corresponding to few PeV primary energy. Few authors, particularly Stenkin, however, objected the existence of the knee in the primary energy spectrum noting that the muon size spectrum of cosmic ray EAS does not show any prominent break against the expectations.

It is found from the present analysis that the EAS-TOP observations on total charged particle and muon spectra consistently infer a knee in the primary energy spectrum provided the primary is pure unchanging iron whereas no consistent primary spectrum emerges from simultaneous use of the KASCADE observed total charged particle and muon spectra.

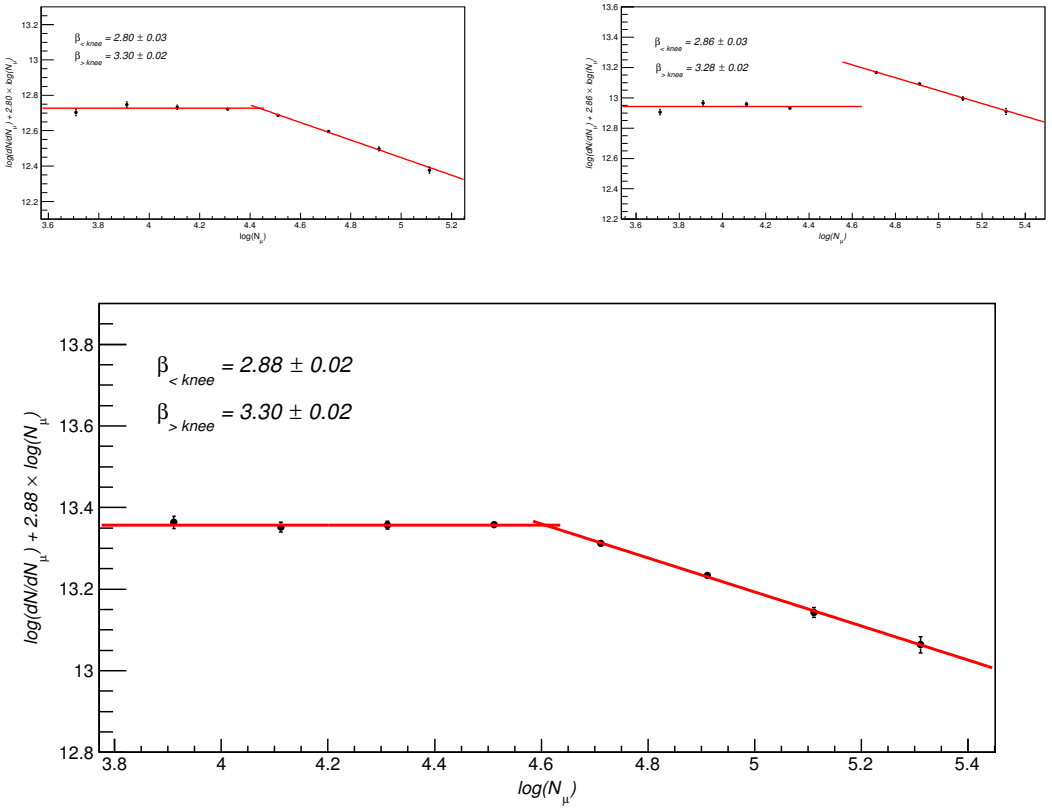

FIGURE 5.6: Same as figure 5.5 but for muon spectrum

It is further found from Monte Carlo simulation results that for pure unchanging proton or iron primaries the difference in spectral slopes below and above the knee of the size spectrum is larger for muon spectrum than the electron spectrum. However, when mass composition changes across the knee the situation becomes quite complex. In such a situation estimation of β properly is problamatic, particularly for total charged particle spectrum. The β_{ch} and the position of the knee depend on primary composition both below and above the knee of the primary energy spectrum when the data points close to the knee in the size spectra are incorporated to determine them. A different choice of data points may change the overall slope considerably. For instance in the simple situation where proton and Fe are the dominating component below and above the knee of the primary energy spectrum, the contribution of Fe, which gives a comparative lower total number of charged particles, leads to a flatter shower size spectrum below the knee, unless the points closed to the knee in the size spectrum are totally ignored to evaluate the slopes. On the other hand iron induced EAS contains comparatively larger number of muons. Hence the slopes of the muon size spectrum does not alter much for the stated changing composition scenario but there will be a mismatch

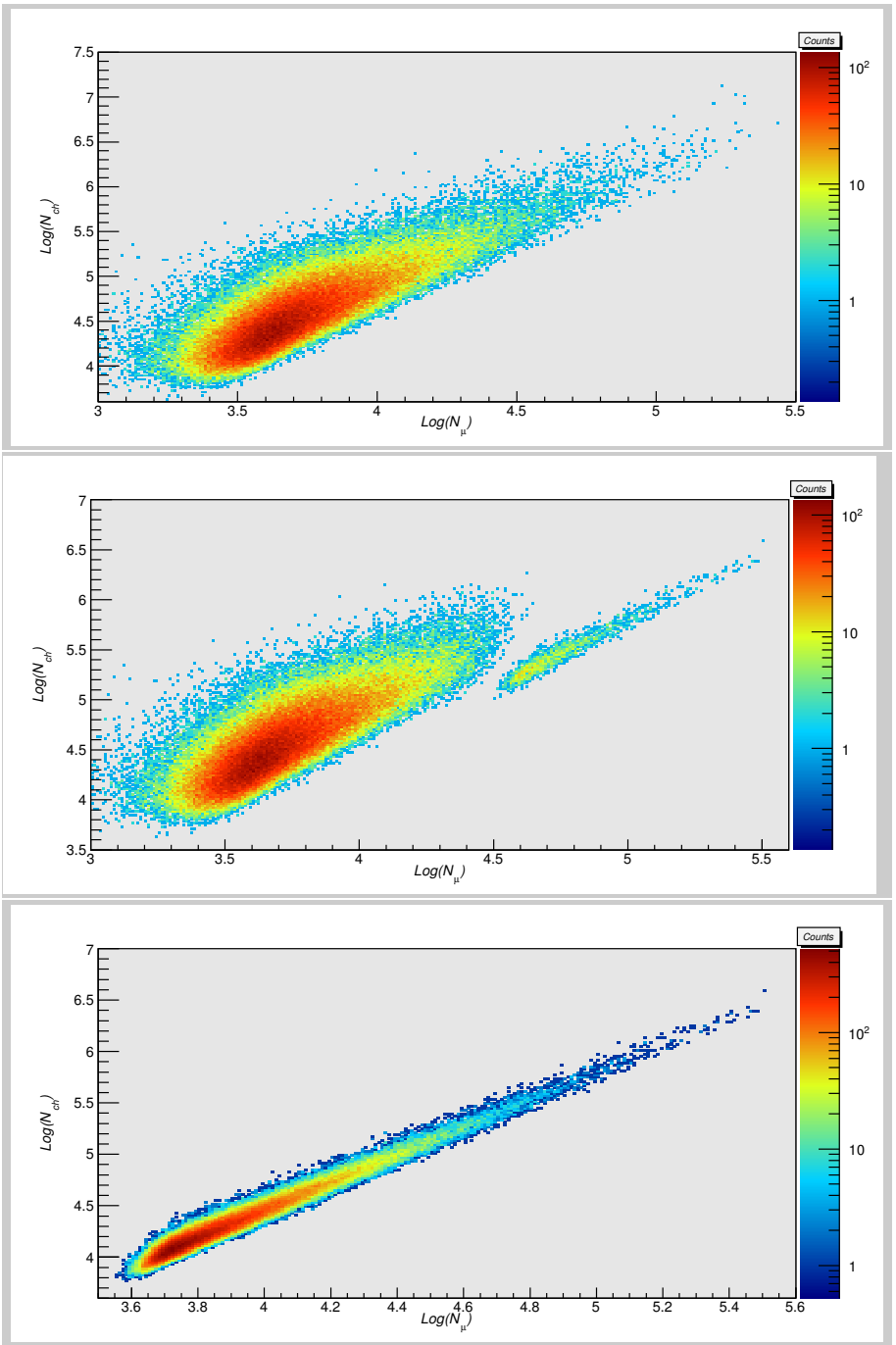

FIGURE 5.7: 2-dimentional charged particles - muon spectrum for different composition scenario around the knee

in the flux at the knee of the muon size spectrum. Non observation of any break in flux level at the knee position of the muon size spectrum in any experiment suggests that there is no abrupt change in primary composition across the knee; the composition either changes slowly above the knee or it changes from a lighter dominating mixed composition to heavier dominated mixed composition without appreciable change in average primary mass.

It is thus concluded that though the derivation of the size spectrum from observed data looks to be rather straight forward process, but in practice it is a quite complex issue, particularly owing to the uncertainty in primary mass composition. The simultaneous use of the measured EAS total charged particle and muon size spectra to infer the primary energy spectrum is certainly a better approach but it requires a careful and experiment specific analysis. The two-dimensional differential spectrum contents substantially higher information than those of two one-dimensional ones and hence used to infer primary spectrum and composition but one dimensional spectra also carry important and exclusive signatures about primary energy spectrum and composition which should also be accommodated to get reliable information about cosmic ray primaries.

Chapter 6

Progenitor model of Cosmic Ray knee

6.1 Introduction

Ever since their discovery more than a hundred years back now, the origin of cosmic rays has been one of the central question of physics. But despite many efforts so far there is no consistent and complete model of the origin of cosmic rays.
The energy spectrum of cosmic rays provides important clues about their origin. The most intriguing feature of the energy spectrum is that though it extends a wide range of energies, from sub GeV to at least 3×10^{20} eV (the highest energy observed so far), it can be well represented by a steeply falling power law for energies above the solar modulated one. However, the spectrum has a knee around 3 PeV where it steepens sharply as discovered more than half a century ago by Kulikov and Khristiansen of the Moscow State University [4]. The spectrum also has an ankle at an energy about 3 EeV where it flattens again to its pre-knee slope. It is relatively easier to interpret the flattening of the spectrum above the ankle as the eventual superseding of a harder cosmic ray component which is sub-dominant at lower energies. In contrast the feature of knee is more difficult to explain. The existence of the knee in the spectrum is definitely an important imprint of the true model of origin of cosmic rays and hence a proper explanation of the knee is expected to throw light on the problem of cosmic ray origin.
Several mechanisms have been proposed so far to explain the knee. Shortly after the discovery of the knee, this spectral feature was interpreted as an effect of the

reduced efficiency of galactic magnetic field to confine the cosmic ray particles with energies above the knee within galaxy [12, 286, 287, 303, 311]. Since the magnetic rigidity of a particle is proportional to its atomic number (Z), cosmic ray protons should start escaping first and hence the observed knee is the proton knee as per this model.

The knee has also been explained based on acceleration mechanism [5, 15, 108, 265, 281, 292]. For reasons of the power required to maintain the observed cosmic ray energy density, it is widely accepted that cosmic rays up to the ankle energy are of galactic origin whereas those having energies above this energy are extragalactic though there are also suggestions for lower transitional energies [254, 255, 268]. Among the galactic sources supernova remnants (SNRs) satisfy the energy budget of cosmic rays. The power law behavior of the energy spectrum on the other hand suggests that cosmic rays are most probably energized by diffusive shock acceleration. The maximum energy that a charged particle can gain by diffusive shock acceleration is proportional to Z. The knee has been assigned in this model as the maximum energy that protons can have under diffusive shock acceleration in SNRs.

A critical analysis of the world data on energy spectrum suggests that the knee is very sharp, the spectral slop changes rather abruptly at the knee position [18]. In contrast, the above mentioned rigidity dependent explanations of the knee predict a smooth change in the spectral slope at the knee because of sum of the contributions of different atomic nuclei having cut-offs at different energies (depending on Z values). To accommodate the sharp knee feature, a few proposals were advanced. In the single source model the dominant contribution of the cosmic ray flux at the knee is by a nearby source [18, 20, 264, 309] which is superimposed on a galactic modulated component in which spectral slop is changing smoothly with energy. In another model the sharp knee is explained in terms of cosmic ray acceleration by a variety of supernovae [23, 25]. The later proposal relies on the fact that the explosion energy of all the supernovae are not the same. The sharp knee also could be due to interaction of cosmic ray particles from a pulsar with radiation from the parent supernova remnant [291].

The mass composition of cosmic rays will be heavier beyond the knee if the knee is a proton knee. Several Extensive Air Shower (EAS) measurements (till now the study of cosmic rays above 1 PeV is of indirect nature via the EAS observations) have been made to determine the mass composition of cosmic rays in the concerned energy region but the measurements have not yielded mutually consistent results

yet due to the weak mass resolution of the measured shower observables [288]. Most of the findings [79, 248, 282, 301] based on electron content relative to muon content (or *vice versa*) in EAS suggest that composition becomes heavier with energy beyond the knee though Haverah Park and few other observations (particularly underground muon telescopes) [252, 253, 261, 266, 267, 271, 276, 296, 299] found opposite trend of mass composition. Mass composition estimated from measurement of the depth of shower maximum through observation of Cerenkov [6, 80, 260, 269, 273, 279, 280, 295] or fluorescence radiation [249–251, 293, 310] on the other hand suggest lighter mass composition beyond the knee differing from those obtained with muon to electron content ratio [263, 288, 290]. The mass composition picture of primary cosmic rays is thus still inconclusive in the PeV and higher energy region.

Considering the possibility that mass composition may become lighter beyond the knee an alternative explanation of knee was suggested based on nuclear photo-disintegration at the sources [13, 16, 115]. In this scenario heavier components of cosmic rays, particularly Fe nuclei undergo nuclear photo-disintegration in interaction with the radiation field of the source so that flux of heavier nuclei decreases with energy beyond the knee whereas protons loose energy by photo-meson production.

A major problem with the standard scenario of diffusive shock acceleration of cosmic rays at SNRs is that a cosmic ray particle hardly attain the knee energy under this SNR shock acceleration scenario. Such a problem can be overcome in the Cannonball model [112, 114, 277, 278] in which masses of baryonic plasma or the so called cannonballs, ejected ultra-relativistically in bipolar supernova explosions, are considered as universal sources of hadronic galactic cosmic rays. In this model the knee corresponds to maximum energy gained by nuclei by elastic magnetic scattering of ambient ISM particles in the Cannonball while re-acceleration of cosmic rays by Cannonballs of other supernova explosions causes the extra steepness above the knee.

There is also proposal of explaining the knee based on a change in the characteristics of high energy interactions [302]. In this model the knee is not a feature of the primary cosmic ray energy spectrum itself, but is caused by change in high-energy interaction characteristics, either producing a new type of a heavy particle unseen by air shower experiments, or an abrupt increase in the multiplicity of produced particles. However, this proposal is ruled out at present as the assumed interaction features have not been observed in the LHC experiment.

None of the prevailing models of knee are free from problems. If the knee corresponds to break in proton spectrum, either because of it is the maximum energy to which proton can accelerate in a galactic cosmic ray source or due to begin of proton leakage from the galaxy at this energy with or without modifications for the sharp knee, then there should be a Fe knee around 10^{17} eV. Hence a special variety of supernovae or some other type of galactic or extra-galactic source has to be invoked as generator of cosmic rays between $\sim 10^{17}$ eV and the ankle or galactic extra-galactic transition should occur at around 10^{17} eV. The problem with the later proposal is that it requires fine-tuning to match both the flux and the energy at the point of taking over. The cannonball model also suffers the same fine tuning problem at the knee energy. There are other problems such as lower than expected observed gamma ray fluxes from SNRs. The dilemma of the knee thus still continues.

The viable sources of cosmic rays include X-ray binaries, SNRs, pulsars, Gamma Ray Bursts (GRBs), Active Galactic Nuclei (AGN) etc. Whatever may be the sources, there is little doubt that they are products of stellar evolution process. And an interesting fact is that the zero age mass spectrum (ZAMS) of stars also exhibits power law behavior [297, 300, 306]. This immediately suggests that the cosmic ray energy spectrum might have some connection with the mass distribution of progenitor of their sources. In the present work the idea is explored and a model for the cosmic ray origin is proposed in which the knee of the primary cosmic ray energy spectrum at ~ 3 PeV is a consequence of mass distribution of progenitor of cosmic ray sources. The proposed model is free from any fine tuning problem and it also overcomes the issue of maximum attainable energy.

The organization of the article is as follows. The model proposed in this work is presented in the next section. The outcome of the present model is discussed in section 6.3. The results of the model are compared with observations in section 6.4. Finally the results are concluded in section 6.5.

6.2 The proposed model

Here a model of origin of cosmic rays is proposed in which there is a single class of major cosmic ray sources in the galaxy.

The basic conjectures of the present model are the followings:

1) Cosmic rays at least up to the ankle energy are produced either in gravitational explosions (core collapse) of massive stars those lead to formation of black holes rather than neutron stars/white dwarf or in accretion onto black holes. No other type of galactic or extra-galactic source dominates at least up to the ankle energy. Here the source has not been identified. The probable candidate sources of cosmic rays include hypernova, Active Galactic Nuclei (AGNs) and Gamma Ray Bursts (GRBs).
2) Particles are accelerated by expanding shock waves up to a maximum energy E_{max}. The maximum attainable energy E_{max} is, however, not the same for all the sources (of same kind) but depending on energy released in explosion/accretion, it has a range. The minimum E_{max} that is possible for the cosmic ray sources is equal to the knee energy. It will argued in the following section that the correspondence of minimum E_{max} with the knee energy is quite plausible and suggestive.
The observed cosmic ray luminosity demands that the cosmic ray sources must be energetically very powerful and are most likely to be powered by gravitational energy. The gravitational collapse that ultimately leads to formation of black hole or accretion onto black hole is expected to release maximum gravitational energy. This is the reason for considering the first conjecture. The maximum energy that a cosmic ray particle can attain in shock acceleration usually depends on the explosion energy. Since black hole has no limiting mass, energy released in black hole formation should varry with progenitor mass and hence the maximum attainable energy of cosmic ray particles are expected to be varry rather than having a fixed value. Essentially this is the logic behind the second conjecture.

6.2.1 The Progenitor connection

Perhaps occurrence of relativistic shock and non-relativistic shock depends whether a black hole (BH) or a neutron star (NS) is formed in the stellar evolution processes. Through stellar core collapse progenitor stars with $M < 20M_{\odot}$ are supposed to give rise to a neutron star or white dwarf whereas stars more massive than 20 to $25M_{\odot}$ form a black hole [283–285] though such end point fate also depends on metallicity [289]. The formation of white dwarf or neutron star is usually associated with supernova explosion. The masses of white dwarfs and neutron stars have to be within the Chandrasekhar limit and Openheimer-Volkof limit respectively. Consequently the energy released in all ordinary supernova explosions are nearly the same. Since black hole has no such upper mass limit the energy released in

core collapse of massive stars leading to black holes should depend on the mass of the progenitor star.

The gravitational collapse of massive stars to black holes involves some complex, still poorly understood aspects of stellar physics. In the collapsar mechanism [312], a black hole is formed when the collapse of a massive star fails to produce a strong supernova explosion, leading to ultimate collapse into a black hole. If the stellar material falling back and accreting onto the black hole has sufficient angular momentum, it can hang up, forming a disk. This disk, by neutrino annihilation or magnetic fields, is thought to produce the jets which finally results in Active Galactic Nuclei (AGN) or hypernova.
In the gravitational collapse of a spherical mass distribution of rest mass M leading to formation of black hole, the maximum energy of extraction out of the collapse will be [272, 305].

$$E_{max}^{collapse} = Mc^2/2 \tag{6.1}$$

During the final stages of stellar evolution, a massive star losses a significant amount of mass. But if a black hole is formed stellar material likely to fall back and accreting onto the black hole [312]. The mass of the final produced black hole is thus expected to increase linearly with the mass of progenitor.

Instead of collapse and resulting explosion, large amount of energy also can be released through accretion process. The Eddington luminosity limit, the maximum steady-state luminosity that can be produced is given by $L_{ed} = 4\pi GMm_pc/\sigma_\tau$ where M is the mass of the black hole, m_p is the proton mass and σ_τ is the Thomson cross-section. The luminosity is thus also proportional to the mass of the black hole.

During the final stages of stellar evolution, a massive star losses a significant amount of mass. But if a black hole is formed stellar material likely to fall back and accreting onto the black hole [312]. The mass of the final produced black hole is thus expected to increase linearly with the mass of progenitor, and hence the distribution of released energy is expected to follow the mass distribution of progenitors.

6.3 Outcomes of the proposed model

Now the outcomes of the proposed model regarding the main cosmic ray observables such as luminosity, maximum attainable energy, energy spectrum and nuclear composition will be found out.

6.3.1 The cosmic Ray Luminosity:

The average energy released in BH formation should be around 5×10^{53} ergs as per the equation (1) which is more than two order higher than that released in supernova explosion. Stars more massive than 20 to $25M_{\odot}$ usually form a black hole. The rate of stars having $M > 20M_{\odot}$ is 2×10^{-3} yr^{-1}. However, not all massive stars will end up as black holes. If the probability of BH formation for a star massive than 20 $M_{\odot}$ is denoted by ρ_{BH}, the total energy released in BH production during the cosmic ray confinement period of about 10^6 years in the galaxy is about $\rho_{BH}10^{57}$ ergs which yields a luminosity $3\rho_{BH}\zeta \times 10^{43}$ ergs/s, where ζ is the efficiency of conversion of explosion energy into cosmic ray energy. Typically ζ ranges from 0.01 to 0.1 whereas ρ_{BH} may be taken as 0.5 [274].

6.3.2 The Maximum attainable Energy:

The maximum energy that a particle with charge Ze can be attained in a bulk magnetized flow on a scale R_s, with velocity $c\beta_s$ and magnetic field B is [116]

$$E_{max} = ZeB\Gamma_s\beta_s R_s \tag{6.2}$$

where Γ_s is the Lorentz factor of the relativistic shock wave. This value of E_{max} is a factor Γ_s larger than that obtained from the Hillas condition. In a BH formation scenario, a fraction of all kinetic energy carries a debris ejected with the largest Lorentz factor thereby generating gamma ray emission in the form of burst, but the bulk of ejecta is less relativistic or even sub-relativistic. Note that if $\sim 10M_{\odot}$ is given $\sim 10^{54}$ ergs then typical velocity of the mass would be 10^{10} cm i.e. $c/3$. GRBs are likely to occur in BH formation collapse and a hint on typical values of Γ_s may be found from GRBs. The GRB observations suggest minimum Γ_s of the burst is few tens [298, 304, 313]. Therefore, the minimum E_{max} for BH producing

explosion should be of few PeV.

Let us consider a more rigorous desscription. In the standard scenario the acceleration of cosmic rays occurs at (non-relativistic) shocks of isolated supernova remnants (SNRs). The maximum energy that can be attained by a cosmic ray particle in an ordinary SNR when the remnant is passing through a medium of density $N_H\ cm^{-3}$ is [15, 265, 281]

$$E_{max} \simeq 4 \times 10^5 Z \left(\frac{E_{SN}}{10^{51}\ erg}\right)^{1/2} \left(\frac{M_{ej}}{10 M_\odot}\right)^{-1/6} \left(\frac{N_H}{3 \times 10^{-3}\ cm^{-3}}\right)^{-1/3} \left(\frac{B_o}{3\mu G}\right)\ GeV \tag{6.3}$$

which is falling short of the knee by about one order of magnitude. Energy released in BH formation explosions is at least two order higher than that in SN explosion. Moreover, as stated before, for relativistic shock acceleration E_{max} will be a factor Γ_s higher. Hence the minimum E_{max} for BH producing explosion should be of few PeV.

An important question for such a BH formation explosion origin of cosmic rays is whether or not E_{max} could reach the ankle energy. Unlike almost constant energy released in SN explosions, energy output in such a scenario varies and it may go at least up to 2 order high from its minimum value. And such high energy events are expected to occur in more rarefied medium. Hence it is very likely that the maximum E_{max} will exceed the ankle energy.

Interestingly for AGN minimum E_{max} is about 3 PeV [307] which is the knee energy and the maximum E_{max} can be many order higher than that owing to the wide range of luminosities of AGNs.

6.3.3 Energy Spectrum:

In the proposed model cosmic rays are accelerated in diffusive relativistic shock acceleration. The energy spectrum of accelerated particles in each source is, therefore, given by a power law

$$\frac{dn}{dE} = AE^{-\gamma} \tag{6.4}$$

with γ is around 2.2, and A is the normalization constant

$$A \equiv \frac{\epsilon}{(\gamma-2)(E_{min}^{-\gamma+2} - E_{max}^{-\gamma+2})} \tag{6.5}$$

where E_{min} and E_{max} are respectively the minimum and maximum attainable energies of cosmic ray particles in the source.

All the sources do not have the same E_{max}. Above the minimum possible E_{max}, which is denoted as E_{max}^{min}, the spectrum will be modified due to the distribution of E_{max}. To get the spectrum beyond the E_{max}^{min} it is needed to obtain maximum energy distributions of the cosmic ray sources from the mass distribution of their progenitors. The calculation involves a sequence of steps. Using the expression for explosion energy as function of progenitor mass as obtained in the previous section, the resulting explosion energy-progenitor mass relation is convolved with the initial mass function of the progenitors to obtain explosion energy distribution. Subsequently using the relation of maximum energy that a cosmic ray particle may attain in relativistic shock acceleration process with explosion energy, the maximum energy distribution for main cosmic ray sources is derived. Using such distribution the energy spectrum of cosmic rays beyond the E_{max}^{min} is obtained.

The stellar initial mass function, or distribution of masses with which stars are formed can be represented by a declining power law

$$\frac{dn}{dM} \propto M^{-\alpha} \tag{6.6}$$

with the universal (Salpeter) value of the exponent $\alpha = -2.35$ over the whole mass range above $3M_{\odot}$ [297, 300, 306]. Since explosion energy (ϵ) scales linearly with M, the expected explosion energy distribution of massive progenitor stars, is also represented by $\frac{dn}{d\epsilon} \propto \epsilon^{-\alpha}$.

The Lorentz factor of relativistic shock is nearly equal to the initial Lorentz factor of the jet i.e. $\Gamma_s \sim \gamma_o$. The relativistic shock waves must carry a significant fraction of the explosion energy which subsequently convert to energies of cosmic rays. Hence Γ_s should be proportional to explosion energy. On the other hand E_{max} is also proportional to Γ_s. So for the proposed model, $E_{max} \propto \epsilon$. Thus

$$\frac{dn}{dE_{max}} \propto E_{max}^{-\alpha} \tag{6.7}$$

. Therefore, the number of sources having $E_{max} \geq E$ is $j(E_{max} \geq E) \propto E_{max}^{-\alpha+1}$. As the minimum E_{max} of a source is equal to E_{max}^{min} all such sources will contribute

to cosmic ray flux when cosmic ray energy is below or equal E_{max}^{min}. However, for energies above the E_{max}^{min} ($E > E_{max}^{min}$) only sources having $E_{max} \geq E$ will contribute. The resultant cosmic ray spectrum above the E_{max}^{min} will be

$$\begin{aligned} \frac{dn}{dE} &= \int_E \frac{dn}{dE_{max}} A E^{-\gamma} dE_{max} \\ &\propto E^{-\gamma-\alpha+2} \end{aligned} \tag{6.8}$$

Therefore beyond the E_{max}^{min} the spectrum should be steepen by 0.35 in spectral index as observed. Note that the difference in power of energy by one between the above equation and the Eq.(3) of Kachelriess and Semikoz [294], where power law distribution of maximum attainable energy of sources was assumed, is due to the fact that our normalization constant A is proportional to the explosion energy (and hence to maximum attainable energy) unlike the explosion energy independent normalization constant as adopted in [294].

6.3.4 Mass composition

According to the proposed model, cosmic rays below and just above the E_{max}^{min} are produced in BH formation explosions of comparable progenitor's mass. Hence there should not be any abrupt change in mass composition through the E_{max}^{min}. In this model higher energy particles originate from the sources of heavier progenitor. Since BH is the last stage of evolution of massive stellar objects, the composition is unlikely to change much for BHs of heavier progenitors. Therefore, the resulting composition of accelerated cosmic rays in the proposed model is expected to remain almost unaltered with energy or may become slightly heavier at higher energies.

6.4 Discussion

Now the outcomes of the proposed model will be compared against the observational features of cosmic rays.

The conventional estimate of cosmic ray luminosity of our galaxy is $\sim 5{\times}10^{40}\ erg\ s^{-1}$. As shown the previous section, the proposed model yields a cosmic ray luminosity equals to $3\rho_{BH}\zeta \times 10^{43}$ ergs/s. Typically ζ ranges from 0.01 to 0.1 whereas ρ_{BH} is around 0.5 [cla15]. Therefore, the power from the BH producing explosions in

the galaxy satisfies the power requirement for accelerating all galactic cosmic rays. Note that with the rate of occurrence one per thirty years and the average energy released in each supernova explosion around 10^{51} ergs, SNRs satisfy the energy budget of observed cosmic rays (hence favored as main source of cosmic rays) provided energy conversion efficiency parameter ζ is relatively higher, around 0.1 to 0.2.

The maximum energy that can be attained by a cosmic ray particle in relativistic shock acceleration under the framework of the proposed model varies from source to source (of the same kind). Because of the relativistic effect (through the Lorentz factor) and owing to the much larger explosion energy, the minimum E_{max} for cosmic rays is found equal to few PeV as shown in the previous section which can be identified as the knee energy. Interestingly the minimum E_{max} for AGN is about 3 PeV [307]. Whereas the maximum E_{max} is found to exceed even the ankle energy. So the maximum attainable energy requirement is satisfied in a generic way. In contrast the maximum energy that can be attained by a cosmic ray particle in an ordinary SNR is 0.3 PeV which is falling short of the knee by about one order of magnitude unless the idea of magnetic amplification is invoked. Even with magnetic amplification it is difficult to exceed 100 PeV and thereby a new source of unknown nature is required between 100 PeV and the ankle energy. Since the proposed model relies on the standard shock acceleration theory, the overall cosmic ray production spectrum will follow power law behavior with spectral index equals to -2.2. Due to diffusive propagation of cosmic rays through the interstellar medium the slope of the spectrum observed at the Earth should be steepen to ~ 2.7 till the knee of the spectrum and the knee should be a sharp one as observed. Above the knee the spectrum will be modified by 0.35 due to the distribution of E_{max} as demonstrated in section 6.3.3. Thus the proposed model explains well the observed features of energy spectrum of primary cosmic rays.

In respect to mass composition of cosmic rays, particularly above the knee energy,the model predicted composition is similar to that of the cannonball model but different than the prediction of supernova model of cosmic ray origin.

Very recent findings by the KASCADE-GRANDE collaboration about the existence of a Fe-knee around 80 PeV along with the heavier dominated composition scenario [257–259] together with earlier results of KASCADE experiment for a proton knee at 3 PeV [256] do not support the composition picture predicted by the proposed model. Importantly in the overlapping energy region around 1 EeV, the composition scenario inferred from the KASCADE-GRANDE or ICETOP findings

of mixed composition with nearly same contribution from proton and Iron [256] is not in agreement with a proton dominated chemical composition as emerged from the observations of Pierre Auger Observatory [251] , HiRes [249, 250] and Telescope Array [293, 310]. This only shows the difficulty in estimating primary masses from air shower experiments that rests on comparisons of data to EAS simulations with the latter requires hadronic interaction models as input which are still uncertain to a large extent at present. Moreover, the uniqueness of solutions of primary energy spectra in the knee region from EAS data is also questioned [308] . It is expected that the mass composition scenario predicted by the present model will motivate newer experiments, exploiting both e/m and optical techniques, to establish unambiguous cosmic ray mass composition in the knee region and in particular to confirm the KASCADE-Grande results including the Fe-knee.
An important question is to identify the sources or more precisely identifying the gravitational explosions those lead to formation of black holes. The viable galactic sources resulting in BH formation include SN 1b/1c, hypernovae whereas GRB and AGN seem possible extragalactic sources. The observed rate of Type 1b and 1c SNe is around $10^{-3}\ yr^{-1}$ which is close to the rate of stars having mass greater than $20M_{\odot}$. Radio observations suggest that about 5% SN 1b/1c can be produced in GRBs [262]. Earlier Sveshnikova demonstrated that hypernovae can satisfy the power requirement for accelerating all galactic cosmic rays [25] assuming the rate of hypernovae is about $10^{-4}\ y^{-1}$. Extragalactic origin of cosmic rays is usually considered as unlikely on the energetic grounds. However, such a problem can be circumvented by employing flux trapping hypothesis as proposed in [111, 270]. Hence the possibility of GRB/AGN as the sole kind of dominate source of cosmic ray source cannot be totally ruled out from energetic consideration.

6.5 Conclusion

In summary, the proposed speculative BH based model of origin of cosmic rays can account all the major observed features about cosmic rays without any serious contradiction to observational results. The knee of the energy spectrum has been ascribed as the consequence of the mass distribution of progenitor of cosmic ray source. Such a philosophy seems applicable to the Cannonball model of cosmic ray origin replacing the original proposal of second order Fermi acceleration of cosmic rays by Cannonballs of other SN explosions as the cause of spectral steepening

above the knee [112, 114, 277, 278]. Precise measurement of primary mass composition can be used to discriminate the proposed model from most of the standard prevailing models of cosmic ray knee. No definite cosmic ray sources could be identified at this stage within the framework of the proposed model which would be an important future task for further development of the proposed model.

Chapter 7

Discussion

7.1 Summary and discussion

The problem of origin of the knee in the cosmic ray energy spectrum is a difficult one to explain or even understand. It is widely believe that the knee in the energy spectrum is an inscription of either cosmic ray sources or acceleration mechanism or propagation characteristics and hence proper understanding of this interesting spectral feature may shed light on the long standing problem of cosmic ray origin.

In the present thesis work we first examine critically the existence of the knee in the primary energy spectrum. The knee feature in the primary energy spectrum is inferred mainly from the size (total number of particles) spectrum of electrons in cosmic ray EAS. It is also expected from theoretical consideration that the knee feature also should reveal from EAS muon size spectrum. We, therefore, have checked whether the knee in the primary energy spectrum is revealed consistently from both electron size and muon size spectra by analysing results obtained by EAS-TOP and KASCADE experiments. The interpretation of the EAS results in terms of primary cosmic rays requires Monte Carlo simulation study of EAS that relies on the high energy particle interaction models. Since our knowledge of particle interactions is somewhat uncertain at high energies as the accelerator data for relevant target-projectile combinations covering the whole kinematic region are not yet available, we first compare the simulated atmospheric proton and antiproton spectra obtained with different low energy hadronic interaction models with those measured by BESS experiment at high altitude. We found that out of the different models used, UrQMD describes the overall experimental data better.

At higher energies QGSJET -1c is found to describe the LHC data, at least major features such as pseudo-rapidity distribution, transverse momentum distribution, cross-section and multiplicity, reasonably well. Hence we choose combination of these two interaction models, QGSJET and UrQMD, as input in our Monte Carlo simulation study of EAS.

It was found from the present analysis that the EAS-TOP observations on total charged particle and muon spectra consistently infer a knee in the primary energy spectrum provided the primary is pure unchanging iron whereas no consistent primary spectrum emerges from simultaneous use of the KASCADE observed total charged particle and muon spectra. However, it has been noted from the analysis that the derivation of the size spectrum from observed data is a quite complex issue, particularly owing to the uncertainty in primary mass composition. The simultaneous use of the measured EAS total charged particle and muon size spectra to infer the primary energy spectrum requires a careful and experiment specific analysis.

Finally a model of knee has been proposed in which the steepening of the spectrum beyond the knee is explained in terms of the mass distribution of the progenitor of the cosmic ray source. The proposed speculative model can account for all the major observed features of cosmic rays without invoking any fine tuning to match flux or spectra at any energy point. A prediction of the proposed model is that the mass composition of primary cosmic rays should remain almost the same below and above the knee energy which is consistent what we found from EAS-TOP data after simultaneous use of the measured EAS total charged particle and muon size spectra to infer the primary energy spectrum. Such a prediction about primary mass composition is quite different from most of the prevailing models of the knee, and thereby can be discriminated from future precise experimental measurements of the primary composition. Other observational consequences, if any, of the proposed models will be investigated in future.

Bibliography

[1] V. Hess, *Phys.Zeitsch.* 13 (1912), 1084–1091.

[2] J. Blümer et al., *ProgressinParticleandNuclearPhysics* 63 (2009) 293–338.

[3] G.V. Kulikov, G.B. Khristiansen, *Zh.Éksp.Teor.Fiz.*, 35:635–640, 1958

[4] G.V. Kulikov, G. B. Khristiansen, *JETP*, **35**, 441-444 (1959).

[5] Stanev T., et al., 1993, *Astron.&Astroph.* 274, 902

[6] Swordy S. P. et al., 2001, *Astropart.Phys.* 13, 137

[7] A.A. Lagutin et al., *Nucl.Phys.B(Proc.Suppl.)* 97 (2001) 267.

[8] A.A. Lagutin et al., *Proc.27thInt.CosmicRayConf.*, Hamburg 5 (2001) 1896 and 1900.

[9] V.S. Ptuskin et al., *Astron.&Astroph.* 268 (1993) 726.

[10] S. Ogio, F. Kakimoto, *Proc.28thInt.CosmicRayConf.*, Tsukuba 1 (2003) 315.

[11] R. Roulet, preprint $astro - ph/0310367$, J. Candia et al., *JournalofCosmologyandAstropart.Phys.* 0305 (2003) 003

[12] Candia, J., Roulet, E., and Epele, N. 2002, *JHEP* 0212, 033

[13] Candia, J., Epele, L. N. and Roulet, E. 2002 *Astropart.Phys.* 17, 23

[14] Candia, J et al., *JHEP* 0212 (2002) 032.

[15] Berezhko, E.G. and Ksenofontov, L.T., 1999, *JETP* 89, 391

[16] Karakula, S. and Tkaczyk, W., 1993 *Astropart.Phys.* 1, 229

[17] W. Tkaczyk, *Proc.27thInt.CosmicRayConf.*, Hamburg 5 (2001) 1979

[18] Erlykin, A.D. and Wolfendale, A.W., 1997 $J.Phys.G : Nucl.Part.Phys.$ 23, 979

[19] A.D. Erlykin and A.W. Wolfendale, $J.Phys.G : Nucl.Part.Phys.$ 27 (2001) 1005 and references therein.

[20] Erlykin, A. D., Martirosov, R. and Wolfendale, A. 2011, $CERNCourier$, 51, 21

[21] D. Kazanas and A. Nicolaidis, eprint $arXiv : astro - ph/0103147$ (2001).

[22] D. Kazanas and A. Nicolaidis, eprint $arXiv : astro - ph/0109247$ (2001).

[23] Sveshnikova, L. G., 2003 Astron. Astroph. 409, 799

[24] Sveshnikova, L. G., $Proc.28thInt.CosmicRayConf.$, Tsukuba 1 (2003) 307.

[25] Sveshnikova, L. G., 2004 $Astron.Letts.$ 30, 41

[26] Greisen, K., 1966, $Phys.Rev.Lett.$ 16, 748

[27] Zatsepin, G. T. and Kuz'min, V.A., 1966, $Zh.Eksp.Teor.Fiz., PismaRed.$ 4, 144

[28] Zatsepin, G. T. and Kuz'min, V.A., 1966, $Sov.Phys.JETPLett.$ 4, 78

[29] Watson A. A., 2007, $HighlightTalkat30thICRC(Mérida, Mexico)$

[30] Abraham, J. et al, 2008, $Phys.Rev.Lett.$ 101, 061101

[31] J. Hörandel, $Adv.SpaceRes.$ 38 (2006) 1549.

[32] J. Simpson, $Ann.Rev.Nucl.Part.Sci.$ 33 (1983) 323–381.

[33] K. Lodders, $Astrophys.J.$, 591 (2003) 1220.

[34] J. Alcaraz, et al., $Phys.Lett.B$ 490 (2000) 27.

[35] N. L. Grigorov et al., $Sov.J.Nucl.Phys.$ 11 (1970), 1058–1069.

[36] N. L. Grigorov et al., $Proc.12thInt.CosmicRayConf.$, Hobart 5, 1971, p. 1760

[37] P. Fowler, et al., $Astrophys.J.$ 314 (1987) 739.

[38] P. Fowler, et al., $Nucl.Instrum.Methods$ 147 (1977) 195.

[39] W. Binns, et al., *Astrophys.J.* 346 (1989) 997.

[40] E. Shirk, et al., *Astrophys.J.* 220 (1978) 719.

[41] D. Lawrence, et al., $Nucl.Instrum.MethodsA$ 420 (1999) 402.

[42] B. Weaver, et al. in: $Proc.of27thInt.CosmicRayConf.$, Hamburg 5, 2001, p. 1720.

[43] J. Tueller, M. Israel, W.R. Binns, et al., Ap. J. 247 (1981) L115.

[44] J. Donelly, et al. in: $Proc.of26thInt.CosmicRayConf.$, Salt Lake City 3, 1999, p. 109.

[45] I. Ivanenko, et al. in: $Proc.of23rdInt.CosmicRayConf.$, Calgary 2, 1993, p. 17.

[46] V. Zatsepin, et al. in: $Proc.of23rdInt.CosmicRayConf.$, Calgary 2, 1993, p. 14.

[47] W. Webber, et al. in: $Proc.of20thInt.CosmicRayConf.$, Moscow 1, 1987, p. 325.

[48] D. Müller, et al., *Astrophys.J.* 374 (1991) 356

[49] J. Wefel, et al. in: $Proc.of29thInt.CosmicRayConf.$, Pune 3, 2005, p. 105.

[50] T. Sanuki et al., *AstrophysJ.* **545** (2000) 1135.

[51] T. Sanuki et al., *Phys.Lett.B* **577** (2003) 10.

[52] T. Sanuki, M. Honda, T. Kajita, K. Kasahara and S. Midorikawa, *Phys.Rev.D* **75** (2007) 043005.

[53] M. Boezio, et al., *Astropart.Phys.* 19 (2003) 583.

[54] M.D. Vernois, et al. in: $Proc.of27thInt.CosmicRayConf.$, Hamburg 5, 2001, p. 1618.

[55] M. Ichimura, et al., *Phys.Rev.D* 48 (1993) 1949.

[56] M. Menn, et al., *Astrophys.J.* 533 (2000) 281.

[57] K. Asakimori, et al. in: $Proc.of24thInt.CosmicRayConf.$, Rome 2, 1995, p. 707.

[58] K. Asakimori, et al., *Astrophys.J.* 502 (1998) 278.

[59] R. Bellotti, et al., *Phys.Rev.D* 60 (1999) 052002.

[60] P. Papini, et al. in: *Proc.of23rdInt.CosmicRayConf.*, Calgary 1, 1993, p. 579.

[61] V. Derbina, et al., *Astrophys.J.* 628 (2005) L41.

[62] L. Smith, et al., *Astrophys.J.* 180 (1973) 987.

[63] D. Müller, et al. in: *Proc.of29thInt.CosmicRayConf.*, Pune 3, 2005, p. 89.

[64] E. Diehl, et al., *Astropart.Phys.* 18 (2003) 487.

[65] M. Ryan, et al., *Phys.Rev.Lett.* 28 (1972) 985.

[66] P. Auger, R. Maze, and T. Grivet-Meyer, C. R. Acad. *Sci.*, 206:1721–1723, 1938.

[67] W. Kolhörster, I. Matthes, and E. Weber, *Naturwissenschaften*, 26(35):576, 1938. doi: 10.1007/BF01773491.

[68] R. Engel, et al., *Annu.Rev.Nucl.Part.Sci.* 2011. 61:467–89

[69] Haungs, A., *Rep.Prog.Phys.* 66 (2003) 1145–1206

[70] Lawrence M A, Reid R J O and Watson A A 1991 *J.Phys.G.* : *Nucl.Part.Phys.* 17 733

[71] Baltrusaitis R M et al 1985 *Nucl.Instrum.MethodsPhys.Res.A* 240 410

[72] Bird D et al 1995 *Astrophys.J.* 441 144

[73] Abu-Zayyad T et al 2001 *Astrophys.J.* 557 686

[74] Nagano M et al 1984 *J.Phys.G* : *Nucl.Phys.* 10 1295

[75] Nagano M et al 1992 *J.Phys.G* : *Nucl.Phys.* 18 423

[76] M. Aglietta et al. (EAS-TOP collab.) *ILNuovoCim.9C*, 262 (1986)

[77] M. Aglietta et al. (EAS-TOP collab.), 1999 *Astropart.Phys.* 10 1

[78] Glasmacher M. A. K., et al, 1999, *Astropart.Phys.* 10, 291

[79] Glasmacher, M. et al.(CASA-MIA Collab.), 1999, *Astropart.Phys.* 12, 19

[80] Fowler, J. W., et al, 2001 *Astropart.Phys.* 15, 49

[81] Arqueros, F et al 2002 *Astron.Astrophys.* 359 682

[82] Knurenko, S et al 2001 $Proc.27thICRC(Humburg)$ vol 1 p 145

[83] Gupta, S. et al 2005 $NuclearInstrumentsandMethodsinPhysicsResearchA$ 540 (2005) 311–323

[84] Ogio, S. et al 2004 *Astrophys.J.* 612 268

[85] Antoni, T. et al 2005 *Astropart.Phys.* 24 1

[86] Amenomori, M. et al 2008 $arXiv : 0801.1803v2$

[87] Hillas, A. M., 1985, $Proc.19thICRC(LaJolla)$ vol 1, p 155

[88] Engel, J., et al, 1992, $Phys.Rev.D$ 46, 5013

[89] Fletcher, R S et al, 1994, $Phys.Rev.D$ 50, 5710

[90] Engel, J., et al, 1999, $Proc.26thICRC(SaltLakeCity, USA)$ vol 1, p 415

[91] Heck, D. et al 1998 $FZKA$ 6019 (Institut für Kernphysik, Forschungszentrum Karlsruhe)

[92] Heck, D. and Knapp J 1998 $FZKA$ 6097 (Forschungszentrum Karlsruhe)

[93] Kalmykov, N. N. and Ostapchenko, S. S. 1993 Yad. Fiz. 56 105

[94] N. N. Kalmykov, S. S. Ostapchenko and A. I. Pavlov, $Nucl.Phys.B(Proc.Suppl.)$ **52** (1997) 17.

[95] Ostapchenko, S. S. 2006 $Phys.Rev.D$ 74 014026

[96] H. Ulrich et al. (KASCADE Collaboration), $Proc.27thInt.CosmicRayCon.$, Hamburg 1 (2001) 97

[97] H. Ulrich et al. (KASCADE Collaboration), $Nucl.Phys.B(Proc.Suppl.)$ 122 (2003) 218.

[98] M. Roth et al. (KASCADE Collaboration), $Nucl.Phys.B(Proc.Suppl.)$ 122(2003) 317.

[99] M. Roth et al. (KASCADE Collaboration), $Proc.28thInt.CosmicRayConf.$, Tsukuba 1 (2003) 139.

[100] J.R. Hörandel et al. (KASCADE Collaboration), preprint $astro-ph/0311478$.

[101] M. Aglietta et al., *AstroparticlePhysics* 19 (2003) 329.

[102] M. Bertaina et al., $Proc.28thInt.CosmicRayConf.$, Tsukuba 1 (2003) 115.

[103] D.Horns et al., $Proc.27thInt.CosmicRayConf.$, Hamburg 1 (2001) 101.

[104] W.R. Nelson, H. Hirayama and D.W.O. Rogers, $ReportSLAC265(1985), StanfordLinearAcceleratorCenter$, http://www.slac.stanford.edu/pubs/slacreports/slac-r-265.html, http://www.irs.inms.nrc.ca/inms/irs/EGS4/get egs4.html

[105] H. Fesefeldt, $RWTHAachenReportNo.PITHA-85/02$, 1985.

[106] K. Werner, *Phys.Rep.* **232** (1993) 87.

[107] K. Werner, F. M. Liu and T. Pierog, *Phys.Rev.C* **74** (2006) 044902.

[108] Kobayakawa, K. et al., 2002, *Phys.Rev.D* 66, 083004

[109] K.M. Schure, A.R. Bell, eprint $arXiv:1209.3043v1$ (2012)

[110] H.J. Volk and V.N. Zirakashvili, $Proc.28thInt.CosmicRayConf.$, Tsukuba 4 (2003) 2031.

[111] Plaga, R. 2001 *Astron.Astrophys.*330, 833

[112] Plaga, R., 2002 $NewAstronomy$, 7, 317

[113] M.T. Dova et al, $astro-ph/0112191$

[114] De Rujula, A., 2005 $Int.J.Mod.Phys.A20$, 6562

[115] Hillas, A. M., 1979 $Proc.16thInt.CosmicRayConf.$, 8, 7

[116] Hillas, A. M. 1984, *Ann.Rev.Astron.Astrophys.* 22, 425.

[117] Kasahara, K, Torii S and Yuda T 1979 $Proc.16thICRC(Kyoto)$ vol 13 p 70

[118] K. Amako, $NuclearInstrumentsandMethodsinPhysicsResearchA$, Vol. 453, P. 455, 2000.

[119] "GEANTDetector description and simulation tool",$CERNProgramLibrary$ Long Write-up W5013, CERN

[120] L. A. Anchordoqui et al, $arXiv : astro - ph/0006141$

[121] S. Béné et al, *Geosci.Instrum.Method.DataSyst.*, 2, 11–15, 2013, doi:10.5194/gi-2-11-2013

[122] M. S. Sabra et al, $APSAprilMeeting$2015, Baltimore, MD, document ID : 20150006841

[123] http://geant4.web.cern.ch/geant4/G4UsersDocuments/UsersGuides/PhysicsReferenceMa

[124] R.J. Glauber, in "$HighEnergyPhysicsandNuclearStructure$", edited by S. Devons (Plenum Press, NY 1970).

[125] Sciutto, S. J. 1999 $arXiv : astroph/9911331$

[126] Ding, L. K. et al 1984 $Proc.Int.Symp.onCosmicRaysandParticlePhysics(InstituteforC$ ed T. Yuda and A. Ohsawa p 142

[127] H. J. Drescher, M. Hladk, S. Ostaptchenko, T. Pierog and K. Werner, *Phys.Rep.* **350** (2001) 93.

[128] T. Pierog, H. J. Drescher, F. Liu, S. Ostapchenko and K. Werner, $Nucl.Phys.A$ **715** (2003) 895c.

[129] J. Ranft, $Phys.Rev.D51$ (1995) 64

[130] J. Ranft, 1999, $arXiv : hep - ph/9911213$

[131] J. Ranft, 1999, $arXiv : hep - ph/9911232$

[132] S. Roesler, R. Engel and J. Ranft, hep-ph/0012252, in *Proceedings of the Monte Carlo 2000 Conference (Lisbon)* (Springer, Berlin, 2001), p. 1033.

[133] S. A. Bass et al., $Prog.Part.Nucl.Phys.$ **41** (1998) 225.

[134] M. Bleicher et al., $J.Phys.G$**25** (1999) 1859.

[135] G. Battistoni, S. Muraro, P. R. Sala, F. Cerutti, A. Ferrari, S. Roesler, A. Fassò, and J. Ranft in (M. Albrow and R. Raja eds.) *Proceedings of the Hadronic Shower Simulation Workshop, Fermilab 6-8 September 2006*, AIP Conference Proceeding **896** (2007) p. 31.

[136] A. Ferrari, P. R. Sala, A. Fassò and J. Ranft, $ReportCERN - 2005 -$ 10(2005), INFN-TC_05/11, SLAC-R-773 (2005).

[137] A.A. Lagutin, A.V. Plyasheshnikov, and V.V. Uchaikin, *Proc.*16*thInt.CosmicRayConf.*, Kyoto (Japan), 7 (1979) 18;

[138] J.N. Capdevielle for KASCADE Collaboration, *Proc.*22*ndInt.CosmicRayConf.*, Dublin (Ireland), 4 (1991) 405

[139] V. N. Gribov, *Sov.Phys.JETP* **26** (1968) 414.

[140] T. Sjostrand, *Comp.Phys.Comm.* 82 (1994) 74

[141] B. Andersson et al., *Phys.Rep.* 97 (1983) 31

[142] T. Sjostrand, *Comp.Phys.Comm.* 39 (1986) 347

[143] A. Ferrari, J. Ranft, S. Roesler and P.R. Sala, *Z.Phys.* C70 (1996) 413, *Z.Phys.* C71 (1996) 75

[144] R.J. Glauber and G. Matthiae, *Nucl.Phys.B* 21 (1970) 135

[145] K.G. Boreskov and A.B. Kaidalov, *Sov.J.Nucl.Phys.* 48 (1988) 367

[146] F. M. Liu, J. Aichelin, M. Bleicher, H. J. Drescher, S. Ostapchenko, T. Pierog and K. Werner, *Phys.Rev.D* **67** (2003) 034011.

[147] M. Bleicher, A. Keränen, J. Aichelin, S. A. Bass, F. Becattini, K. Redlich and K. Werner, *Phys.Rev.Lett.* **88** (2002) 20251.

[148] Werner, K., *NuclearPhysicsB*(*Proc.Suppl.*) 175–176 (2008) 81–87

[149] T. Pierog and K. Werner, *Nucl. Phys. Proc. Suppl.* **196** (2009) 102-105.

[150] D. S. Barton et al., *Phys.Rev.D* **27** (1983) 2580.

[151] V. N. Gribov, *Sov.Phys.JETP* **29** (1969) 483.

[152] V. N. Gribov, *Sov.Phys.JETP* **30** (1970) 709.

[153] A. Ferrari and P. R. Sala, in *Proceedings of the 1993 Conference on Monte Carlo Simulation in High Energy and Nuclear Phys. (Tallahassee, USA)* (World Scientific, Singapore, 1994) p. 277.

[154] A. Fassò, A. Ferrari, J. Ranft and P. R. Sala in *Proceedings of the Specialists Meeting on Shielding Aspects of Accelerators, Targets and Irradiation Facilities (Arlington, USA)* (OECD/NEA, 1994) p. 287.

[155] ALICE collaboration, *PhysicsLettersB*, Volume 753, 10 February 2016, Pages 319–329, doi:10.1016/j.physletb.2015.12.030

[156] B. Abelev et al. (ALICE Collaboration), *Phys.Rev.D* (2015) 91, 112012 – Published 22 June 2015

[157] G. Aad et al. (ATLAS Collab.), arXiv:1104.0326[hep-ex].

[158] C̃sörgö, T. et al (for the TOTEM Collaboration), 2012, *Prog. Theor. Phys. Suppl.* **193** 180

[159] Pierog, T., 2011, $Proc.32ndInt.CosmicRayConf.$, Beijing 5 (2011) 70.

[160] Pierog, T., *VHEPU*, Quy Nhon, Vietnam, 14^{th} August, 2015

[161] Pierog, T., *Prospectives IPHC*, Strasbourg, France, 18^{th} March, 2015

[162] S. Chatrchyan et al. (CMS Collab.), [arXiv:1104.3547 [hep-ex]].

[163] K. Aamodt et al. (ALICE) (2010), 1004.3514

[164] J. W. Mitchell et al., *Phys.Rev.Lett.* **76** (1996) 3057.

[165] M. Kamionkowski and M. S. Turner, *Phys.Rev.D* **43** (1991) 1774.

[166] G. Jungman, M. Kamionkowski and K. Griest, *Phys.Rep.* **267** (1996) 195.

[167] G. Bertone, D. Hooper and J. Silk, *Phys.Rep.* **405** (2005) 279.

[168] S. W. Hawking, $Nature(London)$ **248** (1974) 30.

[169] P. Kiraly, J. Szabelski, J. Wdowczyk and A. W. Wolfendale, $Nature(London)$ **293** (1981) 120.

[170] O. Adriani et al., *Phys.Rev.Lett.* **102** (2009) 051101.

[171] O. Adriani et al., *Phys.Rev.Lett.* **105** (2010) 121101.

[172] T. Abbott et al., *Phys.Rev.C* **47** (1993) R1351.

[173] F. Abe et al., *Phys.Rev.D* **50** (1994) 5550.

[174] K. Abe et al., *Phys.Lett.B* **564** (2003) 8.

[175] K. Abe et al., *Phys.Lett.B* **645** (2007) 472.

[176] N. Abgrall et al., $CERN - SPSC - 2008 - 018$ (2008).

[177] O. Adriani et al., *Nature* **458** (2009) 607.

[178] C. W. Akerlof et al., *Phys.Rev.D* **3** (1971) 645.

[179] J. Alcaraz et al., *Phys.Letts.B* **472** (2000a) 215.

[180] J. Alcaraz et al., *Phys.Letts.B* **494** (2000b) 193.

[181] N. A. Amos et al., *Phys.Rev.Lett.* **68** (1992) 2433.

[182] M. Aguilar et al., *Phys.Rep.* **366** (2002) 331.

[183] N. Antoniou et al., $CERN-SPSC-2007-004$ (2007); $CERN-SPSC-2007-019$ (2007).

[184] C. Avila et al., *Phys.Lett.B* **445** (1999) 419.

[185] M. Baker and K. A. Ter-Martirosyan, *Phys.Rep.* **28** (1976) 1.

[186] H. B. Barber et al., *Phys.Rev.D* **22** (1980) 2667.

[187] B. Baret, L. Derome, C. -Y. Huang and M. Buénerd, *Phys.Rev.D* **68** (2003) 053009.

[188] I. G. Bearden et al., *Phys.Letts.B* **607** (2005) 42.

[189] A. Bhadra, S. K. Ghosh, P. S. Joarder, A. Mukherjee and S. Raha, *Phys.Rev.D* **79** (2009) 114027.

[190] F. W. Bopp, J. Ranft, R. Engel and S. Roesler, *Phys.Rev.C* **77** (2008) 014904.

[191] T. Bowen and A. Moats, *Phys.Rev.D* **33** (1986) 651.

[192] A. Capella, U. Sukhatme, C.-I. Tan and J. Tran Thanh van, *Phys.Rep.* **236** (1994) 225.

[193] P. Capiluppi et al., *Nucl.Phys.B* **79** (1974) 189.

[194] M. Cirelli, M. Kadastik, M. Raidal and A. Strumia, *Nucl.Phys.B* **813** (2009) 1.

[195] F. Donato et al., *Astrophys.J.* **563** (2001) 172.

[196] H. J. Drescher, M. Bleicher, S. Soff and H. Stöcker, *Astropart.Phys.* **21** (2004) 87.

[197] R. P. Duperray, C. -Y. Huang, K. V. Protasov, and M. Buénerd, *Phys.Rev.D* **68** (2003) 094017.

[198] R. P. Duperray et al., *Phys.Rev.D* **71** (2005) 083013.

[199] T. K. Gaisser, M. Honda, P. Lipari and T. Stanev, in $Proceedings of the 27th International Cosmic Ray Conference$, Hamburg, Germany, 2001, Vol. 5, p. 1643.

[200] L. G. Gleeson and W. I. Axford, *AstrophysJ.* **154** (2004) 1011.

[201] S. Haino et al., *Phys.letts.B* **594** (2004) 35.

[202] D. Heck, J. Knapp, J. N. Capdevielle, G. Schatz and T. Thouw, $Forschungszentrum Karlsruhe Report No. FZKA6019$, 1998.

[203] D. Heck, $Nucl.Phys.B(Proc.Suppl.)$ **151** (2006) 127.

[204] D. Hooper, A. Stebbins and K. M. Zurek, *Phys.Rev.D* **79** (2009) 103513.

[205] C. -Y. Huang, L. Derome and M. Buénerd, *Phys.Rev.D* **68** (2003) 053008.

[206] J. R. Johnson et al., *Phys.Rev.D* **17** (1978) 1292.

[207] A. B. Kaidalov, $Surveys High Energ.Phys.$ **13** (1999) 265.

[208] M. Lattanzi and J. I. Silk, *Phys.Rev.D* **79** (2009) 083523.

[209] J. Linsley (private communication).

[210] K. G. McCracken, F. B. McDonald, J. Beer, G. Raisbeck and F. Yiou, *J.Geophys.Res.* **109** (2004) A12103.

[211] I. V. Moskalenko, A. W. Strong, J. F. Ormes and M. S. Potgieter, *Astrophys.J.* **565** (2002) 280.

[212] S. S. Ostapchenko, $Nucl.Phys.B(Proc.Suppl.)$ **151** (2006) 143 and 147.

[213] S. S. Ostapchenko, *Phys.Rev.D* **74** (2006) 014026.

[214] V. S. Ptuskin, I. V. Moskalenko, F. C. Jones, A. W. Strong and V. N. Zirakashvili, *Astrophys.J.* **642** (2006) 902.

[215] T. J. Sabaka, R. A. Langel and J. A. Conrad, *J.Geomag.Geoelect.* **49**, (1997) 157.

[216] M. A. Shea and D. F. Smart, *J.Geophys.Res.* **72** (1967) 2021.

[217] M. Simon, A. Molnar and S. Roesler, *Astrophys.J.* **499** (1998) 250.

[218] S. A. Stephens, *Astrophys.SpaceSci.* **76** (1981) 87.

[219] S. A. Stephens, *Astropart.Phys.* **6** (1997) 229.

[220] S. A. Stephens, *Adv.SpaceRes.* **35** (2005) 142.

[221] Y. Sugaya et al., *Nucl.Phys.A* **634** (1998) 115.

[222] I. G. Usoskin, A. -H. Katja, G. A. Kovaltsov and K. Mursula, *J.Geophys.Res.* **110** (2005) A12108.

[223] B. Weibel-Sooth, P. L. Biermann and H. Mayer, *Astron.Astrophys.* **330** (1998) 389.

[224] K. Yamato et al., *Phys.Lett.B* **632** (2006) 475.

[225] C. E. Fichtel, and J. Linsley, *Astrophys.J.* **300**, 474 (1986)

[226] V. L. Ginzburg, and S. I. Syrovatskii, 1964, $TheOriginofCosmicRays$, Macmillan, NewYork.

[227] A. D. Erlykin, A. W. Wolfendale, $J.Phys.G$: $Nucl.Part.Phys.$ **23**, 979 (1997).

[228] B. Bijay and A. Bhadra, Res. $Astron.Astrophys.(toappear)$ (2015); eprint $arXiv$: 1412.0818.

[229] S. I. Nikolsky, and V. A. Romachin, $PhysicsofAtomicNuclei$, **63**, 1799 (2000).

[230] D. Kazanas and A. Nicolaidis, eprint $arXiv : astro - ph/0103147$ (2001).

[231] Yu. V. Stenkin, $Mod.Phys.Lett.$ **A18** 1225 (2003) .

[232] Yu. V. Stenkin, $Nucl.Phys.B(Proc.Suppl.)$ **151**, 65 (2006)

[233] D M Gromushkin et al., $J.Phys.(Conf.Series)$ **409**, 012044 (2013).

[234] D. Heck, J. Knapp, J. N. Capdevielle, G. Schatz and T. Thouw, $ForschungszentrumKarlsruheReportNo.FZKA6019$, (1998).

[235] J. Matthews, *Astropart.Phys.* **22** 387 (2005).

[236] J. R. Hoerandel, *Mod.Phys.Lett.A* **22** 1533 (2007)

[237] N. N. Kalmykov, S. S. Ostapchenko and A. I. Pavlov, *Nucl.Phys.B, Proc.Suppl.* **52** 17 (1997).

[238] M. Bleicher et al., *J.Phys.G***25** 1859 (1999).

[239] K. Werner, F. M. Liu and T. Pierog, *Phys.Rev.C* **74** 044902 (2006).

[240] H. Fesefeldt, *RWTH Aachen Report No. PITHA* – 85/02, (1985).

[241] H. J. Drescher, M. Bleicher, S. Soff and H. Stöcker, *Astropart.Phys.* **21** 87 (2004).

[242] A. Bhadra, S. K. Ghosh, P. S. Joarder, A. Mukherjee and S. Raha, *Phys.Rev.D* **79** 114027 (2009).

[243] T. Antoni, et.al. (KASCADE collab.), *Nucl.Instru.Meth.* **513** 490 (2003)

[244] R. Glasstetter et al., *Proc.Int.CosmicRayConf.* **6**, 157 (1997)

[245] T. Antoni et. al (KASCADE collab.), *Astropart.Phys.* **16** 373 (2002)

[246] G. Navarra et al (EAS-TOP collab.), *Nucl.Phys.B*(*Proc.Suppl.*) 60, 105 (1998)

[247] kcdc.ikp.kit.edu (KIT, Karlsruhe Institute of Technology)

[248] Aartsen, M.G. et al. (ICETOP Coll.), 2013 *Phys.Rev.D* 88, 042004

[249] Abbasi, R. et al., 2008, *Phys.Rev.Lett.* 100, 101101

[250] Abbasi, R. et al., 2004, *Phys.Rev.Lett.* 92, 151101

[251] Abraham, J., 2010, *Phys.Rev.Lett.* 104, 091101

[252] Aglietta, M. et al., 1990 *Nucl.Phys.*(*Proc.Supl.*) 14B, 193

[253] Ahlen, S. et al., 1992 *Phys.Rev.D* 46, 4836

[254] Aloisio, R., Berezinsky, V. and Gazizov, A., 2012 *Astropart.Phys.* 39-40, 129

[255] Amato, E., 2014 Int. *J.Mod.Phys.D*, 23, 1430013

[256] Apel, W.-D. et al.(KASCADE Collaboration), 2010 *Astropart.Phys.* 31, 86

[257] Apel, W.-D. et al.(KASCADE Collaboration), 2011 *Phys.Rev.Lett.* 107, 171104

[258] Apel, W.-D. et al.(KASCADE Collaboration), 2012 *Astropart.Phys.* 36, 183

[259] Apel, W.-D. et al.(KASCADE Collaboration), 2013 *Phys.Rev.D*87, 081101

[260] Arqueros, F. et al., 2000, *Astron.Astrophys.* 359, 682

[261] Bakatanov, V. N. et al., 1999 *Astropart.Phys.* 12, 19

[262] Berger, E. et al., 2003 ApJ599, 408

[263] Bhadra, A. and Sanyal, S., 2005, in $Proc.29thInt.CosmicRayConf.$, 6, 137

[264] Bhadra, A., 2005 $Proc.29thInt.CosmicRayConf.$ 3, 117

[265] Biermann, P. L., 1993, *Astron.&Astroph.* 271, 649

[266] Blake, P. R. and Nash, M.F., 1995 $J.Phys.G : Nucl.Part.Phys.$ 21, 1731

[267] Blake, P. R. and Nash, M.F., 1998 $J.Phys.G : Nucl.Part.Phys.$ 24, 217

[268] Blasi, P. 2014 *R.Physique* 15, 329

[269] Boothby, K., et al., 1997 *Astrophys.J* 491, L35

[270] Burbidge, G., 1962 *Prog.Theor.Phys.* 27, 999

[271] Chakrabarty, C. et al., 1998 $ILNuovoCim.$ 21, 215

[272] Christodoulou, D. and Ruffini, R. 1971 *Phys.Rev.D* 4, 3552

[273] Cherev, D. et al., 2004, $astro-ph/0411139$

[274] Clausen, D., Piro, A.L. and Ott, C. D., 2015 *Astrophys.J.* 799, 190

[275] C. W. Akerlof et al., *Phys.Rev.D* **3** (1971) 645.

[276] Danilova, E. V. et al., 1995 $Proc.24thInt.CosmicRayConf$, 1, 286

[277] Dar, A. and Plaga, R. 1999 *Astron.&Astroph.* 349, 259

[278] Dar, A., 2005 $NuovoCim.B$ 120, 767

[279] Dickinson, J. E. et al., 1999, in $Proc.26thIntCosmicRayConf.$ 3, 136

[280] Efimov, N. N. et al., 1991, $Proc.Int.Symp.astrophysicalaspectsofmostenergeticcosmicra$
Ed. M. Nagano, and F. Takahara, p 20

[281] Fichtel, C.E. and Linsley, J. 1986, ApJ300, 474

[282] Fomin, Y. et al., 1996 $J.Phys.G : Nucl.Part.Phys.$ 22, 1839

[283] Fryer, C. L. 1999 ApJ522, 413

[284] Fryer, C. L. and Heger, A. 2000 ApJ541, 1033

[285] Fryer, C. L. 2003 $Class.QuantumGrav.$ 20, S73

[286] Giacinti, G., Kachelrie, M., and Semikoz, D. V. 2014, *Phys.Rev.D* 90, 041302(R)

[287] Ginzburg, V. L. and Syrovatskii, S. I. 1964, $TheOriginofCosmicRays$, Macmillan, NewYork

[288] Haungs, A., 2011 $SpaceSc.Trans$, 7, 295

[289] Heger, A. and Fryer, C. L. 2003 ApJ591, 288

[290] Hörandel, J.R., 1993, $AIPConf.Proc.$, 1516, 185

[291] Hu, H-B., et al, 2009, ApJ, 700, L170

[292] Jokipii, J.R. and Morfill, G.E. 1986, ApJ312, 170

[293] Jui, C. C., 2012, $J.Phys.Conf.Ser.$ 404, 012037

[294] Kachelriess, M. and Semikoz, D. V. 2005 $arXiv : astro - ph/0510188$

[295] Karle, A. et al., 1995, $Astropart.Phys.$ 3, 321

[296] Kasahara, S. et al., 1997 *Phys.Rev.D* 55, 5282

[297] Kroupa, P. 2002 *Science* 295, 82

[298] Lithwick, Y. and Sari, R. 2001 ApJ555, 540

[299] Longley, N. et al., 1995 *Phys.Rev.D* 52, 2760

[300] Massey, P. et al. 1995 ApJ454, 151

[301] Navarra, G. et al. (EAS TOP Collab.), 1998 $Nucl.Phys.(Proc.Supl.)$ 12, 1

[302] Nikolsky, S. I. and Romachin, V. A. 2000 $Physicsof AtomicNuclei$, 63, 1799

[303] Ptuskin, V. S., 1993, *Astron.&Astroph.* 268, 726

[304] Racusin, J. L. et al., 2011 ApJ738, 138

[305] Ruffini, R. and Vitagliano, L., 2003 $Int.J.Mod.Phys.D$, 12, 121

[306] Salpeter, E. E., 1955 ApJ121, 161

[307] Stecker, F. W., Done, C, Salamon, M. H. and Sommers, P., 1991 *phys.Rev.Letts* 66, 2697

[308] Ter-Antonyan, S., 2007, *Astropart.Phys.* 28, 321

[309] Ter-Antonyan, S., 2014 *Phys.Rev.D.* 89, 123003

[310] Tsunesada, Y., Preprint $arXiv$: 1111.2507

[311] Wdowczyk, J. and Wolfendale, A.W. 1984, *J.Phys.G*, 10, 1453

[312] Woosley, S. E. 1993 ApJ405, 273

[313] Zou, Y.-C., Fan, Y.-Z., Piran T., 2011, ApJ726, L2

Index

Astroparticle Physics 35 (2012) 277–286

Contents lists available at SciVerse ScienceDirect

Astroparticle Physics

journal homepage: www.elsevier.com/locate/astropart

Influence of microscopic particle interaction models on the flux of atmospheric antiprotons

Arunava Bhadra [a], Biplab Bijay [a], Sanjay K. Ghosh [b,c], Partha S. Joarder [c], Sibaji Raha [b,c,*]

[a] High Energy & Cosmic Ray Research Centre, University of North Bengal, Siliguri 734013, West Bengal, India
[b] Department of Physics, Bose Institute, 93/1 A.P.C. Road, Kolkata 700009, India
[c] Centre for Astroparticle Physics and Space Science, Bose Institute, Block EN, Sector V, Salt Lake, Kolkata 700091, India

ARTICLE INFO

Article history:
Received 18 February 2011
Received in revised form 30 July 2011
Accepted 12 September 2011
Available online 25 September 2011

Keywords:
Antiproton
BESS observations
Particle interaction models
PAMELA experiment

ABSTRACT

We study the effect of particle interaction models on the theoretical estimates of atmospheric antiproton flux by comparing the BESS observations of antiproton spectra with the spectra obtained by means of a full three dimensional Monte Carlo simulation program. For such a purpose, we use two popular microscopic interaction models, namely FLUKA and UrQMD, to simulate antiproton spectra at multiple observation levels. In this article, we further compare the atmospheric antiproton fluxes predicted by a few popular microscopic high energy particle interaction models with each other to get an idea about the influence of such models at energies beyond the BESS upper cutoff up to about 100 GeV. We find that the simulated antiproton flux has strong dependence on the choice of interaction models. The present analysis seems to further indicate that the theoretical prediction of galactic antiproton spectrum may be uncertain by an appreciable amount due to our limited knowledge of particle interaction characteristics.

1. Introduction

Antiprotons ($\bar{p}$) in cosmic rays are supposed to provide information on the sources of cosmic rays and their propagation in the Galaxy as well as the matter–antimatter asymmetry of the local universe [62]. They are also believed to play crucial role in indirect dark matter search [23,53,56]. Primary $\bar{p}$ may as well be produced from the evaporation of primordial black holes (PBH) [47,57]. Observations of $\bar{p}$ spectrum with appropriate features may, therefore, be considered for probing into the possible signatures of the PBH.

Recently, the PAMELA instruments attached to the Russian Resurs-DK1 satellite have made a precise measurement of $\bar{p}$ spectrum in the energy range from 60 MeV to 180 GeV [6,8]. Comparison with several theoretical estimates [32,66,75] seems to support the view that the PAMELA $\bar{p}$ spectrum is consistent with a scenario of pure secondary production of $\bar{p}$ *via.* cosmic ray interactions in the interstellar medium (ISM) [6,8].

An accurate estimation of the secondary antiproton flux is, however, a difficult task. This is because of the fact that such an estimate requires precise knowledge of three factors, namely, the detailed features of cosmic ray propagation in the Galaxy, the characteristics of high energy particle interactions and the effect of solar modulation on the cosmic rays. While we have a reasonable understanding of the solar modulation effect, major uncertainties in the predicted flux still arise from our incomplete knowledge of cosmic ray propagation and the high energy particle interactions.

Over the past few years, the BESS experiments have reported the results of the precise measurements of atmospheric $\bar{p}$ spectra in an energy range 0.2–3.4 GeV at three observation levels, namely, the balloon altitude, mountain altitude and the sea level [72,84]. It is interesting to note that the cosmic rays traverse a depth (5–6 g cm^{-2}) of matter in the Galaxy that is close to the average atmospheric depth (10.7 g cm^{-2}) of the BESS-2001 balloon observation at the location of Ft. Sumner, USA [84]. As the $\bar{p}$ production mechanism in the atmosphere is likely to be similar to that in the Galaxy, a study of such atmospheric $\bar{p}$ at balloon altitude would possibly provide us with an opportunity to quantify the uncertainty in the theoretical estimate of interstellar $\bar{p}$ flux that may be caused by our limited knowledge of high energy particle interactions.

A good knowledge of particle interactions in the energy range from sub-GeV to about 100 GeV is required to understand the production and transport of the BESS-detected atmospheric $\bar{p}$s with their energies in the range between 0.2 GeV to a few GeV. Due to the steeply falling energy spectra of the primary cosmic rays, the contribution of primary particles with energies above 80 GeV/n to such BESS-observed atmospheric $\bar{p}$ spectrum has been recently

* Corresponding author at: Department of Physics, Bose Institute, 93/1 A.P.C. Road, Kolkata 700009, India.
E-mail addresses: aru_bhadra@yahoo.com (A. Bhadra), biplabbijay@rediffmail.com (B. Bijay), sanjay@bosemain.boseinst.ac.in (S.K. Ghosh), partha@bosemain.boseinst.ac.in (P.S. Joarder), sibaji@bosemain.boseinst.ac.in (S. Raha).

0927-6505/$ - see front matter © 2011 Elsevier B.V. All rights reserved.
doi:10.1016/j.astropartphys.2011.09.002

found to be insignificant [24]. GHEISHA (version 2002d) [40], UrQMD (version 1.3) [20,25] and FLUKA (version 2008.3b) [21,39] are among the most popular models for describing particle interactions in the relevant energy range. Such models are useful for the study of the development of cosmic ray cascades in the atmosphere. Among the three models mentioned above, GHEISHA is based on the parametrization of accelerator data, while UrQMD and FLUKA describe particle interactions microscopically.

The purpose of the present work is to study the influence of high energy particle interaction models on the atmospheric $\bar{p}$ spectra through the three dimensional Monte Carlo (MC) simulation methods. For such a purpose, we first simulate the atmospheric $\bar{p}$ spectra at multiple observation levels by using FLUKA and UrQMD models and then compare such simulated spectra with the BESS observations. The interaction model GHEISHA is not considered here (except in Fig. 3(b)) as the model is known to have shortcoming in describing fixed target accelerator data as well as the atmospheric cosmic ray data [24,34,49]. The present study is also prompted by the recently reported fact [24] that the BESS-measured atmospheric $\bar{p}$ flux at mountain altitude [72] is substantially less than the simulated flux obtained from FLUKA, while the flux obtained from UrQMD is consistent with experimental measurements. It is important to know whether such a discrepancy between the simulated and the experimental fluxes persists even at a very high (balloon) altitude or at the sea level. Such a study may have important bearing on our understanding of the reasons behind the disagreement between the FLUKA-derived results and the BESS measurements.

We here note that several MC simulations [18,36,51,77,78], relying mostly on phenomenological description of high energy particle interactions, have been carried out in the past to study the atmospheric $\bar{p}$ spectra. Such an approach does not usually satisfy many of the conservation laws in a single hadronic interaction and also suffers from various other inconsistencies (see, for instance, [27]). Besides, an understanding of the atmospheric $\bar{p}$ production also requires a good estimation of cosmic ray secondaries (mostly protons) in the atmosphere that was not considered in many of such earlier studies. In the present study, we further take the residual effect of the galactic $\bar{p}$ flux at the observation level into consideration that was mostly ignored in the calculations mentioned above.

The BESS-measured $\bar{p}$ spectra are limited to 3.4 GeV that corresponds to the mean vertical geomagnetic rigidity cutoff at the location of Ft. Sumner, USA. A simulation study of atmospheric $\bar{p}$ at very high altitude, that corresponds with the BESS observations at Ft. Sumner, is therefore relevant only for the low energy end of the galactic $\bar{p}$ spectrum measured by the PAMELA experiment [6,8]. To simulate the atmospheric $\bar{p}$ flux up to about 100 GeV, a good understanding of particle interactions up to at least a few hundred GeV is necessary. Due to the paucity of experimental data [35] on the inclusive $\bar{p}$ production and annihilation cross sections over the whole kinematic region in hadron–hadron, hadron–nucleus and nucleus–nucleus collisions in the stated energy range, one has to strongly rely on various theoretical models of particle interactions. In the absence of experimental data, we here compare the predictions of the well known high energy interaction models QGSJET (version 01c) [55], VENUS (version 4.12) [82], NEXUS (version 3.97) [33,67] and EPOS (version 1.6) [83], each in combination with FLUKA (version 2008.3b) for the description of hadronic interactions below 80 GeV/n, to get some idea about the theoretical uncertainties in the predicted $\bar{p}$ flux at energies beyond the upper cutoff for the BESS-2001 balloon experiment, i.e., over an energy range of about 3–100 GeV.

In a recent work [24], we found that the atmospheric proton spectrum, as measured by the BESS detector at mountain altitude [72], may be reasonably described by the FLUKA model; whereas, the model UrQMD works well at relatively higher energies. Such a proton flux deep in the atmosphere results from the production of protons in the interactions of primary/secondary cosmic rays with air nuclei as well as the absorption of such protons during their propagation through the Earth's atmosphere. Secondary proton spectrum at very high altitude, on the other hand, is likely to contain cleaner information on proton production alone. As the major fraction of such secondary protons arises from hadronic interactions in the forward kinematic region, a study of such proton spectra at very high altitude is likely to provide us with an opportunity to investigate particle production in the forward region. As a continuation of our study in [24], we therefore examine the dependence of atmospheric proton flux at balloon altitude on various hadronic interaction models in this article apart from the study of such a dependence on the atmospheric $\bar{p}$ spectrum as is already mentioned in the previous paragraphs.

Apart from the ambiguity in high energy particle interactions, a dominant systematic error in evaluating the flux of cosmic ray secondaries arises from the uncertainties involved in the estimation of input fluxes of primary cosmic rays. To minimize such uncertainties, spectra of different primary particles measured by the BESS-98 experiment [71] are used as the inputs in our simulations such that the systematic errors in the calculation of atmospheric fluxes are nearly eliminated as we compare with the BESS experimental fluxes of atmospheric protons/antiprotons at different altitudes.

The plan of the article is outlined as in the following. In the next section, we briefly describe the production mechanisms of $\bar{p}$ in high energy collisions and the ways in which different models implement such mechanisms. In Section 3, we give a brief description of the adapted simulation technique. In Section 4, we present the results of our MC simulations. Summary and discussion are presented in Section 5.

2. Production and transport of antiprotons in the atmosphere

2.1. General aspects

Antiproton flux in the atmosphere relies mainly on two factors, namely, the inclusive $\bar{p}$ production cross section in cosmic ray-air nuclei collisions and the propagation of $\bar{p}$ in the atmosphere. The latter factor also includes ionization energy loss, loss of $\bar{p}$ due to annihilation and other interactions.

Antiprotons are produced in the atmosphere in high energy interactions of primary and secondary cosmic ray hadrons/nuclei with air nuclei. A typical example could be the interaction $p + N \rightarrow \bar{p} + p + p + p + N$ with N representing a nucleon. The threshold proton energy for such interaction is about 6.6 GeV in the rest frame of the target nucleon. In addition to the above interactions, meson-nucleon interactions may also lead to the excitation of color flux tubes and their subsequent decay into baryon–antibaryon pairs.

The final state in high energy hadron–nucleon collisions often consists of many particles. Basic reaction for the production of $\bar{p}$ is, therefore, the inclusive $N + N \rightarrow \bar{p} +$ anything process and the inclusive $\bar{p}$ production cross section is one of the main ingredients for the calculation of atmospheric $\bar{p}$ flux. Such $\bar{p}$ production is likely to take place in the central kinematic region rather than the fragmentation region. Antibaryon absorption can also be important in the case of massive nuclear collisions. The $\bar{p}$ mean multiplicity is the other main input for the $\bar{p}$ production spectrum. For propagation of $\bar{p}$ through the atmosphere, the annihilation cross-section of $\bar{p}$ due to its collisions on light nuclei (N and O) are of primary importance.

In the instant case, several $\bar{p}$ production cross-section data on the collisions of proton with various fixed target nuclei in the

(laboratory) energy range of a few GeV to about 400 GeV are available. A complete data set is, however, available for p, π, and K projectiles at 100 GeV (lab) energy on p, C, Cu, Sn and Pb targets where the momenta of the secondary antiprotons are measured [19]. Apart from such data, some measurements on the $\bar{p}p$ and $\bar{p}C$ collisions in the sub-GeV to hundreds of GeV energy range are also available [1,9,30,52,79]. A semi-phenomenological fit to such data can, therefore, be employed for the calculation of atmospheric $\bar{p}$ flux with some level of accuracy and this has been a popular approach [17,28,76–78] for more than 25 years.

A precise estimation of the atmospheric $\bar{p}$ flux additionally requires reliable estimates for the secondary cosmic ray flux that may, in turn, produce further $\bar{p}$ by colliding with air nuclei. Tertiary $\bar{p}$s (arising from inelastically scattered secondaries) also contribute at low energies. One needs to further consider the residual galactic component of $\bar{p}$ in the case of very high (balloon) altitude.

2.2. Importance of high energy interaction models

Computation of hadron production, particularly at low transverse momenta, is not yet possible from first principles within quantum chromodynamics (QCD). One, therefore, relies on phenomenological models that are appropriately tuned to match with the prevailing experimental data. Even a parametrization of such models may be difficult as the accelerator data for the relevant target-projectile combinations covering the whole kinematic region are not available. Experimental data on hadron–hadron interactions in the forward kinematic region at high energies and the data on hadron–nucleus and nucleus–nucleus interactions at all energies covering the whole kinematic range are particularly scarce. One has to resort to theoretical models of particle interactions in such cases. Microscopic models are preferred over the parametrized inclusive models in view of the preservation of correlations such that the basic conservation laws are maintained at every single interaction level. Moreover, such microscopic models have predictive power in the regions in which experimental data are not available.

Hadronic interactions are well described by resonance production and subsequent resonance decay near the particle production threshold; whereas, such particle production scenario becomes too complex at higher ($E_{lab} > 5$ GeV) energies. In the latter situation, most of the particles are produced with low transverse momenta and, therefore, along the projectile direction so that a very large number of resonances of very short lifetimes have to be considered to describe particle production that may not be possible in practice. Such a difficulty gives rise to a number of attempts to develop various hadronic interaction models. Among such models, the string-based phenomenological models such as the Quark-Gluon Strings (QGS) model [54] and the Dual Parton Model (DPM) [29] are of particular interest as they are found to describe particle production at high energies reasonably well.

2.3. Outline of various particle interaction models

The interaction model FLUKA [21,39] employs resonance superposition from threshold to about 5 GeV but incorporates the two-strings interaction model (DPM) at higher energies. In this model, the resonance energies, widths, cross sections and the branching ratios are extracted from data and from the conservation laws by making explicit use of the spin and isospin relations. For high energy hadron–nucleus interactions, the model exploits the Glauber–Gribov cascade [44,45]; whereas, it uses the pre-equilibrium-cascade model PEANUT [37,38] below about 5 GeV. The nucleus-nucleus interactions above a few GeV/n are treated in FLUKA (version 2008.3b) by interfacing with the DPMJET-III [69] model.

The UrQMD (Ultra-relativistic Quantum Molecular Dynamics, version 1.3) model [25] was originally designed for simulating the relativistic heavy ion collisions in the (center of mass) energy range from around 1 AGeV to a few hundred AGeV for the RHIC experiment. This particular model inherits the basic treatment of the baryonic equation of motion in quantum molecular dynamic approach and describes the phenomenology of hadronic interactions at low to intermediate energies in terms of the interactions between known hadrons and their resonances. The model does not use an intrinsic cross section calculation. Instead, the projectile is allowed to hit a sufficiently large disk involving maximum collision parameters as a result of which the program consumes rather long a CPU time. We may add here that both UrQMD and FLUKA describe the fixed-target data reasonably well.

In the string-based models, the high energy nucleonic interactions lead to the excitation of color flux tubes. Antiprotons are produced *via.* the decay of such color flux tubes and also in antiresonance decays; whereas, the $\bar{p}$ annihilation is modeled *via.* the annihilation of quark-antiquark pairs and the formation and subsequent decay of two color flux tubes with baryon number zero. The annihilation of baryon–antibaryon pairs proceeds in UrQMD according to rearrangement diagrams. Here, the formation of two $\bar{q}q$-strings of equal energies in the c.m. system is assumed, while the remaining constituent quarks are rearranged into newly produced hadrons.

At higher energies, the interactions of nucleons and nuclei are calculated on the basis of the Gribov–Regge theory [43] that describes the observed rise of cross-sections at high energies as a consequence of the exchange of multiple supercritical Pomerons [16]. All observed scattering processes are successfully described with the Reggeon–Pomeron scattering scheme [16]. Presently, the Gribov–Regge theory-based interaction models used for cosmic rays include the QGSJET 01c [55], VENUS 4.12 [82], DPMJET-III [69], NEXUS 3.97 [33,67] and the EPOS 1.6 [83] models. Such different models in this class differ from each other in the details concerning the precise formulation of string formation and decay, treatment of the remnants, etc.

Being based on the quark-gluon string description of high energy interactions, the QGSJET model treats the hadronic and nuclear collisions in the framework of Gribov's Reggeon approach [44] as the multiple scattering processes. The individual scattering contributions are phenomenologically described in this model as Pomeron exchanges. The VENUS model considers color exchange between the quarks as well as the antiquarks. In this model, an individual collision leads to color exchanges between the quarks and between the antiquarks with such color rearrangements being the origin of color string formation. After all the strings have been formed due to color exchanges, they are fragmented into the observable hadrons by using an iterative fragmentation cascade. The fragmentation is assumed to be the same as in lepton scattering. Which nucleons from the projectile and the target nuclei collide with each other is determined from geometrical considerations.

While none of the mentioned models violates important theoretical principles, NEXUS and EPOS are the only models in which the theoretically predicted energy–momentum sharing between the hadron constituents is consistently implemented in the construction of scattering amplitudes. Being based on partons and strings, the NEXUS 3.97 [67] and the EPOS 1.6 [83] models employ the multiple scattering approach through a "three object picture" – a parton ladder between two interacting partons, one of which is from the projectile and the other is from the target, along with two excited colorless remnants formed by the spectator partons of the projectile and the target nucleons. The parton ladder describes successive parton emission through the soft and the hard interactions with the soft interaction being described by the traditional soft Pomeron exchange; whereas, the hard interaction is

realized through perturbative QCD within the concept of the semi-hard Pomeron. According to the number of quarks and antiquarks, to the phase space and to an excitation probability, a remnant decays into mesons, baryons and antibaryons [60]. The remnants produce particles mostly at large rapidities whereas the parton ladders emit particles mainly at central rapidities. Such "three object picture" of the parton-ladder and the two remnants solve the multistrange problem of conventional high energy models [26].

To implement energy conserving multiple scattering, these models consider both the open parton ladders as well as the closed parton ladders. Although the parton ladders of the latter category do not contribute to particle production, they nevertheless play a crucial role in the calculation of partial cross sections through interfering contributions. The NEXUS/EPOS models use relativistic string approach to obtain observable hadrons from partons *via.* two steps, namely, the formation of strings from the partons and then the string fragmentation into hadrons.

Being the successor to NEXUS, EPOS has adopted some additional aspects such as the nuclear effects related to Cronin transverse momentum broadening, parton saturation and screening. The model also puts special emphasis on high parton densities. The particle production scenario is expected to be very different depending on whether the interaction is with a peripheral nucleon or with a nucleon from the high density central part. This aspect has been accomplished in EPOS by allowing splitting (as well as merging) of parton ladders based on an effective treatment of lowest order Pomeron–Pomeron interaction graphs with the corresponding parameters being adjusted from the comparison with RHIC data.

In the case of meson projectile, the EPOS model leads to an increase of baryon and antibaryon production in the forward direction in agreement with the low energy pion-nucleus data [19]. In fact, the EPOS model seems to be the only model used both for EAS simulations and accelerator physics that is able to reproduce almost all the experimental data from 100 GeV lab to 1.8 TeV center of mass energy, including antibaryons, multistrange particles, ratios and p_t distributions.

3. Implementation of the simulations

In the present work, we generate atmospheric cosmic ray proton and antiproton spectra by employing the interaction models FLUKA 2008.3b and UrQMD 1.3 in the framework of the cosmic ray EAS simulation code CORSIKA (version 6.735) [48]. Following the default settings of the CORSIKA code, FLUKA and UrQMD have been used up to 80 GeV/n, while the model QGSJET 01c has been used above such energy threshold. As mentioned in Section 1, we also use the high energy interaction models VENUS 4.12, NEXUS 3.97 and EPOS 1.6, each in combination with the FLUKA model, to compare various theoretical estimates of the atmospheric $\bar{p}$ flux at energies beyond the BESS upper cutoff up to about 100 GeV. Other considerations/settings used in this work are briefly described in the following.

3.1. The primary spectra

Uncertainties in the determination of primary cosmic ray flux have been substantially reduced in recent years due to the precise measurements of such flux by the BESS-98 [71], BESS-TeV [46] and the AMS [10,11] experiments. The observed total primary nucleon flux below 100 GeV/n is found to agree within an accuracy of 4.0% in the above three experiments [41,73]. For such a reason, and considering the fact that we would compare our results with the BESS observations, we choose the BESS-98 spectra as the input primary spectra in our simulations while extending the maximum (kinetic + rest-mass) energy of the primary particles up to 1 PeV/n. For reproducing the BESS-observed primary spectra in CORSIKA, the effect of solar modulation on the spectra has been handled by using the *force field approximation* [42,61] in which the primary particle flux is expressed in terms of a time dependent *solar modulation potential* $\phi(t)$ that takes on different values for different epochs of solar activity [80]. For the BESS balloon-borne measurements of the atmospheric proton and antiproton fluxes in September 2001 at Ft. Sumner, USA [3,4,84], the primary cosmic ray spectra are generated by taking a solar modulation potential $\phi = 891$ MV [80] into account. Again, for the BESS sea-level measurements of the antiproton fluxes [84] at Tsukuba, Japan during 6th–11th May and 7th–13th December 1997, we consider $\phi = 410$ MV [80] as the mean value of the solar modulation potential.

3.2. The geomagnetic rigidity cutoff

The geomagnetic rigidity cutoff calculations have been performed by using the (back) trajectory-tracing technique [74]. The quiescent International Geomagnetic Reference Field (IGRF) model of 1995 [70] for the Earth's magnetic field has been used for such calculations. Both the umbra and the penumbra regions in the rigidity range of a primary particle in any particular direction have been taken into consideration [24] in our treatment of the rigidity cutoff. In Fig. 1, we display the values of the mean geomagnetic rigidity cutoff for the primary cosmic ray particles entering the atmosphere at the location of Ft. Sumner from various directions as an example of our rigidity calculations. Such cutoff calculations are used in the simulations to modify the primary cosmic ray spectra obtained from CORSIKA, although the calculation of the re-entrant albedo cosmic ray flux is not incorporated in the present simulations; see Section 5.

3.3. Other settings

The fluxes of cosmic ray particles also depend on the atmospheric density profile. Such a density profile, in turn, has latitudinal and seasonal variations. The effect of such variations on the atmospheric cosmic ray spectra is, however, expected to be small, particularly in the case of very high altitude observations. We, therefore, consider the US-standard atmospheric model [59] with a planar approximation in the present work.

Proton, helium and the heavier nuclei up to iron are considered here as the primary cosmic ray particles. Instead of taking each of the elements individually, the primary nuclei heavier than helium are taken in three separate groups, namely, medium ($5 < Z < 10$, $\langle A\rangle \approx 14$), heavy ($11 < Z < 20$, $\langle A\rangle \approx 24$) and very heavy ($21 < Z < 30$, $\langle A\rangle \approx 56$) nuclei respectively [24]. The spectra for such groups are taken from the compilation of Ref. [81]. The sum of the fluxes of individual elements in a group is taken as the flux of that particular group and the weighted average value of the power indices of such individual elements is taken as the power index of the group [24].

Particular care should, however, be taken for the simulation of atmospheric antiproton flux at a very high altitude. Such atmospheric antiprotons may, in fact, have significant contribution from the residual galactic $\bar{p}$s arriving at the observation level. In this work, we generate a secondary $\bar{p}$ spectrum by combining the simulation-generated (and normalized to the BESS-98 spectrum) primary proton spectrum with the recent measurement of antiproton to proton flux ratio obtained in the PAMELA experiment [6]. The resultant secondary $\bar{p}$ spectrum, adjusted for the location of Ft. Sumner and for a solar modulation potential appropriate for the BESS-2001 experiment, is considered along with the usual primary cosmic ray particles as the inputs in the simulations. However, the integrated secondary $\bar{p}$ flux is found to be only about $1.4–1.5 \times 10^{-4}$ times the integrated primary proton flux in our

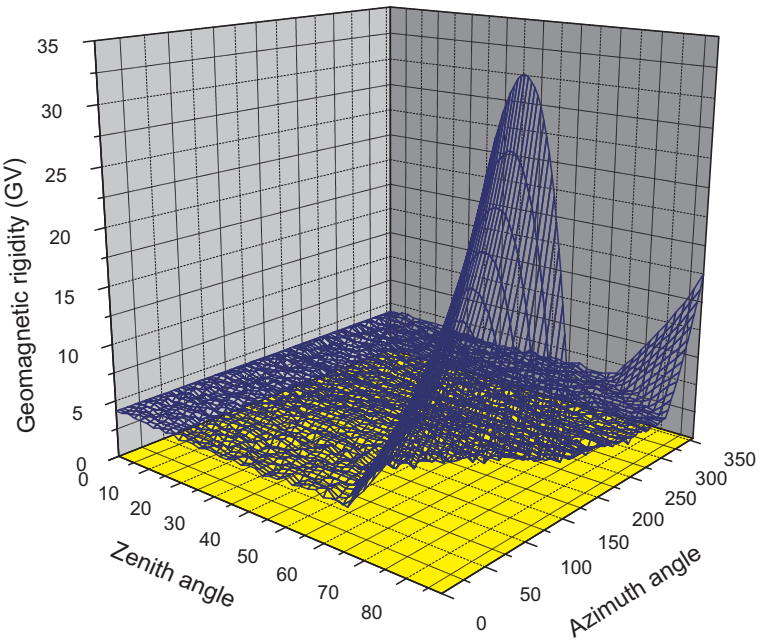

Fig. 1. Directional dependence of the mean geomagnetic rigidity cutoff for primary cosmic rays at the location of Ft. Sumner, USA.

simulations. We have checked that such interstellar $\bar{p}$ flux, in fact, have negligible effects on the generated atmospheric antiprotons within the energy range considered by the BESS experiments and even beyond.

Note that the fluxes of atmospheric shower particles obtained by using CORSIKA have statistical as well as systematic errors. In the present work, nearly 4–20 $\times$ 10^7 events have been generated in each of our simulations for the estimation of the fluxes of atmospheric shower particles, the results of which are presented in the following.

4. Simulated results and comparison with observations

The BESS-2001 experiment [3] is a balloon-borne experiment that was carried out in September 2001 at Ft. Sumner, USA. It consisted of a high resolution spectrometer with a large acceptance capable of performing precise measurements of absolute fluxes of various cosmic rays and their dependence on the atmospheric depth. The secondary proton and helium spectra in an energy range 0.5–10.0 GeV/n and the atmospheric muon spectra in a momentum range 0.5–10.0 GeV/c were measured at atmospheric depths ranging from 4.5 to 28.0 g cm^{-2} during the slow descending period of the balloon flight [3,4]. Atmospheric antiproton flux was also measured in the energy range 0.2–3.4 GeV and, reportedly, at a mean atmospheric depth 10.7 g cm^{-2} [84]. The zenith angle θ_z of the BESS-2001 measurements was limited to $\cos\theta_z \geqslant 0.9$ to obtain nearly vertical fluxes of atmospheric particles [3].

The BESS experiment also measured the sea-level antiproton flux at KEK, Tsukuba during 6th–11th May and 7th–13th December 1997 at a mean atmospheric depth 994.0 g cm^{-2} in the energy range 0.2–3.4 GeV [84].

Fig. 2 depicts the simulated atmospheric proton flux at the location of Ft. Sumner at the atmospheric depths (a) 10.5 g cm^{-2} and (b) 26.4 g cm^{-2}. Corresponding BESS-measurements [3,4] are also shown in the figure. We note that the statistical errors in the simulated spectra are quite small and fall within the widths of the representing lines in Fig. 2.

The BESS-2001-observed proton spectra in Fig. 2 show the following characteristic features. With the increase of energy from about 0.3 GeV, the differential flux initially decreases thus attaining a minimum value at about 2.5 GeV. Such a minimum is followed by an increase in flux up to a maximum at around 3.4 GeV above which the flux decreases again. Above about 2.5 GeV, bulk of the contribution to the observed flux is from primary protons with the peak being due to the geomagnetic cutoff effect. Below 2.5 GeV, the observed spectrum is due to secondary protons produced by the interaction of primary cosmic rays with atmospheric nuclei.

In Fig. 2, we find that the spectra derived from FLUKA and UrQMD models have features similar to those in the measured spectra. Both the models, however, yield fluxes that are lower than the measured values particularly at energies below 1.0 GeV. We also note that the simulated results match better with the measurements at 26.4 g cm^{-2} in Fig. 2(b) than at 10.5 g cm^{-2} in Fig. 2(a).

Fig. 2 shows an additional peak in the UrQMD-derived spectrum at about 1.4 GeV. In this context, we note that the kinetic energy corresponding to the mean vertical geomagnetic rigidity cutoff at Ft. Sumner [84] is also about 1.4 GeV/n for the threshold primary helium nuclei. To investigate if the anomalous peak in the UrQMD-derived flux in Fig. 2 is due to such primary α particles, we plot the separate contributions of (a) primary proton and (b) primary α components to the secondary proton flux in Fig. 3(a) and (b) at an atmospheric depth 10.5 g cm^{-2} at the location of Ft. Sumner. It is clear from this figure that the additional peak in UrQMD in Fig. 2 is indeed contributed by the primary helium nuclei. To check if there is any error in our simulations, we also compute the secondary proton flux from primary α particles in Fig. 3(b) by using the GHEISHA model. We find no additional peak in the GHEISHA model, the result of which is consistent with the FLUKA result. Fig. 3 thus seems to suggest that the fragmentation channel for quasi-elastic interactions between helium and air nuclei is overestimated in the UrQMD model. Such a finding is somewhat unexpected as the UrQMD model was primarily developed to address the nucleus–nucleus interactions and the model is known to well-reproduce the accelerator data. Further study on the stated feature in UrQMD seems, therefore, to be necessary. In Fig. 2, we also note that the results simulated with FLUKA and UrQMD models show very close agreement with each other at low energies, below about 1.0 GeV.

Fig. 4 shows the simulated atmospheric $\bar{p}$ fluxes in comparison with the BESS-measurements at balloon altitude, at mountain altitude and at the sea-level. The bandwidth of each of the bands

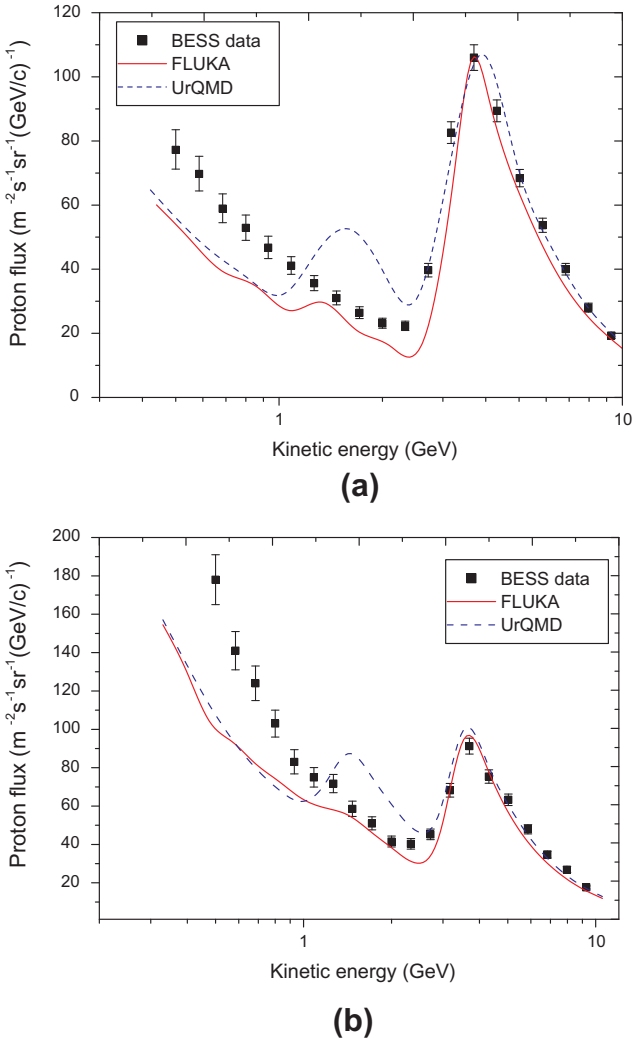

Fig. 2. Differential spectra of vertical atmospheric proton flux at the location of Ft. Sumner, USA that are obtained by using two hadronic interaction models at the atmospheric depths (a) 10.5 g cm^{-2} and (b) 26.4 g cm^{-2}. The results of the BESS-2001 observations at such depths [3,4] are also given for comparison.

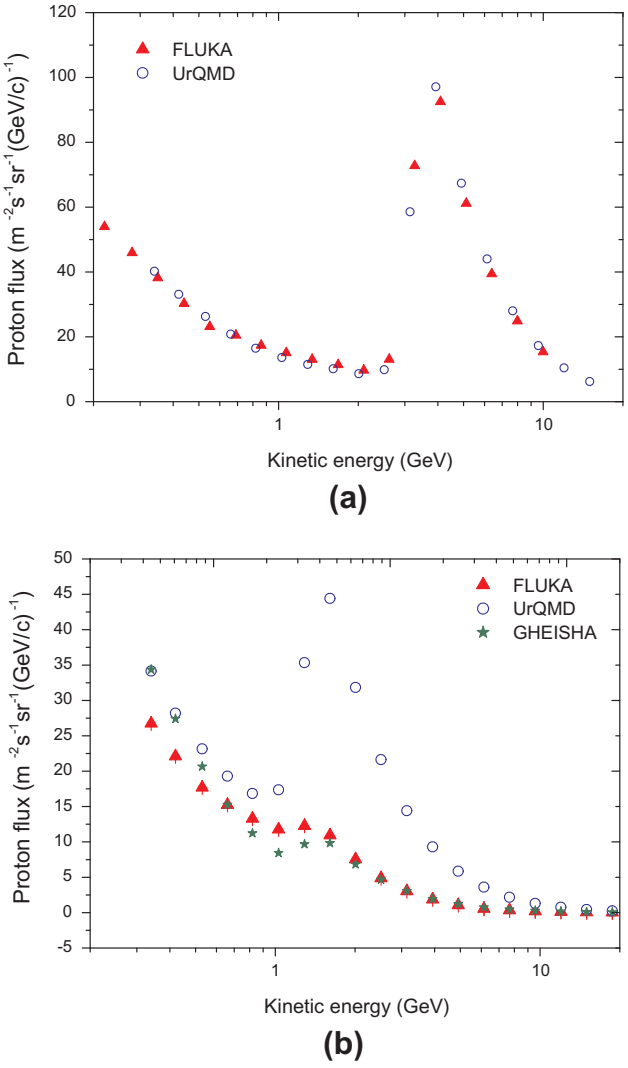

Fig. 3. Contributions from (a) primary protons and (b) primary α particles to the simulated vertical secondary proton flux at an atmospheric depth 10.5 g cm^{-2} at the location of Ft. Sumner. The proton fluxes are generated by using various hadronic interaction models as indicated in the diagram.

displayed in this diagram represents the magnitude of statistical error in the simulations.

At mountain altitude and at the sea-level, the $\bar{p}$ fluxes generated by UrQMD are found to be consistent with the BESS measurements within error bars. Such UrQMD-derived fluxes are, however, higher than the measured values at very high altitude. On the other hand, the FLUKA-generated fluxes are consistently higher than the measured values at all the atmospheric depths. The disagreement between the FLUKA-derived $\bar{p}$ spectra and the BESS observations is maximum at very high altitude and minimum at the sea level.

The results of our simulation for antiproton flux up to about 100 GeV at an atmospheric depth 10.7 g cm^{-2} is displayed in Fig. 5. To minimize statistical fluctuations, 40–50 million events are generated to obtain the flux from each model in this figure. The BESS measurements at Ft. Sumner [84] are also compared in Fig. 5. The fluxes generated by UrQMD + QGSJET and FLUKA + QGSJET combinations are found to differ significantly at the lower energy end; whereas, they predict nearly the same flux at higher (above about 5.0 GeV) energies. As we move to higher energies, the simulated $\bar{p}$ flux is increasingly influenced by the particle interaction characteristics at higher energies. We have, so far, considered just a single model (QGSJET) for describing particle interactions above 80 GeV/n. It is, therefore, expected that the stated combinations of models will give nearly the same flux at such higher energies.

To probe further into the situations at energies ranging roughly from about 10 GeV to 100 GeV, we simulate additional sets of data by replacing QGSJET by VENUS, NEXUS and EPOS interaction models to describe particle interactions above 80 GeV/n, while continuing with FLUKA below 80 GeV/n. The spectra obtained from such combinations are also shown in Fig. 5. In the absence of any experimental data, we could not judge the merit of the VENUS, NEXUS or the EPOS model over the QGSJET model as far as the $\bar{p}$ production in the atmosphere is concerned. It is, however, clear from the comparison of $\bar{p}$ fluxes in Fig. 5 that the theoretically predicted antiproton flux has strong dependence on high energy interaction models over the energy range considered here.

A characteristic feature of the atmospheric antiproton spectrum is that it peaks at around 2 GeV, decreasing rapidly towards lower energies, that is reflected in the simulated spectra as displayed in Fig. 5. Such a feature is not clearly visible in the BESS atmospheric observations because of the limited energy range of the experimental spectra.

To quantify the uncertainties in the theoretical $\bar{p}$ fluxes to a certain extent, we plot the ratios of average $\bar{p}$ fluxes predicted by each

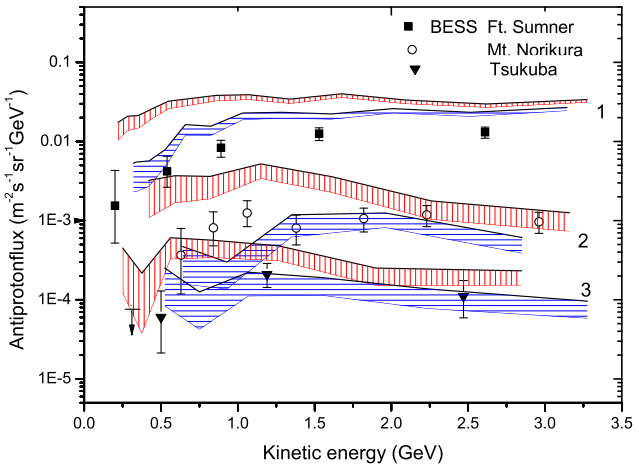

Fig. 4. A diagram depicting the simulated differential spectra of vertical atmospheric antiprotons at multiple atmospheric depths. In this figure, the red (vertically striped) bands and the blue (horizontally striped) bands represent the results simulated with FLUKA and UrQMD models; whereas, the uppermost (marked by the numeral 1), middle (marked by the numeral 2) and the lowermost (marked by the numeral 3) pair of bands represent $\bar{p}$ fluxes at balloon altitude (at the location of Ft. Sumner, USA), at mountain altitude (Mt. Norikura, Japan) and at the sea-level (Tsukuba, Japan) respectively. Corresponding measurements by BESS-2001 [84], BESS-1999 [72] and BESS-1997 [84] experiments are also given for comparison. Note that the bands marked by the numeral 2 are obtained from our previous simulations [24]. (For interpretation of the references to colour in this figure legend, the reader is referred to the web version of this article.)

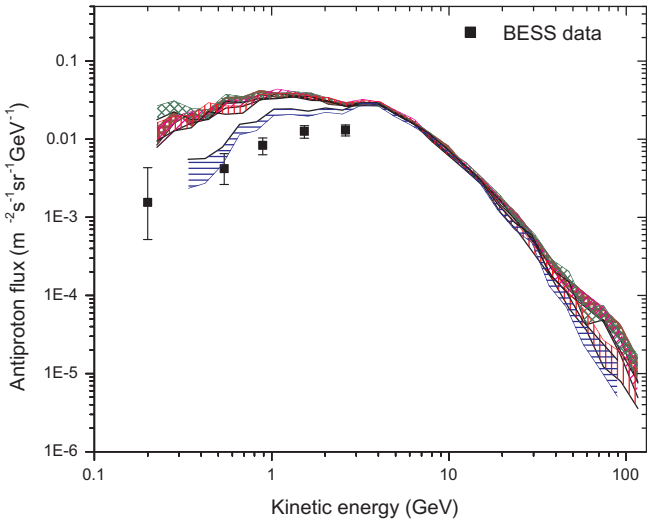

Fig. 5. Atmospheric vertical antiproton flux simulated with UrQMD + QGSJET, FLUKA + QGSJET, FLUKA + VENUS, FLUKA + NEXUS and FLUKA + EPOS models at an atmospheric depth 10.7 g cm^{-2} at the location of Ft. Sumner, USA for the kinetic energy of antiprotons within a range 0.2–100 GeV. Here, the blue (horizontally striped) band depicts the UrQMD + QGSJET combination, the red (vertically striped) band depicts the FLUKA + QGSJET combination, the magenta band (shaded by right-tilted lines) represents the FLUKA + NEXUS combination, the green (cross-hatched) band represents the FLUKA + VENUS combination and the brown (square-hatched) band represents the FLUKA + EPOS combination. Fluxes obtained by the BESS-2001 observation are also given for comparison. (For interpretation of the references to colour in this figure legend, the reader is referred to the web version of this article.)

of the FLUKA + QGSJET, UrQMD + QGSJET, FLUKA + VENUS and the FLUKA + EPOS combinations to the average fluxes obtained from the FLUKA + NEXUS combination (arbitrarily chosen as reference for the comparison) that are displayed in Fig. 6. While such ratios are found to be close to unity in the energy range around 3 – 10 GeV for all the models, they significantly deviate from each

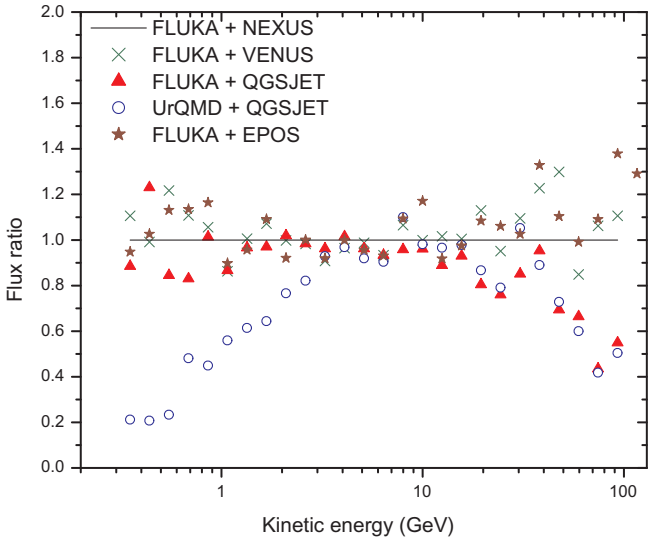

Fig. 6. Ratios of the mean atmospheric antiproton fluxes simulated with each of the FLUKA + QGSJET, FLUKA + VENUS, FLUKA + EPOS and the UrQMD + QGSJET combinations to the ones simulated with the FLUKA + NEXUS model for various values of kinetic energy of the antiprotons at a mean atmospheric depth 10.7 g cm^{-2} at the location of Ft. Sumner, USA.

other at higher energies. The flux-ratios even show more than 60% variation for different models at energies around 100 GeV. In Fig. 6, we find that the QGSJET-predicted mean flux at kinetic energies above about 10 GeV is substantially lower than those predicted by the NEXUS or the VENUS model. The EPOS1.6 model follows a trend similar to that shown by VENUS at such high energies. Below about 3 GeV, the UrQMD model gives appreciably lower fluxes than those obtained by the FLUKA model as was already noted in Fig. 5. Possibilities of statistical fluctuations are, of course, present in such results, but such systematic deviations as depicted in Fig. 6 can not be accommodated in terms of statistical fluctuations.

Since all the interaction models used here are appropriately tuned to the results obtained from the known collider and other experiments, the difference between the predictions of such models are mainly due to our limited understanding of high energy particle interactions.

5. Summary and discussion

Atmospheric proton and antiproton fluxes at different atmospheric levels are calculated in this article by using MC simulations with different particle interaction models and compared to the BESS experimental results. For spectra below about 10 GeV, corresponding to the experimental measurements, only the interaction models FLUKA and UrQMD are relevant. Here, we further extend our study of the atmospheric $\bar{p}$ flux up to 100 GeV where the high energy particle interaction models QGSJET01c, VENUS4.12, NEXUS3.97 and EPOS1.6 start to influence the simulated flux. As a consequence, we can examine the effect of such interaction models on the calculated $\bar{p}$ spectra in this article. The results of such study lead to the following observations.

1. It is interesting to note that the predictions of $\bar{p}$ fluxes obtained from FLUKA and UrQMD show significant deviations from each other, particularly at energies below about 3 GeV.
   The model UrQMD presents reasonable description of the BESS $\bar{p}$ data at mountain altitude and at sea level; whereas, it overestimates the antiproton flux at very high altitude thus possibly indicating that there is an enhanced production of $\bar{p}$ followed

by an enhanced annihilation in this particular model. Such an enhanced production of $\bar{p}$ in UrQMD may not be entirely unexpected as the model yields a higher multiplicity in comparison with the fixed target experiments.

The fact that FLUKA consistently yields a higher $\bar{p}$ flux than the measurements at all the observation levels possibly indicates a strongly enhanced $\bar{p}$ production in this model unless we assume that the BESS experiments have missed a sizable $\bar{p}$ events. The latter possibility is, however, thin as the fluxes obtained from UrQMD is consistent with the measured fluxes at sea-level and at mountain altitude. Atmospheric $\bar{p}$ annihilation also appears to be slightly enhanced in the FLUKA model as the disagreement between the FLUKA-generated $\bar{p}$ spectra and the ones obtained from the BESS measurements is found to decrease with increasing atmospheric depth.

As mentioned in Section 2, FLUKA mainly exploits the DPMJET-III model in describing high energy nucleon-nucleus interactions. DPMJET-III is known to moderately reproduce the energy dependence of antiproton to proton ratio at $y_{cm} = 0$ in proton-proton collisions as measured in the accelerator experiments [27]. It also reproduces the BRAHMS findings (from the RHIC experiment) regarding the dependence of antiproton to proton ratio on cms rapidity practically within experimental errors [22]. Although the consistency of the model parameters can not be checked in the energy range relevant for the present study as there is no direct experimental data on antiproton rapidity distribution in collisions with air or similar targets, the disagreement between the FLUKA-based fluxes and the measured fluxes on such a scale as noticed in the present study is, nevertheless, not an expected one.

It is worthwhile to note that the $\bar{p}$ flux obtained by Stephens [78] through a three dimensional MC simulation within a phenomenological framework was also found to be substantially higher in comparison with the BESS-observed flux at balloon altitude and in comparison with the theoretical unidirectional flux. Stephens [78] ascribed such a discrepancy to the use of the global spectra of primary cosmic ray particles instead of those observed by the BESS experiments. Such a possibility seems to be unlikely as the difference between the measured flux and the theoretically predicted flux is rather large in this particular case. As mentioned earlier, the balloon in the BESS-2001 experiment at Ft. Sumner was initially floated at an atmospheric depth 4.5 g cm^{-2} from where it started to descend slowly to an atmospheric depth of around 30.0 g cm^{-2} before the termination of the experiment [84]. In the absence of any knowledge regarding the effective observation time at each atmospheric depth, the $\bar{p}$ flux at balloon altitude is computed in the present investigation (and in [78]) at 10.7 g cm^{-2} that was the mean atmospheric depth for the BESS-2001 experiment. As the $\bar{p}$ flux in the atmosphere does not vary linearly with the atmospheric depth, such an inability to precisely determine the atmospheric depth could be at least one of the possible reasons for the difference between the simulated and the measured fluxes at the balloon altitude.

We here note that a few phenomenological MC simulations yield $\bar{p}$ fluxes that are consistent with the BESS observation at balloon altitude except below 1.0 GeV unless it is assumed that the tertiary antiprotons do not loose their energy in collisions with atmospheric nuclei [84]. Notwithstanding such assumptions, none of the above simulations consistently describe the BESS measurements of $\bar{p}$ spectra at all the observation levels. The present study, on the other hand, seems to suggest that the BESS observations of $\bar{p}$ spectra are relatively well described by the UrQMD model.

2. The results presented in this article show a significant discrepancy between the BESS-observed secondary proton spectra at very high altitude below the geomagnetic rigidity cutoff and the ones obtained from the interaction models FLUKA and UrQMD, particularly at the low energy part of the observed spectra. It is worth noting here that the re-entrant albedo particles, a consideration of which has been left out of the present investigation, are unlikely to be the cause of such a difference between the measured and the simulated flux of the secondary protons. This is because of the fact that the flux of such re-entrant albedo protons, as measured by the AMS experiment [13], is smaller by more than an order in comparison with the BESS-observed secondary proton flux below the geomagnetic cutoff till down to at least 0.3 GeV. We also note that the BESS collaboration (see the footnote in Ref. [3]) found no such re-entrant albedo proton flux in their observation at the balloon altitude.

   The difference that we find between the simulated and the observed proton spectra at very high altitude is in apparent contradiction with the results of our earlier simulations [24] that display reasonable agreement with the BESS-observed proton flux at mountain altitude. Fig. 2(a) and (b) in Section 4, however, demonstrate that the model-predicted proton fluxes at a lower altitude are indeed closer to the observed proton fluxes in comparison with those at a higher altitude. We may thus infer from the above results that the BESS observations seem to favor a higher production rate of protons in the nucleon-air collisions than the ones implemented in the FLUKA and the UrQMD models. We, however, note that the results of a single experimental measurement may contain uncertainties so that further observations of cosmic ray proton fluxes at multiple altitudes, along with the corresponding MC simulations, may be required to arrive at a definite conclusion on this particular issue.

3. The recent findings of the PAMELA experiment on positron excess [7,8] but no antiproton excess [6] in the energy range from sub-GeV to about 180 GeV lead to a nontrivial constraint on dark-matter models that try to account for the positron excess [31,50,58]. In the stated findings, the excess is determined by comparing with the background predictions from cosmic ray propagation models. The background $\bar{p}$ spectrum, that originates from the hadronic production induced by cosmic rays on the ISM, is generally calculated with the GALPROP numerical propagation code either by applying the parametrization of the invariant $\bar{p}$ production cross section [63] or by implementing the DTUNUC MC code [75]. Uncertainties in $\bar{p}$ flux due to the uncertainties in nuclear parameters, that are estimated from the parametrization of the maxima and the minima of the measured inclusive $\bar{p}$ cross sections in hadron-hadron and hadron-nucleus collisions, were found earlier to be about 22–25% [32]; whereas, the uncertainties in the nuclear parameters of the DTUNUC program, that essentially rests on the DPM model, were estimated to be about 40% [75].

   The present study also indicates, albeit indirectly, that the theoretical galactic $\bar{p}$ spectrum may contain large uncertainties due to the uncertainties in our knowledge of the particle interaction characteristics. Our investigation shows that at energies below about 3 GeV, the BESS observed atmospheric antiproton fluxes, at an atmospheric depth roughly comparable to the depth traversed by the cosmic rays in the Galaxy, are substantially lower than those obtained with the model FLUKA that may be regarded as a DPM class of model. At energies above about 10 GeV, the model predictions cannot be tested experimentally but, importantly, the predictions from different popular microscopic high energy interaction models tend to differ appreciably. In this context, we note that the model EPOS is known to produce more baryons/antibaryons in comparison with most of the other models including QGSJET that seems to be reflected in our results; see Figs. 5 and 6 in Section 4. Our investigation in

Fig. 6, in fact, suggests that the amount of uncertainty between different model predictions is not the same at all energies. Around 300 MeV, such uncertainty is as large as 80% that reduces substantially towards higher energies, particularly above about 3 GeV. Above 10 GeV, the uncertainty, however, increases again with energy and even becomes more than 60% at about 100 GeV. In the near future, we plan to take up a further investigation on the secondary antiproton spectrum by extending the maximum kinetic energy of such antiprotons to about 180 GeV or even beyond and by exploiting the updated versions of high energy interaction models, such as the QGSJET-II [64,65] and the EPOS 1.99 [68] models, in the framework of CORSIKA 6.980 (along with FLUKA 2011.2 to simulate below 80 GeV/n) for a better understanding of the recent PAMELA observations [8]. It may also be important here to note that the proposed measurements of $p + C \to \bar{p}$ and $\pi + C \to \bar{p}$ by the NA61/SHINE fixed-target experiments [5,14] at a few hundred GeV (lab) energy is expected to assist us in improving our understanding on the production of antiprotons thereby resolving the noted discrepancies between the interaction models in near future.

Finally, we may argue that the magnitude of uncertainties quoted in the theoretical calculations of $\bar{p}$ flux, that are obtained by employing semi-phenomenological fit to the experimental data, should perhaps be taken with some caution. This is because of the fact that the errors in the experimental results, based on which the model parameters are fitted or parametrized, are often underestimated or overlooked that may, in turn, affect the entire theoretical prediction. Well known examples are the inelastic $p - \bar{p}$ cross-sections that were measured by three different experiments at FERMILAB and the values at $\sqrt{s} = 1800$ GeV were found to vary from 80.03 ± 2.24 mb to 71.71 ± 2.02 mb [2,12,15]. Therefore, it is obvious that the model parameters that were tuned in accordance with the earlier quoted experimental $p - \bar{p}$ cross-sections would suffer from additional uncertainties. Thus, the consistencies of the predictions of a model in different circumstances may alone provide the validity of its inputs. In view of the results of the present analysis, a detailed study of the galactic $\bar{p}$ flux by exploiting different microscopic interaction models seems to be worth pursuing in the context of the PAMELA observation and its interpretation in terms of the standard/non-standard (dark matter, etc.) sources.

Acknowledgements

A.B. and B.B. acknowledge the support provided by the Department of Science and Technology (DST, Govt. of India) through the Grant No. SR/S2/HEP-14/2007. S.K.G., P.S.J. and S.R. thank the DST (Govt. of India) for support under the IRHPA scheme. We thank two anonymous reviewers for their constructive criticisms on an earlier version of the manuscript that has helped us to improve the quality of this version. We also thank Dr. R. Engel and Dr. T. Pierog for helping us with certain aspects of the CORSIKA code.

References

[1] T. Abbott et al., Phys. Rev. C 47 (1993) R1351.
[2] F. Abe et al., Phys. Rev. D 50 (1994) 5550.
[3] K. Abe et al., Phys. Lett. B 564 (2003) 8.
[4] K. Abe et al., Phys. Lett. B 645 (2007) 472.
[5] N. Abgrall et al., CERN-SPSC-2008-018, 2008.
[6] O. Adriani et al., Phys. Rev. Lett. 102 (2009) 051101.
[7] O. Adriani et al., Nature 458 (2009) 607.
[8] O. Adriani et al., Phys. Rev. Lett. 105 (2010) 121101.
[9] C.W. Akerlof et al., Phys. Rev. D 3 (1971) 645.
[10] J. Alcaraz et al., Phys. Lett. B 472 (2000) 215.
[11] J. Alcaraz et al., Phys. Lett. B 494 (2000) 193.
[12] N.A. Amos et al., Phys. Rev. Lett. 68 (1992) 2433.
[13] M. Aguilar et al., Phys. Rep. 366 (2002) 331.
[14] N. Antoniou et al., CERN-SPSC-2007-004, 2007; CERN-SPSC-2007-019, 2007.
[15] C. Avila et al., Phys. Lett. B 445 (1999) 419.
[16] M. Baker, K.A. Ter-Martirosyan, Phys. Rep. 28 (1976) 1.
[17] H.B. Barber et al., Phys. Rev. D 22 (1980) 2667.
[18] B. Baret, L. Derome, C.-Y. Huang, M. Buénerd, Phys. Rev. D 68 (2003) 053009.
[19] D.S. Barton et al., Phys. Rev. D 27 (1983) 2580.
[20] S.A. Bass et al., Prog. Part. Nucl. Phys. 41 (1998) 225.
[21] G. Battistoni, S. Muraro, P.R. Sala, F. Cerutti, A. Ferrari, S. Roesler, A. Fassò, J. Ranft, in: M. Albrow, R. Raja (Eds.), Proceedings of the Hadronic Shower Simulation Workshop, Fermilab 6–8 September 2006, AIP Conference Proceeding, vol. 896, 2007, p. 31.
[22] I.G. Bearden et al., Phys. Lett. B 607 (2005) 42.
[23] G. Bertone, D. Hooper, J. Silk, Phys. Rep. 405 (2005) 279.
[24] A. Bhadra, S.K. Ghosh, P.S. Joarder, A. Mukherjee, S. Raha, Phys. Rev. D 79 (2009) 114027.
[25] M. Bleicher et al., J. Phys. G 25 (1999) 1859.
[26] M. Bleicher, A. Keränen, J. Aichelin, S.A. Bass, F. Becattini, K. Redlich, K. Werner, Phys. Rev. Lett. 88 (2002) 20251.
[27] F.W. Bopp, J. Ranft, R. Engel, S. Roesler, Phys. Rev. C 77 (2008) 014904.
[28] T. Bowen, A. Moats, Phys. Rev. D 33 (1986) 651.
[29] A. Capella, U. Sukhatme, C.-I. Tan, J. Tran Thanh van, Phys. Rep. 236 (1994) 225.
[30] P. Capiluppi et al., Nucl. Phys. B 79 (1974) 189.
[31] M. Cirelli, M. Kadastik, M. Raidal, A. Strumia, Nucl. Phys. B 813 (2009) 1.
[32] F. Donato et al., Astrophys. J. 563 (2001) 172.
[33] H.J. Drescher, M. Hladk, S. Ostaptchenko, T. Pierog, K. Werner, Phys. Rep. 350 (2001) 93.
[34] H.J. Drescher, M. Bleicher, S. Soff, H. Stöcker, Astropart. Phys. 21 (2004) 87.
[35] R.P. Duperray, C.-Y. Huang, K.V. Protasov, M. Buénerd, Phys. Rev. D 68 (2003) 094017.
[36] R.P. Duperray et al., Phys. Rev. D 71 (2005) 083013.
[37] A. Fassò, A. Ferrari, J. Ranft, P.R. Sala, in: Proceedings of the Specialists Meeting on Shielding Aspects of Accelerators, Targets and Irradiation Facilities (Arlington, USA) (OECD/NEA, 1994), p. 287.
[38] A. Ferrari, P.R. Sala, in: Proceedings of the 1993 Conference on Monte Carlo Simulation in High Energy and Nuclear Phys. (Tallahassee, USA), World Scientific, Singapore, 1994, p. 277.
[39] A. Ferrari, P.R. Sala, A. Fassò, J. Ranft, Report CERN-2005-10 (2005), INFN-TC_05/11, SLAC-R-773 (2005).
[40] H. Fesefeldt, RWTH Aachen Report No. PITHA-85/02, 1985.
[41] T.K. Gaisser, M. Honda, P. Lipari, T. Stanev, in: Proceedings of the 27th International Cosmic Ray Conference, Hamburg, Germany, vol. 5, 2001, p. 1643.
[42] L.G. Gleeson, W.I. Axford, Astrophys. J. 154 (2004) 1011.
[43] V.N. Gribov, Sov. Phys. JETP 26 (1968) 414.
[44] V.N. Gribov, Sov. Phys. JETP 29 (1969) 483.
[45] V.N. Gribov, Sov. Phys. JETP 30 (1970) 709.
[46] S. Haino et al., Phys. Lett. B 594 (2004) 35.
[47] S.W. Hawking, Nature (London) 248 (1974) 30.
[48] D. Heck, J. Knapp, J.N. Capdevielle, G. Schatz, T. Thouw, Forschungszentrum Karlsruhe Report No. FZKA 6019, 1998.
[49] D. Heck, Nucl. Phys. B, Proc. Suppl. 151 (2006) 127.
[50] D. Hooper, A. Stebbins, K.M. Zurek, Phys. Rev. D 79 (2009) 103513.
[51] C.-Y. Huang, L. Derome, M. Buénerd, Phys. Rev. D 68 (2003) 053008.
[52] J.R. Johnson et al., Phys. Rev. D 17 (1978) 1292.
[53] G. Jungman, M. Kamionkowski, K. Griest, Phys. Rep. 267 (1996) 195.
[54] A.B. Kaidalov, Surv. High Energy Phys. 13 (1999) 265.
[55] N.N. Kalmykov, S.S. Ostapchenko, A.I. Pavlov, Nucl. Phys. B, Proc. Suppl. 52 (1997) 17.
[56] M. Kamionkowski, M.S. Turner, Phys. Rev. D 43 (1991) 1774.
[57] P. Kiraly, J. Szabelski, J. Wdowczyk, A.W. Wolfendale, Nature (London) 293 (1981) 120.
[58] M. Lattanzi, J.I. Silk, Phys. Rev. D 79 (2009) 083523.
[59] J. Linsley, private communication.
[60] F.M. Liu, J. Aichelin, M. Bleicher, H.J. Drescher, S. Ostapchenko, T. Pierog, K. Werner, Phys. Rev. D 67 (2003) 034011.
[61] K.G. McCracken, F.B. McDonald, J. Beer, G. Raisbeck, F. Yiou, J. Geophys. Res. 109 (2004) A12103.
[62] J.W. Mitchell et al., Phys. Rev. Lett. 76 (1996) 3057.
[63] I.V. Moskalenko, A.W. Strong, J.F. Ormes, M.S. Potgieter, Astrophys. J. 565 (2002) 280.
[64] S.S. Ostapchenko, Nucl. Phys. B (Proc. Suppl.) 151 (2006) 143–147.
[65] S.S. Ostapchenko, Phys. Rev. D 74 (2006) 014026.
[66] V.S. Ptuskin, I.V. Moskalenko, F.C. Jones, A.W. Strong, V.N. Zirakashvili, Astrophys. J. 642 (2006) 902.
[67] T. Pierog, H.J. Drescher, F. Liu, S. Ostapchenko, K. Werner, Nucl. Phys. A 715 (2003) 895c.
[68] T. Pierog, K. Werner, Nucl. Phys. Proc. Suppl. 196 (2009) 102–105.
[69] S. Roesler, R. Engel, J. Ranft, in: Proceedings of the Monte Carlo 2000 Conference (Lisbon), Springer, Berlin, 2001, p. 1033. Available from: <hep-ph/0012252>.
[70] T.J. Sabaka, R.A. Langel, J.A. Conrad, J. Geomag. Geoelect. 49 (1997) 157.
[71] T. Sanuki et al., Astrophys. J. 545 (2000) 1135.

[72] T. Sanuki et al., Phys. Lett. B 577 (2003) 10.
[73] T. Sanuki, M. Honda, T. Kajita, K. Kasahara, S. Midorikawa, Phys. Rev. D 75 (2007) 043005.
[74] M.A. Shea, D.F. Smart, J. Geophys. Res. 72 (1967) 2021.
[75] M. Simon, A. Molnar, S. Roesler, Astrophys. J. 499 (1998) 250.
[76] S.A. Stephens, Astrophys. Space Sci. 76 (1981) 87.
[77] S.A. Stephens, Astropart. Phys. 6 (1997) 229.
[78] S.A. Stephens, Adv. Space Res. 35 (2005) 142.
[79] Y. Sugaya et al., Nucl. Phys. A 634 (1998) 115.
[80] I.G. Usoskin, A.-H. Katja, G.A. Kovaltsov, K. Mursula, J. Geophys. Res. 110 (2005) A12108.
[81] B. Weibel-Sooth, P.L. Biermann, H. Mayer, Astron. Astrophys. 330 (1998) 389.
[82] K. Werner, Phys. Rep. 232 (1993) 87.
[83] K. Werner, F.M. Liu, T. Pierog, Phys. Rev. C 74 (2006) 044902.
[84] K. Yamato et al., Phys. Lett. B 632 (2006) 475.

The knee in the cosmic ray energy spectrum from the simutaneous EAS charged particles and muon density spectra

Biplab Bijay[1,a], Prabir Banik[1,b] and Arunava Bhadra[1,c]
[1] *High Energy & Cosmic Ray Research Centre, University of North Bengal, Siliguri, West Bengal, India 734013*
[a] *biplabbijay@rediffmail.com,*
[b] *pbanik74@yahoo.com*
[b] *aru_bhadra@yahoo.com*

In this work we examine with help of Monte Carlo simulation whether a consistent primary energy spectrum of cosmic rays emerges from both the experimentally observed total charged particles and muon size spectra of cosmic ray extensive air showers considering primary composition may or may not change beyond the knee of the energy spectrum.

I. INTRODUCTION

The primary energy spectrum of all particle cosmic rays is known to exhibit a power law behavior with few features including a slight bend of the spectrum at about 3 PeV, the so called knee of the spectrum, where the power law spectral index changes from about -2.7 to nearly -3.0. The knee is generally believed to be of astrophysical origin. The common explanations of the knee include rigidity-dependent upper limit on the energy that cosmic ray protons can attain at supernova remnants [1], leakage of cosmic rays from the galaxy [2], a nearby single source [3], mass distribution of progenitors of cosmic ray sources [4] etc.

The primary cosmic ray particles after entering into the Earth's atmosphere interact with the atmospheric nuclei and produce secondary particles. The detection of cosmic rays above the atmosphere is thus the only way to obtain direct measurements of the characteristics of primary cosmic ray particles including their energy spectra and mass composition. The energy spectrum of primary cosmic rays has been measured directly through satellite or balloon borne detectors up to few hundreds TeV. Above such energy direct methods for studying primary cosmic rays become inefficient due to sharp decrease in the flux of primary particles and the study of primary cosmic rays has to perform indirectly, through the observation of cosmic ray extensive air shower (EAS) which are cascades of secondary particles produced by interactions of cosmic ray particles with atmospheric nuclei. From their experimental results the Moscow State University group first noticed that the EAS electron size (total electron content) spectrum had a pronounced increase of slope (β increases suddenly) at a size corresponding to a primary energy of about 3 PeV [5] which was inferred as due to a break or the knee in the cosmic ray primary energy spectrum. Since then many EAS experiments covering this energy range confirm such a break in the spectral index of electron size spectrum and the existence of the knee in the cosmic ray energy spectrum is now considered as a well- established fact.

Some authors, however, cast doubt on the astrophysical origin of the knee. In particular a new type of interaction that transfers energy to a not yet observed component with interaction threshold in the knee region was proposed as the cause of the observed knee feature in the shower size spectrum [6, 7]. However, such a proposal has not received any support from the LHC experiment against the expectations. On the other hand Stenkin [8, 9] refuted the reality of the knee in the primary cosmic ray energy spectrum on the ground that the knee has been noticed observationally only in the electromagnetic component of EAS but not in the muonic and the hadronic components of EAS. In other words the knee feature in the primary cosmic ray energy spectrum is not consistently revealed from electromagnetic, muonic and hadronic components of EAS. Stenkin proposed an alternative explanation of the break in shower size spectrum in terms of coreless EAS [8, 9]. Further a new experiment PRISMA has been proposed to investigate the situation [10].

While arguing against the astrophysical knee, Stenkin did not consider any change in primary mass composition in the knee region on air shower muon and electron spectra [8]. Here it is worthwhile to mention that the almost all the well known models of the knee generally predict for a change in the mass composition of cosmic rays across the knee energy. For instances, the scenarios like rigidity dependent acceleration mechanism in the source or leakage from the Galaxy (which is also a rigidity dependent effect) predict for a heavier cosmic ray mass composition beyond the knee while the models based on nuclear photo-disintegration processes in the presence of a background of optical and soft UV photons in the source region predict for a lighter composition above the knee. The modern precise EAS experiments estimated primary energy spectra of different mass groups or even of various elements based on the deconvolution of either measured electron size distribution along with the information of muon content (as a function of electron size) or from a measured two-dimensional electron muon number distribution. Though conclusions of different experiments on primary mass composition in the knee region are not unequivocal, majority conclude that the knee represents the

energy at which proton component exhibits cut-off [4] i.e. the knee of the spectrum has been ascribed as the proton knee.

It is thus imperative to examine whether the primary knee feature is consistently revealed in electron and muon components of EAS when primary composition changes from lighter primaries to heavier primaries beyond the knee energy. This is precisely the objective of the present work. Our main emphasis will be to check whether the different EAS observables suggest for consistent spectral indices in the primary cosmic ray energy spectrum before and after the knee considering the fact that primary composition may or may not change across the knee. For this purpose we shall perform a detailed Monte Carlo simulation study of EAS using CORSIKA [11] in the concerned energy range and we will analyze different experimental data on size spectrum of various EAS observables to check the inner consistency. We will also estimate the spectral indices of electron and muon size spectra for different primary composition scenario assuming primary cosmic ray energy spectrum has a knee. The hadronic component is not considered in this work as only few data in this regard are available and more importantly the uncertainties are quite large.

The organization of the paper is as follows. In the next section the principle of deriving the cosmic ray energy spectrum from the EAS observables is outlined briefly in the framework of Bhabha-Heitler theory of electromagnetic cascade . In section III we describe our analysis of cosmic rsy EAS size spectra based on the Monte Carlo simulation study. The procedure adapted for the Monte Carlo simulation of cosmic ray EAS is discussed in the subsection III-A. In the subsection III-B we evaluate spectral index of primary energy spectrum from the measured electron and muon size spectra for different primary composition scenario. The expected shower size and muon size spectra for different mass composition scenario assuming the primary energy spectrum has a knee are obtained in the subsection III-C. Finally we discuss the findings and their probable explanations in the section IV.

II. PRIMARY ENERGY SPECTRUM FROM EAS OBSERVATIONS AND THE KNEE

Usually, cosmic ray EAS arrays employ scintillation detectors for detection of electrons, which is the dominating component among the charged particles in EAS. However, such detectors also detect other charged particles including muons. So essentially EAS observations give information about total charged particle spectrum instead of electron size spectrum . The observational charged particle size (often known as shower size) spectrum in EAS is found to exhibit power law behavior i.e.

$$\frac{dN}{dN_{ch}} \propto N_{ch}^{-\beta_{ch}} \tag{1}$$

Though the development of EAS is a very complicated process that can be properly addressed only via Monte Carlo simulation technique but an idea of how electron and other secondary particle sizes are related to primary energy can be obtained based on the Bhabha - Heitler analytical approach of electromagnetic cascade [12, 13]. A cosmic ray particle interacts with the atmospheric nuclei while moving through the atmosphere and produced dominantly charged and neutral pions. There will be also secondary hadrons (leading particles). Neutral pions quickly decay to photons which subsequently initiate electromagnetic cascades. The charged pions may interact with atmospheric nuclei (thereby further produce secondary particles) or decay depending on their energy. The decay of charged pions yields muons and neutrinos. The energy dependence of total number electrons, muons and hadrons at shower maximum (at which the number of particles in a shower reaches its maximum) in EAS initiated by a nucleus with atomic mass number A and energy E_o can be expressed as [12, 13]

$$N_i^{max} = N_i^o E_o^{\alpha_i} \tag{2}$$

where i stands for e (electron), μ (muon) and h (hadron). For pure electromagnetic cascade and under few simple approximations such as the all electrons have the same energy E_e^c (which is the critical energy (85 MeV in air), at which ionization losses and radiative losses are equal) α_e is nearly equal to 1. Similarly when all muons are considered to have the same energy E_π^c (which is the energy at which the probability for a charged pion to decay and to interact are equal) and taking the charged pion production multiplicity is 10 (constant) $\alpha_\mu \sim 0.85$ [13]. When the effect of inelasticity is taken into consideration, α_μ will be slightly higher, ~ 0.90 [13]. If one considers that total primary cosmic ray energy is distributed between electron and muon component, α_e will be slightly higher, about 1.05 [13].

Two important points to be noted are (i) the total number of electrons increases with energy slightly faster than exactly linear whereas the total number of muons grows with energy slightly less than exactly linear. (ii) The electron number decreases with increasing mass number whereas muon number grows with mass number.

After shower maximum, electron (and hadron) size decreases due to attenuation whereas muon size almost remain constant because of its large attenuation length. Hence at a observational level well passed the shower maximum, the equation (2) is not strictly valid, particularly for electrons and hadrons.

Considering that the electron size spectrum and total charged particle size spectrum are more or less the same, from equations (1) and (2) one can infer the primary cosmic ray spectrum as follows

$$\frac{dN}{dE_o} = \frac{dN}{dN_e^{max}} \frac{dN_e^{max}}{dE_o} \propto E_o^{-\gamma} \tag{3}$$

where

$$\gamma \equiv 1 + \alpha_e(\beta_e - 1) \quad (4)$$

will be the slope of primary cosmic ray differential energy spectrum. Since a sudden change in β_e at a size corresponding to a primary energy of about 3 PeV is observed, consequently a change in γ at 3 PeV is inferred which is the so called knee of the cosmic ray energy spectrum.

Equations (2) and (3) imply that muon and hadron size spectra also should exhibit power law behavior with $\beta_i = 1 + (\gamma - 1)/\alpha_i$. Since $\alpha_\mu < \alpha_e$, change in β_μ should be larger than β_e for a change in γ. Observationally, however, no significant change in β_μ is found. This is why Stenkin objected against the existence of a knee in the primary energy spectrum [8, 9].

Note that the semi-analytical expressions described above, though match reasonably well with the simulation results, are approximated description of cosmic ray cascade in the atmosphere. Moreover, the relation between electron size and energy (Eq. 3) is valid only at shower maximum. So a detailed Monte Carlo simulation study needs to be done to draw any concrete conclusion in this regard.

III. MONTE CARLO SIMULATION STUDY OF SIZE SPECTRUM

In the present work we have simulated EAS for three different mass composition scenario: proton as primary over the whole energy range, secondly proton and Fe respectively as primary below and above the knee energy and finaly Fe as primary over the whole energy range. Subsequently we explore whether a consistent mass composition scenario evolve from simultaneous study of electron and muon size spectra in the knee region. We evaluate α_i from simulation data for proton and iron primaries both below and above the knee and using the observed β_i from experiments, we subsequently estimate γ following the equation () and check whether electron, muon and hadron observations give a consistent primary energy spectrum when primary composition is allowed to change across the knee.

A. Simulation procedure adopted

The air shower simulation program CORSIKA (COsmic Ray SImulation for KAscade) (version 6.690) [11] is employed here for generating EAS events. The high energy (above 80GeV/n) hadronic interaction model QGSJET 01 (version 1c) [14] has been used in combination with the low energy (below 80GeV/n) hadronic interaction model UrQMD [15]. A relatively smaller sample has also been generated using the high-energy interaction model EPOS (version 2.1) [16] and low energy interaction model GHEISHA (version 2002d) [17] to judge the influence of the hadronic interaction models on the results. Note that GHEISHA exhibits a few shortcomings [18, 19] but the low energy interaction models has no significant effect on the total number of secondary particles for primaries in the PeV energy range.

The US-standard atmospheric model with planar approximation which works only for the zenith angle of the primary particles being less than 70^o is adopted. The EAS events have been generated for proton and iron nuclei as primaries at several fixed energy points spreaded between 3×10^{14} to 3×10^{16} eV as well as over a continuous energy spectrum between 3×10^{14} to 3×10^{16} eV with differential energy spectrum slop -2.7and -3.1 below and above the knee (3×10^{15} eV) respectively. The EAS events have been simulated at geographical positions correspond to experimental sites of KASCADE [20] and EAS-TOP [21]. The magnetic fields, observation levels, threshold energies of particle detection and zenith angles are provided accordingly.

B. Inferring Primary cosmic ray spectrum from measured EAS size spectra

Only a few EAS experiments so far measured both β_{ch} and β_μ before and after the knee. Here we would consider the results of two experiments, the KASCADE [22, 23] and EAS-TOP [24]. The KASCADE experiment was considered as one of the most precise air shower experiments in the world which was situated in the site of Forschungszentrum Karlsruhe (Germeny) at an altitude 110 m above sea level at 49.1^o N, 8.4^o E, covering an energy range from about 100 TeV to nearly 100 PeV and was in operation during October 1996 to 2003. The experiment consisted an array of electron and muon detectors, spread over 700 m^2 $\times$ 700 m^2, a central hadron calorimeter with substantial muon detection areas and a tunnel with streamer tube muon telescopes. This multidetector system was used for the study of electromagnetic, muonic and hadronic components of EAS. The experiment was later extended to KASCADE-Grande in 2003 to study primary cosmic rays at higher energies. On the other hand the EAS-TOP array was located at Campo Imperatore, National Gran Sasso Laboratories in Italy, 2005 m a.s.l.,(820 $g\ cm^2$) atmospheric depth. This multi-component experiment consisted of detectors of the electromagnetic, muon, hadron and atmospheric Cherenkov light components for the study of EAS over the energy range 100 TeV to about 10 PeV. Two layers of streamer tubes with total surface area $12 \times 12\ m^2$ was used for detection of EAS muons having threshold energy of 1 GeV.

The results of these two experiments on β_{ch} and β_μ are shown in Table 1. Note that the shower size (N_e) and muon size are generally evaluated from the experimental measured particle (electron/muon) densities by fitting with the lateral density distribution function. To minimize the bias by the functional form of the muon

lateral distribution function, KASCADE experiment introduced the quantity truncated muon number which is essentially the muon size within 40 m and 200 m core distance.

Using the public data of KASCADE experiment provided through KCDC [25] we also estimated β. For vertical air showers ($\theta < 18^o$), we find β equals to 2.54 ± 0.06 and 2.97 ± 0.05 below and above the knee are respectively for total charged particles and 2.96 ± 0.08 and 3.24 ± 0.06 for muons below and above the knee respectively which are closed to KASCADE reported β for vertical showers.

Our target is now to evaluate γ both below and above the knee from the measured β_{ch} and β_{μ} considering the results of KASCADE and EAS-TOP, using the expression (). To estimate α we exploit Monte Carlo simulation method.

The figure 1(a) displays the variation of total charged particle number in EAS obtained with Monte Carlo simulation as a function of energy at KASCADE location for proton primary whereas the variation of muon content with primary energy in proton induced EAS is shown in figure 1(b). Power law fits to the data points are also shown in both the figures. We find that the dependence of shower size on primary energy can be described by a power law with constant spectral index. We have also checked whether the data suggest different spectral slops at lower and higher energies by fitting the data below and above the knee separately. But the so fitted slops are found only to differ within the error limits of the single constant spectral index. The estimated power law indices (α_e and α_{μ}) are displayed in table 1 for proton primary. In figure 2 we have plotted the electron and muon sizes in Fe initiated EAS as a function of primary energy. α_e and α_{μ} for Fe primary are also evaluated from power law fitting and are shown in table 2.

Since β_is are known from observations, we have estimated γ straightway using the expression (). We considered both proton and Fe as primaries below the knee as well as above the knee and evaluated γ. Subsequently we computed $\delta\gamma$ across the knee. The results are given in Table 1 for the KASCADE measurements. It is noticed that no consistent γs below and above the knee emerge from the KASCADE measured electron and muon spectra irrespective of the primary composition. The $\delta\gamma$s from the observed electron and muon spectra also differ significantly.

Results of a similar analysis for the EAS-TOP electron and muon spectra are displayed in figures 3 nad 4 from simulation data and in Table 2. In EAS-TOP location the α of charged particles for proton primary is found quite small than that for the KASCADE location which suggests that α changes with atmospheric depth and close to one at shower maximum. For Fe primary, however, no significant difference in α of charged particles noticed in two stated locations which is probably due to the fact that air showers reaches to its maximum development much earlier for heavier primaries. So even at EAS-TOP location, PeV energy Fe initiated showers are quite old. The spectral index (of primary cosmic ray energy spectrum) derived separately from the EAS-TOP observed electron and muon size spectra is found somewhat mutually consistent when cosmic ray primary is dominantly Fe, both before and after the knee. The $\delta\gamma$s from the observed electron and muon spectra also found mutually consistent for unchanging Fe dominated primary.

C. Electron and muon spectra for astrophysical knee

It appears that the main difficulty of arriving a consistent knee from simultaneous charged particles and muon spectra in EAS as observed by KASCADE experiment is the very small spectral slope difference in muon spectrum across the knee relative to the spectral slope difference in charged particle spectrum. However, such an inference is based on the equation () that follows from consideration of the cascade theory which is an approximate description of complex EAS phenomenology. Here we shall estimate the expected spectral slopes in electron and muon spectra for different primary composition scenario assuming that the primary energy spectrum has a knee. The spectral index of the primary energy spectrum below the energy 3 PeV is taken as -2.7 whereas above 3 PeV it is assumed as -3.1. The EAS are generated from the minimum energy of 100 TeV and only vertical showers are generated.

The electron and muon size spectra at KASCADE location from the simulation results are displayed in figures 5. We considered a change in mass composition after the knee from pure proton to pure iron as well as for unchanged (proton and Fe) mass composition. The knee structure is found present in both electron and muon size spectra for all the mass composition scenario considered. The β value obtained from the simulation results are displayed in Table 4 for the different composition scenario. To identify the position of the knee and also to estimate the β values in electron and muon size spectra we multiply the differential total charged particle (muon) numbers by some suitable power (selected by varying the power index slowly) of total charges particles (muons) to emphasize the small difference in slop and plot it against the total charged particles (muons) in log-log scale. It is found that the points below and above a certain total charged particle number have distinct slops. The best fitted slops give the β below and above the size knee whereas the crossing point of the two straight lines (in log-log scale) give the position of the knee in size spectra.

The spectral index of total charged particle spectrum above the knee obtained from the simulation results is found slightly lower than the observational result whereas for muon spectrum the spectral index below the knee from the simulation data is found slightly larger than the observations. It is also noticed that the spectral index below (or above) the knee depends not only primary composition below (above) the knee of the

TABLE I: The measured spectral indices of primary energy spectrum below and above the knee from the electron and the muon size spectra of KASCADE and EAS-TOP observations

Experiment	Component	$\beta_{<knee}$	$\beta_{>knee}$
KASCADE	electron	2.45 ± 0.06	2.94 ± 0.12
KASCADE	muon (> 490 MeV)	3.05 ± 0.006	3.27 ± 0.01
EAS-TOP	electron	2.61 ± 0.01	3.01 ± 0.06
EAS-TOP	muon (> 1 GeV)	3.12 ± 0.03	3.67 ± 0.07

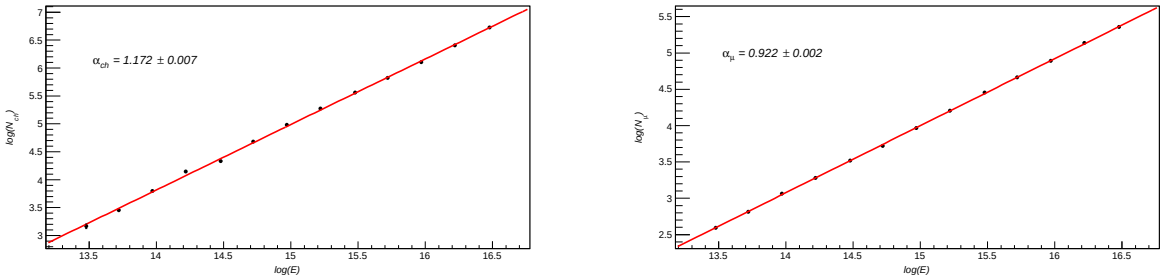

FIG. 1: (Color online) Energy dependence of (a) total charged particles and (b) muon content in proton induced EAS at KASCADE location from the Monte Carlo simulation data.

primary energy spectrum but also the composition above (below) the knee of the energy spectrum, particularly when points close to the knee in the size spectra are considered to determine the spectral index. There are few other important points have been noted:

i) the position of the knee in the charged particles and muon spectra also influence by the primary composition both below and above the knee of the cosmic ray energy spectrum,

ii) the knee in the muon spectrum is slightly more revealing in comparison to that in the electron spectrum for pure proton or Fe primaries over the entire energy range but the same may not be true when primary composition changes across the knee,

and iii) for proton primary before the knee and Fe primary after the knee the muon spectrum exhibits a break not only in the spectral index but also in the flux. The later feature is due to larger muon size in Fe initiated EAS in comparison to proton induced EAS.

A two dimensional plot of electron and muon size spectra for different composition scenario are also obtained and depicted in figures 6 for KASCADE location. An interesting observation is that the knee is not clearly revealed from the two-dimensional plots. Since Fe induced EAS contains lower electrons and higher muons in compare to proton induced EAS, the two dimensional figure exhibits some mismatch in shower and muon sizes around the knee for a sharp change in composition from proton to Fe across the knee which is not observed experimentally.

IV. DISCUSSION AND CONCLUSION

The knee of the primary energy spectrum has long been inferred from the break in shower size spectrum of cosmic ray EAS at certain shower size corresponding to few PeV primary energy. Few authors, particularly Stenkin, however, objected the existence of the knee in the primary energy spectrum noting that the muon size spectrum of cosmic ray EAS does not show any prominent break against the expectations based on cascade theory.

It is found from the present analysis that when a hybrid approach is employed involving cascade theory (to have a relation between the spectral index of primary energy spectrum and the spectral indices of EAS electron and muon size spectra) and the Monte Carlo simulation (invoked to get the relation between electron and muon sizes with primary energy) the EAS-TOP observations on total charged particle and muon spectra consistently infer a knee in the primary energy spectrum provided the primary is pure unchanging iron whereas no consistent primary spectrum emerges from simultaneous use of the KASCADE observed total charged particle and muon spectra.

When a pure Monte Carlo approach is adopted to examine the expected size spectra for a given primary energy spectrum with different mass composition, it is found that for pure unchanging proton or Fe primaries the difference in spectral slops below and above the knee of the size spectrum is larger for muon spectrum than the electron spectrum. However, when mass composition changes across the knee the situation becomes quite complex. In such a situation estimating β properly is challenging, particularly for total charged particle spec-

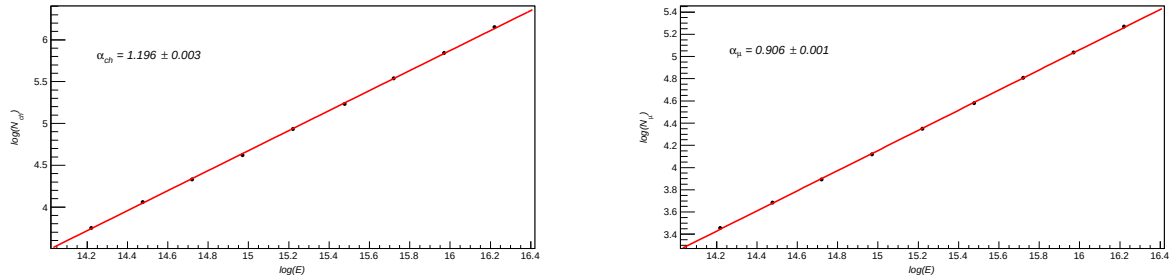

FIG. 2: (Color online) Same as Figure 1 but in Fe initiated EAS.

TABLE II: Spectral indices of primary energy spectrum below and above the knee from the electron and the muon size spectra of KASCADE observations

Primary before the knee	Primary after the knee	Secondary	$\alpha_{<knee}$	$\alpha_{>knee}$	$\gamma_{<knee}$	$\gamma_{>knee}$	$\Delta\gamma$
Proton	Proton	electron	1.172 ± 0.007	1.172 ± 0.007	2.70 ± 0.08	3.27 ± 0.16	0.57 ± 0.24
		Muon (> 490 MeV)	0.922 ± 0.002	0.922 ± 0.002	2.89 ± 0.01	3.09 ± 0.02	0.20 ± 0.04
Proton	Fe	electron	1.172 ± 0.007	1.196 ± 0.003	2.70 ± 0.08	3.32 ± 0.14	0.62 ± 0.22
		Muon (> 490 MeV)	0.922 ± 0.002	0.906 ± 0.001	2.89 ± 0.01	3.05 ± 0.02	0.16 ± 0.03
Fe	Fe	electron	1.196 ± 0.003	1.196 ± 0.003	2.73 ± 0.08	3.32 ± 0.14	0.59 ± 0.22
		Muon (> 490 MeV)	0.906 ± 0.001	0.906 ± 0.001	2.86 ± 0.01	3.05 ± 0.02	0.19 ± 0.03

trum; the β value and the position of the knee depend on primary composition both below and above the knee of the primary energy spectrum and the points close to the knee in the size spectra may change the overall slope considerably. For instance in the simple situation where proton and Fe are the dominating component below and above the knee of the primary energy spectrum, the contribution of Fe, which gives a comparative lower total number of charged particles, leads to a flatter shower size spectrum below the knee, unless the points closed to the knee in the size spectrum are totally ignored to evaluate the slopes. On the other hand Fe induced EAS contains comparatively larger muon number. Hence the slopes of the muon size spectrum does not alter much for the stated changing composition scenario but there will be a mismatch in the flux at the knee of the muon size spectrum. Non observation of any break in flux level at the knee position of the muon size spectrum in any experiment suggests that there is no abrupt change in primary composition across the knee; the composition either changes slowly above the knee or it changes from a lighter dominating mixed composition to heavier dominated mixed composition without appreciable change in average primary mass. In such changing mass composition scenario, the break in EAS muon size spectrum may not be more revealing than that in total charged particle spectrum against the common perception.

We thus conclude that though the derivation of the size spectrum from observed data looks to be rather straight forward process, but in practice it is a quite complex issue particularly owing to the uncertainty in primary mass composition. The simultaneous use of the measured EAS total charged particle and muon size spectra to infer the primary energy spectrum is certainly a better approach but it requires a careful and experiment specific analysis. The two-dimensional differential spectrum contents substantially higher information than those of two one-dimensional ones and hence used to infer primary spectrum and composition but one dimensional spectra also carry important and exclusive signatures about primary energy spectrum and composition which may be accommodated to get more reliable estimates about cosmic ray primaries.

[1] C. E. Fichtel, and J. Linsley, Astrophys. J. **300**, 474 (1986)
[2] V. L. Ginzburg, and S. I. Syrovatskii, 1964, The Origin of Cosmic Rays, Macmillan, NewYork.
[3] A. D. Erlykin, A. W. Wolfendale, J. Phys. G: Nucl. Part. Phys. **23**, 979 (1997).

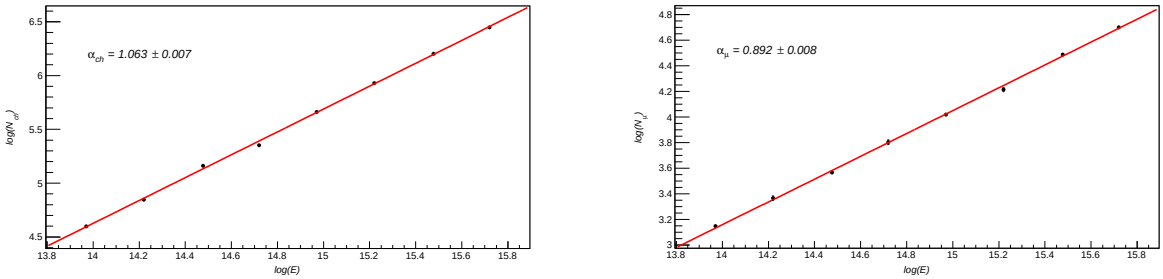

FIG. 3: (Color online) Energy dependence of (a) total charged particles and (b) muon content in proton induced EAS at EASTOP location.

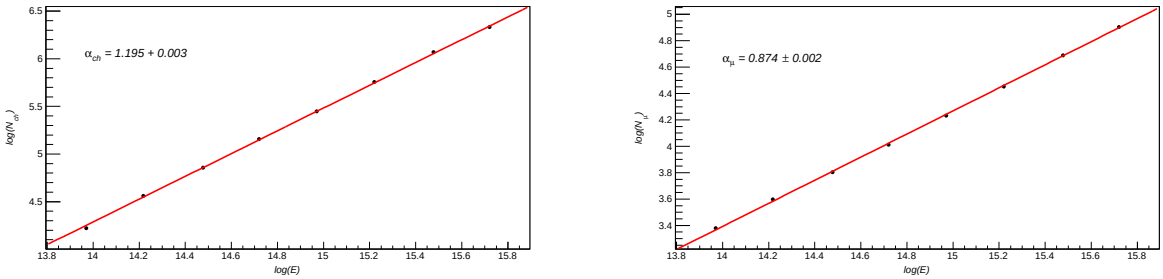

FIG. 4: (Color online) Same as Figure 3 but in Fe initiated EAS .

[4] B. Bijay and A. Bhadra, Res. Astron. Astrophys. (to appear) (2015); eprint arXiv:1412.0818.
[5] G. V. Kulikov, G. B. Khristiansen, JETP, **35**, 441 (1959).
[6] S. I. Nikolsky, and V. A. Romachin, Physics of Atomic Nuclei, **63**, 1799 (2000).
[7] D. Kazanas and A. Nicolaidis, eprint arXiv:astro-ph/0103147 (2001).
[8] Yu. V. Stenkin, Mod. Phys. Lett. **A18** 1225 (2003) .
[9] Yu. V. Stenkin, Nucl. Phys. B (Proc. Suppl.) **151**, 65 (2006)
[10] D M Gromushkin et al., J. Phys. (Conf. Series) **409**, 012044 (2013).
[11] D. Heck, J. Knapp, J. N. Capdevielle, G. Schatz and T. Thouw, Forschungszentrum Karlsruhe Report No. FZKA 6019, (1998).
[12] J. Matthews, Astropart. Phys. **22** 387 (2005).
[13] J. R. Hoerandel, Mod.Phys.Lett.A **22** 1533 (2007)
[14] N. N. Kalmykov, S. S. Ostapchenko and A. I. Pavlov, Nucl. Phys. B, Proc. Suppl. **52** 17 (1997).
[15] M. Bleicher et al., J. Phys. G **25** 1859 (1999).
[16] K. Werner, F. M. Liu and T. Pierog, Phys. Rev. C **74** 044902 (2006).
[17] H. Fesefeldt, RWTH Aachen Report No. PITHA-85/02, (1985).
[18] H. J. Drescher, M. Bleicher, S. Soff and H. Stocker, Astropart. Phys. **21** 87 (2004).
[19] A. Bhadra, S. K. Ghosh, P. S. Joarder, A. Mukherjee and S. Raha, Phys. Rev. D **79** 114027 (2009).
[20] T. Antoni, et.al. (KASCADE collab.), Nucl. Instru. Meth. **513** 490 (2003)
[21] M. Aglietta et al. (EAS-TOP collab.) IL Nuovo Cim. 9C, 262 (1986)
[22] R. Glasstetter et al., Proc. Int. Cosmic Ray Conf. **6**, 157 (1997)
[23] T. Antoni et. al (KASCADE collab.), Astropart. Phys. **16** 373 (2002)
[24] G. Navarra et al (EAS-TOP collab.), Nucl. Phys. B (Proc. Suppl.) 60, 105 (1998)
[25] kcdc.ikp.kit.edu (KIT, Karlsruhe Institute of Technology)

TABLE III: Spectral indices of primary energy spectrum below and above the knee from the electron and the muon size spectra of EAS-TOP observations

Primary before the knee	Primary after the knee	Secondary	$\alpha_{<knee}$	$\alpha_{>knee}$	$\gamma_{<knee}$	$\gamma_{>knee}$	$\Delta\gamma$
Proton	Proton	Electron	1.063 ± 0.007	1.063 ± 0.007	2.71 ± 0.02	3.14 ± 0.07	0.43 ± 0.09
		Muon	0.892 ± 0.008	0.892 ± 0.008	2.89 ± 0.04	3.38 ± 0.09	0.49 ± 0.13
Proton	Iron	Electron	1.063 ± 0.007	1.195 ± 0.003	2.71 ± 0.02	3.40 ± 0.08	0.69 ± 0.10
		Muon	0.892 ± 0.02	0.874 ± 0.002	2.89 ± 0.04	3.33 ± 0.07	0.44 ± 0.11
Iron	Iron	Electron	1.195 ± 0.003	1.195 ± 0.003	2.92 ± 0.02	3.40 ± 0.08	0.48 ± 0.10
		Muon	0.874 ± 0.002	0.874 ± 0.002	2.85 ± 0.03	3.33 ± 0.07	0.48 ± 0.10

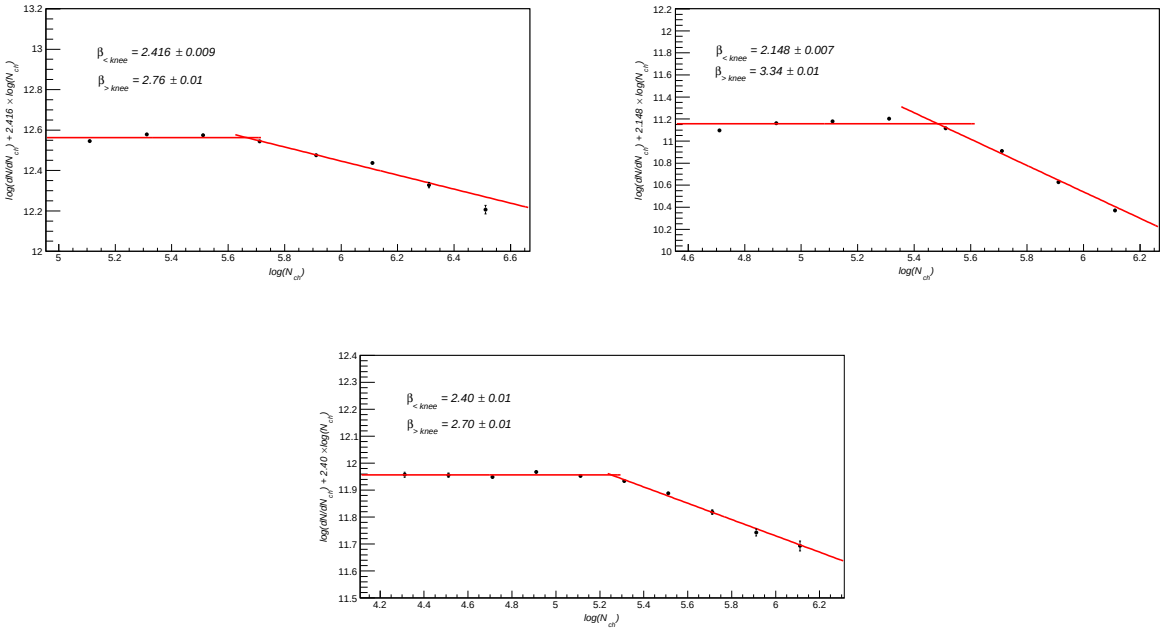

FIG. 5: (Color online) Expected total charged particle size spectrum for different mass composition scenario across the knee (a) unchanged proton primary (b) proton below the knee and Fe above the knee and (c) unchanged Fe primary.

TABLE IV: Spectral indices of the simulated electron and the muon size spectra for cosmic ray energy spectrum with the knee

Primary before the knee	Primary after the knee	Secondary	$\beta_{<knee}$	$\beta_{>knee}$	$\Delta\beta$
Proton	Proton	Electron	2.39 ± 0.01	2.70 ± 0.01	0.31 ± 0.02
		Muon	2.80 ± 0.03	3.30 ± 0.02	0.50 ± 0.05
Proton	Iron	Electron	2.16 ± 0.01	3.03 ± 0.01	0.87 ± 0.02
		Muon	2.86 ± 0.03	3.28 ± 0.02	0.42 ± 0.05
Iron	Iron	Electron	2.40 ± 0.01	2.70 ± 0.01	0.30 ± 0.02
		Muon	2.88 ± 0.02	3.30 ± 0.02	0.42 ± 0.04

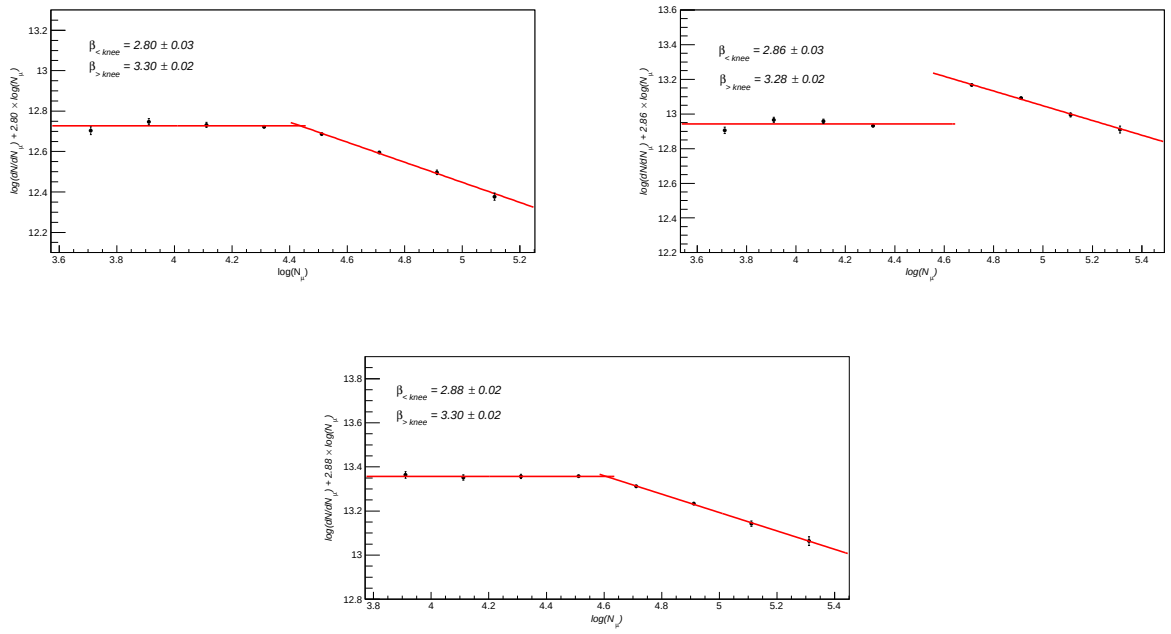

FIG. 6: (Color online) Same as figure 5 but for muon spectrum

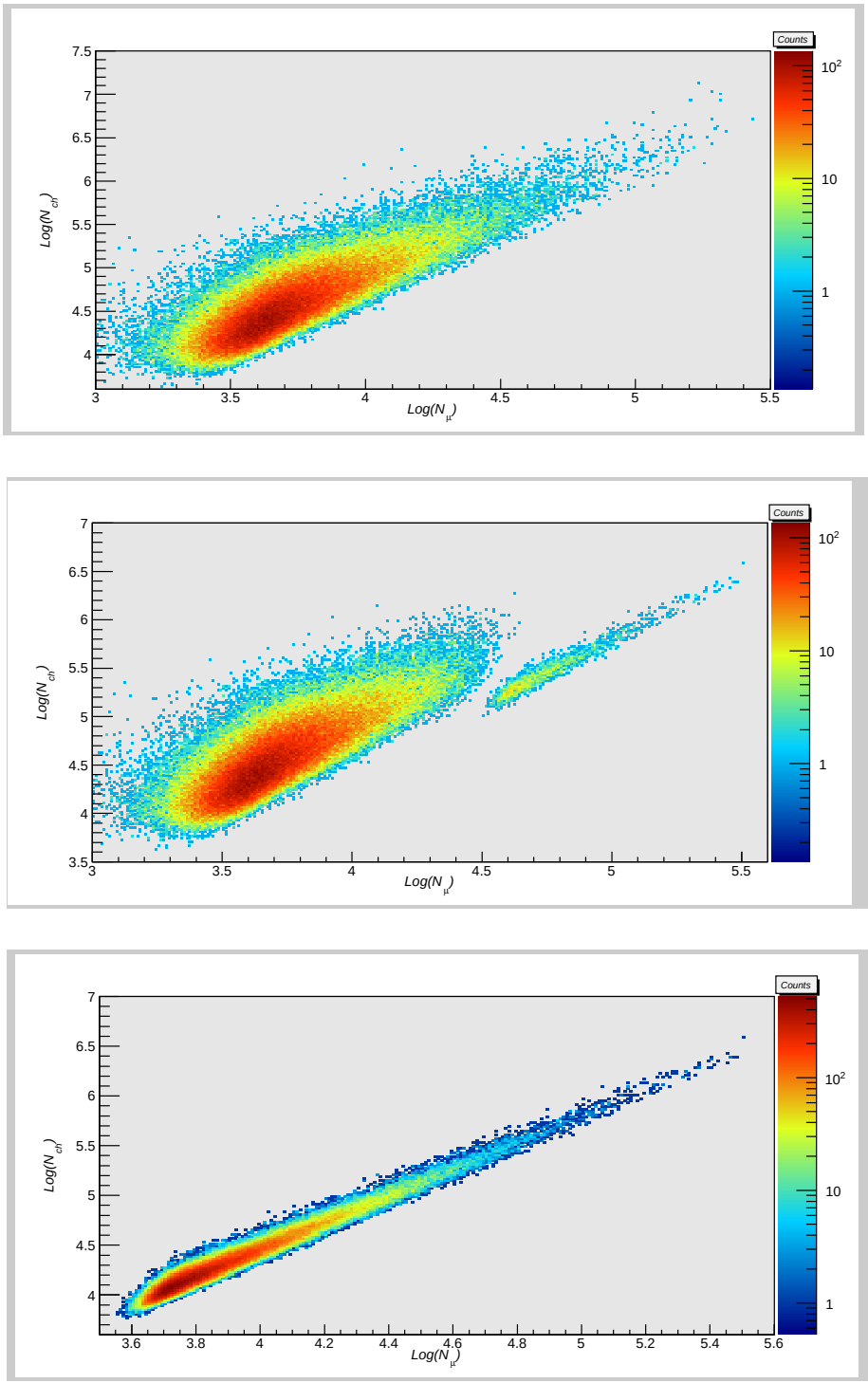

FIG. 7: (Color online) 2-dimentional charged particles - muon spectrum for different composition scenario around the knee

RAA 2015 Vol. **16** No. **1**, 6 (8pp) doi: 10.1088/1674–4527/16/1/006
http://www.raa-journal.org *http://iopscience.iop.org/raa*

Research in Astronomy and Astrophysics

Progenitor model of cosmic ray knee

Biplab Bijay and Arunava Bhadra

High Energy & Cosmic Ray Research Centre, University of North Bengal, Siliguri, WB 734013, India; *aru_bhadra@yahoo.com*

Received 2015 March 07; accepted 2015 July 25

Abstract The primary energy spectrum of cosmic rays exhibits a knee at about 3 PeV where a change in the spectral index occurs. Despite many efforts, the origin of such a feature in the spectrum is not satisfactorily solved yet. Here it is proposed that the steepening of the spectrum beyond the knee may be a consequence of the mass distribution of the progenitor of the cosmic ray source. The proposed speculative model can account for all the major observed features of cosmic rays without invoking any fine tuning to match flux or spectra at any energy point. The prediction of the proposed model regarding the primary composition scenario beyond the knee is quite different from most of the prevailing models of the knee, and thereby can be discriminated from precise experimental measurement of the primary composition.

Key words: cosmic rays — acceleration of particles — black hole physics

1 INTRODUCTION

Ever since their discovery more than a hundred years ago, the origin of cosmic rays has been one of the central questions in physics. But despite many efforts, so far there is no consistent and complete model of the origin of cosmic rays.

The energy spectrum of cosmic rays provides important clues about their origin. The most intriguing feature of the energy spectrum is that although it extends over a wide range of energies, from sub GeV to at least 3×10^{20} eV (the highest energy observed so far), it can be well represented by a steeply falling power law for energies above the solar modulated one. However, the spectrum has a knee around 3 PeV where it steepens sharply as discovered more than half a century ago by Kulikov and Khristiansen of Moscow State University (Kulikov & Khristiansen 1959). The spectrum also has an ankle at an energy of about 3 EeV where it flattens again to its pre-knee slope. It is relatively easier to interpret the flattening of the spectrum above the ankle as the eventual superseding of a harder cosmic ray component which is sub-dominant at lower energies. In contrast, the feature of the knee is more difficult to explain. The existence of the knee in the spectrum is definitely an important imprint of the true model of the origin of cosmic rays and hence a proper explanation of the knee is expected to shed light on the problem of cosmic ray origins.

Several mechanisms have been proposed so far to explain the knee. Shortly after the discovery of the knee, this spectral feature was interpreted as an effect of the reduced efficiency of the galactic magnetic field to confine cosmic ray particles with energies above the knee within the galaxy (Ginzburg & Syrovatskii 1964; Wdowczyk & Wolfendale 1984; Ptuskin et al. 1993; Candia et al. 2002b; Giacinti et al. 2014). Since the magnetic rigidity of a particle is proportional to its atomic number (Z), cosmic ray protons should start escaping first and hence the observed knee is the proton knee as per this model.

The knee has also been explained based on the acceleration mechanism (Fichtel & Linsley 1986; Jokipii & Morfill 1987; Biermann 1993; Berezhko & Ksenofontov 1999; Stanev et al. 1993; Kobayakawa et al. 2002). For reasons of the power required to maintain the observed cosmic ray energy density, it is widely accepted that cosmic rays up to the ankle energy are of galactic origin whereas those having energies above this energy are extragalactic, though there are also suggestions for lower transitional energies (Blasi 2014; Amato 2014; Aloisio et al. 2012). Among the galactic sources, supernova remnants (SNRs) satisfy the energy budget of cosmic rays. The power law behavior of the energy spectrum on the other hand suggests that cosmic rays are most probably energized by diffusive shock acceleration. The maximum energy that a charged particle can gain by diffusive shock acceleration is proportional to Z. The knee has been assigned in this model as the maximum energy that protons can have under diffusive shock acceleration in SNRs.

A critical analysis of data collected at different experiments worldwide in terms of the energy spectrum suggests that the knee is very sharp, and the spectral slope changes rather abruptly at the knee position (Erlykin & Wolfendale 1997). In contrast, the above mentioned rigidity dependent explanations of the knee predict a smooth change in the spectral slope at the knee because of the sum of the contri-

butions of different atomic nuclei having cut-offs at different energies (depending on Z values). To accommodate the sharp knee feature, a few proposals have been advanced. In the single source model the dominant contribution of the cosmic ray flux at the knee is by a nearby source (Erlykin & Wolfendale 1997; Bhadra 2005; Erlykin et al. 2011; Ter-Antonyan 2014) which is superimposed on a galactic modulated component in which the spectral slope is changing smoothly with energy. In another model the sharp knee is explained in terms of cosmic ray acceleration by a variety of supernovae (SNe) (Sveshnikova 2004, 2003). The later proposal relies on the fact that the explosion energy of all SNe is not the same. The sharp knee also could be due to interaction of cosmic ray particles from a pulsar with radiation from the parent SNR (Hu et al. 2009).

The mass composition of cosmic rays will be heavier beyond the knee if the knee is a proton knee. Several Extensive Air Shower (EAS) measurements (till now the study of cosmic rays above 1 PeV has been of an indirect nature via EAS observations) have been made to determine the mass composition of cosmic rays in the energy region of interest, but the measurements have not yielded mutually consistent results yet due to the weak mass resolution of the measured shower observables (Haungs 2011). Most of the findings (Navarra 1998; Glasmacher et al. 1999; Aartsen et al. 2013; Fomin et al. 1996) based on electron content relative to muon content (or *vice versa*) in EAS suggest that composition becomes heavier with energy beyond the knee, though the Haverah Park experiment and a few other observations (particularly underground muon telescopes) (Blake & Nash 1998, 1995; Danilova et al. 1995; Saha et al. 1998; Aglietta et al. 1990; Ahlen et al. 1992; Kasahara et al. 1997; Longley et al. 1995; Bakatanov et al. 1999) found the opposite trend for mass composition. Mass composition estimated from the measurement of the depth of shower maximum through observation of Cerenkov (Boothby et al. 1997; Swordy & Kieda 2000; Fowler et al. 2001; Chernov et al. 2005; Karle et al. 1995; HEGRA-Collaboration et al. 2000; Dickinson 1999; Efimov & et al. 1991) or fluorescence radiation (Abraham et al. 2010; Abbasi et al. 2008, 2004; Tsunesada 2011; Jui & Telescope Array Collaboration 2012), on the other hand, suggests a lighter mass composition beyond the knee differing from that obtained with muon to electron content ratio (Haungs 2011; Hörandel 2013; Bhadra & Sanyal 2005). The mass composition picture of primary cosmic rays is thus still inconclusive in the PeV and higher energy region.

Considering the possibility that mass composition may become lighter beyond the knee, an alternative explanation of the knee was suggested based on nuclear photo-disintegration at the sources (Hillas 1979; Karakula & Tkaczyk 1993; Candia et al. 2002a). In this scenario, heavier components of cosmic rays, particularly Fe nuclei, undergo nuclear photo-disintegration in interactions with the radiation field of the source so that the flux of heavier nuclei decreases with energy beyond the knee whereas protons lose energy by photo-meson production.

A major problem with the standard scenario of diffusive shock acceleration of cosmic rays in SNRs is that a cosmic ray particle can hardly attain the knee energy under this SNR shock acceleration scenario. Such a problem can be overcome in the Cannonball model (Dar & Plaga 1999; Plaga 2002; Dar 2005; de Rújula 2005) in which masses of baryonic plasma or the so called cannonballs, ejected ultra-relativistically in bipolar SN explosions, are considered to be universal sources of hadronic galactic cosmic rays. In this model, the knee corresponds to the maximum energy gained by nuclei through elastic magnetic scattering of ambient particles from the interstellar medium (ISM) in the cannonball while re-acceleration of cosmic rays by cannonballs from other SN explosions causes the extra steepness above the knee.

There is also a proposal of explaining the knee based on a change in the characteristics of high energy interactions (Nikolsky & Romachin 2000). In this model the knee is not a feature of the primary cosmic ray energy spectrum itself, but is caused by the change in high-energy interaction characteristics, either producing a new type of a heavy particle unseen by air shower experiments, or an abrupt increase in the multiplicity of produced particles. However, this proposal has been ruled out at present as the assumed interaction features have not been observed in the Large Hadron Collider experiment.

None of the prevailing models of the knee are free from problems. If the knee corresponds to a break in the proton spectrum, either because it is the maximum energy to which the proton can be accelerated in a galactic cosmic ray source or due to the start of proton leakage from the galaxy at this energy with or without modifications to the sharp knee, then there should be an Fe knee around 10^{17} eV. Hence a special variety of SNe or some other type of galactic or extragalactic source has to be invoked as a generator of cosmic rays between $\sim 10^{17}$ eV and the ankle or galactic-extragalactic transition should occur around 10^{17} eV. The problem with the latter proposal is that it requires fine-tuning to match both the flux and energy at the point where take over occurs. The Cannonball model also suffers the same fine tuning problem at the knee energy. There are other problems such as lower than expected observed gamma ray fluxes from SNRs. The dilemma of the knee thus still continues.

The viable sources of cosmic rays include SNRs, pulsars, gamma ray bursts (GRBs), active galactic nuclei (AGNs), etc. Whatever may be the sources, there is little doubt that they are products of the stellar evolution process. An interesting fact is that the zero age mass spectrum of stars also exhibits power law behavior (Salpeter 1955; Kroupa 2002; Massey et al. 1995). This immediately suggests that the cosmic ray energy spectrum might have some connection with the mass distribution of the progeni-

tor of their sources. In the present work we explore the idea and propose a model for the cosmic ray origin in which the knee of the primary cosmic ray energy spectrum at ~ 3 PeV is a consequence of mass distribution of the progenitor of cosmic ray sources. The proposed model is free from any fine tuning problem and it also overcomes the issue of maximum attainable energy.

The organization of the article is as follows. The model proposed in this work is presented in the next section. The outcome of the present model is discussed in Section 3. The results of the model are compared with observations in Section 4. Finally the results are concluded in Section 5.

2 THE PROPOSED MODEL

Here we propose a model of the origin of cosmic rays in which there is a single class of major cosmic ray sources in the galaxy.

The basic conjectures of the present model are the following:

(1) Cosmic rays, at least up to the ankle energy, are produced either in gravitational explosions (core collapse) of massive stars that lead to formation of black holes (BHs) rather than neutron stars (NSs), or in accretion onto BHs. No other type of galactic or extragalactic source dominates at least up to the ankle energy. Here we have not identified the source. The probable candidate sources of cosmic rays include hypernovae, AGNs and GRBs.
(2) Particles are accelerated by expanding shock waves up to a maximum energy $E_{\rm max}$. The maximum attainable energy $E_{\rm max}$ is, however, not the same for all the sources (of the same kind) but, depending on energy released in explosion/accretion, it has a range. The minimum $E_{\rm max}$ that is possible for cosmic ray sources is equal to the knee energy. We shall argue in the following section that the correspondence of minimum $E_{\rm max}$ with the knee energy is quite plausible and suggestive.

The observed cosmic ray luminosity demands that the cosmic ray sources must be energetically very powerful and are most likely to be powered by gravitational energy. The gravitational collapse that ultimately leads to the formation of a BH or accretion onto a BH is expected to release the maximum gravitational energy. This is the reason for considering the first conjecture. The maximum energy that a cosmic ray particle can attain in shock acceleration usually depends on the explosion energy. Since a BH has no limiting mass, energy released in BH formation should vary with progenitor mass and hence the maximum attainable energies of cosmic ray particles are expected to vary rather than having a fixed value. Essentially, this is the logic behind the second conjecture.

2.1 The Progenitor Connection

Perhaps the occurrence of relativistic shock and non-relativistic shock depends on whether a BH or an NS is formed in the stellar evolution processes. Through stellar core collapse, progenitor stars with $M < 20\ M_\odot$ are supposed to give rise to an NS or white dwarf whereas stars more massive than 20 to 25 $M_\odot$ form a BH (Fryer 1999; Fryer & Heger 2000; Fryer 2003), though such an end point fate also depends on metallicity (Heger et al. 2003). The formation of an NS is usually associated with an SN explosion. The masses of white dwarfs and NSs have to be within the Chandrasekhar limit and Oppenheimer-Volkoff limit respectively. Consequently, the energy released in all ordinary SN explosions is nearly the same. Since a BH has no such upper mass limit, the energy released in the core collapse of massive stars leading to BHs should depend on the mass of the progenitor star.

The gravitational collapse of massive stars to BHs involves some complex, still poorly understood aspects of stellar physics. In the collapsar mechanism (Woosley 1993), a BH is formed when the collapse of a massive star fails to produce a strong SN explosion, leading to its ultimate collapse into a BH. If the stellar material falling back and accreting onto the BH has sufficient angular momentum, it can hang up, forming a disk. This disk, by neutrino annihilation or magnetic fields, is thought to produce the jets which finally results in AGNs or hypernovae.

In the gravitational collapse of a spherical mass distribution with rest mass M leading to formation of a BH, the maximum energy of extraction out of the collapse will be (Ruffini & Vitagliano 2003; Christodoulou & Ruffini 1971),

$$E_{\rm max}^{\rm collapse} = Mc^2/2\,. \qquad (1)$$

During the final stages of stellar evolution, a massive star loses a significant amount of mass. But if a BH is formed, stellar material is likely to fall back and accrete onto the BH (Woosley 1993). The mass of the final produced BH is thus expected to increase linearly with the mass of the progenitor, and hence the distribution of released energy is expected to follow the mass distribution of progenitors.

Instead of a collapse and resulting explosion, a large amount of energy can also be released through the accretion process. The Eddington limit, the maximum steady-state luminosity that can be produced, is given by $L_{\rm ed} = 4\pi GMm_{\rm p}c/\sigma_\tau$ where M is the mass of the BH, $m_{\rm p}$ is the proton mass and σ_τ is the Thomson cross section. The luminosity is thus also proportional to the mass of the BH.

3 OUTCOMES OF THE PROPOSED MODEL

We shall now explore the outcomes of the proposed model regarding the main cosmic ray observables such as luminosity, maximum attainable energy, energy spectrum and nuclear composition.

3.1 The Cosmic Ray Luminosity

The average energy released in BH formation should be around 5×10^{53} erg as per Equation (1), which is more than two orders higher than that released in an SN explosion. Stars more massive than 20 to 25 $M_\odot$ usually form a BH. The rate of stars having $M > 20\ M_\odot$ is $2 \times 10^{-3}\ \mathrm{yr}^{-1}$. However, not all massive stars will end up as BHs. If we denote the probability of BH formation for a star more massive than $20\ M_\odot$ as $\rho_{\rm BH}$, the total energy released in BH production during the cosmic ray confinement period of about 10^6 years in the galaxy is about $\rho_{\rm BH}10^{57}$ erg. This yields a luminosity of $3\rho_{\rm BH}\zeta\times10^{43}$ erg s^{-1}, where ζ is the efficiency of conversion of explosion energy into cosmic ray energy. Typically ζ ranges from 0.01 to 0.1 whereas $\rho_{\rm BH}$ may be taken as 0.5 (Clausen et al. 2015).

3.2 The Maximum Attainable Energy

The maximum energy that a particle with charge Ze can attain in a bulk magnetized flow on a scale $R_{\rm s}$, with velocity $c\beta_{\rm s}$ and magnetic field B, is (Hillas 1984)

$$E_{\rm max} = ZeB\Gamma_{\rm s}\beta_{\rm s}R_{\rm s}\,, \tag{2}$$

where $\Gamma_{\rm s}$ is the Lorentz factor of the relativistic shock wave. This value of $E_{\rm max}$ is a factor $\Gamma_{\rm s}$ larger than that obtained from the Hillas condition. In a BH formation scenario, a fraction of all kinetic energy carries debris ejected with the largest Lorentz factor, thereby generating gamma ray emission in the form of a burst, but the bulk of ejecta is less relativistic or even sub-relativistic. Note that if $\sim 10\ M_\odot$ is given $\sim 10^{54}$ erg then the typical velocity of the mass would be 10^{10} cm, i.e. $c/3$. GRBs are likely to occur in BH formation collapse and a hint on typical values of $\Gamma_{\rm s}$ may be found from GRBs. The GRB observations suggest the minimum $\Gamma_{\rm s}$ of the burst is a few tens (Racusin et al. 2011; Lithwick & Sari 2001; Zou et al. 2011). Therefore, the minimum $E_{\rm max}$ for a BH producing an explosion should be a few PeV.

Let us consider a more rigorous description. In the standard scenario the acceleration of cosmic rays occurs at (non-relativistic) shocks of isolated SNRs. The maximum energy that can be attained by a cosmic ray particle in an ordinary SNR when the remnant is passing through a medium of density $N_{\rm H}\ \mathrm{cm}^{-3}$ is (Fichtel & Linsley 1986; Biermann 1993; Berezhko & Ksenofontov 1999)

$$E_{\rm max} \simeq 4\times10^5 Z \left(\frac{E_{\rm SN}}{10^{51}\ \mathrm{erg}}\right)^{1/2} \left(\frac{M_{\rm ej}}{10\ M_\odot}\right)^{-1/6} \left(\frac{N_{\rm H}}{3\times10^{-3}\ \mathrm{cm}^{-3}}\right)^{-1/3} \left(\frac{B_{\rm o}}{3\mu G}\right)\ \mathrm{GeV}\,, \tag{3}$$

which falls short of the knee by about one order of magnitude. Energy released in BH formation explosions is at least two orders higher than that in SN explosions. Moreover, as stated before, for relativistic shock acceleration $E_{\rm max}$ will be a factor $\Gamma_{\rm s}$ higher. Hence the minimum $E_{\rm max}$ for an explosion that produces a BH should be a few PeV.

An important question for such an explosion that forms a BH in terms of the origin of cosmic rays is whether or not $E_{\rm max}$ could reach the ankle energy. Unlike the almost constant energy released in SN explosions, energy output in such a scenario varies and it may increase at least two orders higher than its minimum value. Such high energy events are expected to occur in a more rarefied medium. Hence it is very likely that the maximum $E_{\rm max}$ will exceed the ankle energy.

Interestingly, the AGN minimum $E_{\rm max}$ is about 3 PeV (Stecker et al. 1991) which is the knee energy and the maximum $E_{\rm max}$ can be many orders higher than that owing to the wide range of luminosities of AGNs.

3.3 Energy Spectrum

In the proposed model, cosmic rays are accelerated in diffusive relativistic shock acceleration. The energy spectrum of accelerated particles in each source is, therefore, given by a power law

$$\frac{dn}{dE} = AE^{-\gamma}\,, \tag{4}$$

with γ around 2.2, and A the normalization constant

$$A \equiv \frac{\epsilon}{(\gamma-2)(E_{\rm min}^{-\gamma+2} - E_{\rm max}^{-\gamma+2})}\,, \tag{5}$$

where $E_{\rm min}$ and $E_{\rm max}$ are respectively the minimum and maximum attainable energies of cosmic ray particles in the source.

The sources do not all have the same $E_{\rm max}$. Above the minimum possible $E_{\rm max}$, which we denote as $E_{\rm max}^{\rm min}$, the spectrum will be modified due to the distribution of $E_{\rm max}$. To get the spectrum beyond $E_{\rm max}^{\rm min}$ we need to obtain the maximum energy distribution of the cosmic ray sources from the mass distribution of their progenitors. The calculation involves a sequence of steps. Using the expression for explosion energy as a function of progenitor mass as obtained in the previous section, we convolve the resulting explosion energy-progenitor mass relation with the initial mass function of the progenitors to obtain the explosion energy distribution. Subsequently using the relation of maximum energy that a cosmic ray particle may attain in the relativistic shock acceleration process with explosion energy, we derive the maximum energy distribution for main cosmic ray sources. Using such a distribution we obtain the energy spectrum of cosmic rays beyond the $E_{\rm max}^{\rm min}$.

The stellar initial mass function, or distribution of masses with which stars are formed, can be represented by a declining power law

$$\frac{dn}{dM} \propto M^{-\alpha}\,, \tag{6}$$

with the universal (Salpeter) value of the exponent $\alpha = -2.35$ over the whole mass range above 3 $M_\odot$ (Salpeter 1955; Kroupa 2002; Massey et al. 1995). Since explosion energy (ϵ) scales linearly with M, the expected explosion energy distribution of massive progenitor stars is also represented by $\frac{dn}{d\epsilon} \propto \epsilon^{-\alpha}$.

The Lorentz factor of a relativistic shock is nearly equal to the initial Lorentz factor of the jet, i.e. $\Gamma_{\rm s} \sim \gamma_o$. The relativistic shock waves must carry a significant fraction of the explosion energy which is subsequently converted to energies of cosmic rays. Hence, $\Gamma_{\rm s}$ should be proportional to explosion energy. On the other hand, $E_{\rm max}$ is also proportional to $\Gamma_{\rm s}$. So for the proposed model, $E_{\rm max} \propto \epsilon$. Thus we have

$$\frac{dn}{dE_{\rm max}} \propto E_{\rm max}^{-\alpha}\,. \tag{7}$$

Therefore, the number of sources having $E_{\rm max} \geq E$ is $j(E_{\rm max} \geq E) \propto E_{\rm max}^{-\alpha+1}$. As the minimum $E_{\rm max}$ of a source is equal to $E_{\rm max}^{\rm min}$, all such sources will contribute to cosmic ray flux when cosmic ray energy is below or equal to $E_{\rm max}^{\rm min}$. However, for energies above $E_{\rm max}^{\rm min}$ ($E > E_{\rm max}^{\rm min}$), only sources having $E_{\rm max} \geq E$ will contribute. The resultant cosmic ray spectrum above $E_{\rm max}^{\rm min}$ will be

$$\frac{dn}{dE} = \int_E \frac{dn}{dE_{\rm max}} A E^{-\gamma} dE_{\rm max} \propto E^{-\gamma-\alpha+2}\,. \tag{8}$$

Therefore, beyond $E_{\rm max}^{\rm min}$ the spectrum should steepen by 0.35 in spectral index as observed. Note that the difference in the exponent of energy by one between the above equation and Equation (3) of Kachelrieß & Semikoz (2006). There the power law distribution of the maximum attainable energy of sources was assumed, due to the fact that our normalization constant A is proportional to the explosion energy (and hence to the maximum attainable energy), unlike the normalization constant that is independent of explosion energy that was adopted in Kachelrieß & Semikoz (2006).

3.4 Mass Composition

According to the proposed model, cosmic rays below and just above $E_{\rm max}^{\rm min}$ are produced in explosions that form a BH comparable to the progenitor's mass. Hence there should not be any abrupt change in mass composition through the $E_{\rm max}^{\rm min}$. In this model, higher energy particles originate from the sources with heavier progenitors. Since a BH is the last stage of evolution for massive stellar objects, the composition is unlikely to change much for BHs from heavier progenitors. Therefore, the resulting composition of accelerated cosmic rays in the proposed model is expected to remain almost unaltered with energy or may become slightly heavier at higher energies.

4 DISCUSSION

We shall now compare the outcomes of the proposed model against the observational features of cosmic rays.

The conventional estimate of cosmic ray luminosity in our galaxy is $\sim 5 \times 10^{40}$ erg s^{-1}. As shown in the previous section, the proposed model yields a cosmic ray luminosity equal to $3\rho_{\rm BH}\zeta \times 10^{43}$ erg s^{-1}. Typically ζ ranges from 0.01 to 0.1 whereas $\rho_{\rm BH}$ is around 0.5 (Clausen et al. 2015). Therefore, the power from explosions that produce BHs in the galaxy satisfies the power requirement for accelerating all galactic cosmic rays. Note that with the rate of occurrence of one per thirty years and the average energy released in each SN explosion of around 10^{51} erg, SNRs satisfy the energy budget for observed cosmic rays (and hence are favored as the main source of cosmic rays) provided the energy conversion efficiency parameter ζ is relatively higher, around 0.1 to 0.2.

The maximum energy that can be attained by a cosmic ray particle in relativistic shock acceleration under the framework of the proposed model varies from source to source (of the same kind). Because of the relativistic effect (through the Lorentz factor) and owing to the much larger explosion energy, the minimum $E_{\rm max}$ for cosmic rays is found to equal a few PeV as shown in the previous section, which can be identified as the knee energy. Interestingly, the minimum $E_{\rm max}$ for an AGN is about 3 PeV (Stecker et al. 1991), whereas the maximum $E_{\rm max}$ is found to exceed even the ankle energy. So, the maximum attainable energy requirement is satisfied in a generic way. In contrast, the maximum energy that can be attained by a cosmic ray particle in an ordinary SNR is 0.3 PeV which falls short of the knee by about one order of magnitude unless the idea of magnetic amplification is invoked. Even with magnetic amplification, it is difficult to exceed 100 PeV and thereby a new source with an unknown nature is required between 100 PeV and the ankle energy.

Since the proposed model relies on standard shock acceleration theory, the overall cosmic ray production spectrum will follow a power law behavior with spectral index equal to –2.2. Due to diffusive propagation of cosmic rays through the ISM, the slope of the spectrum recorded at Earth should steepen to ~ 2.7 till the knee of the spectrum, and the knee should be as sharp as observed. Above the knee, the spectrum will be modified by 0.35 due to the distribution of $E_{\rm max}$ as demonstrated in Section 3.3. Thus

the proposed model explains well the observed features of the energy spectrum of primary cosmic rays.

With respect to the mass composition of cosmic rays, particularly above the knee energy, the composition predicted by the model is similar to that of the Cannonball model but different from the prediction of the SN model that has a cosmic ray origin.

Very recent findings by the KASCADE-GRANDE collaboration regarding the existence of an Fe-knee around 80 PeV along with the composition scenario that is dominated by heavier particles (Apel et al. 2013, 2012, 2011), together with earlier results of the KASCADE experiment for a proton knee at 3 PeV (Apel et al. 2009), do not support the composition picture predicted by the proposed model. Importantly in the overlapping energy region around 1 EeV, the composition scenario inferred from the KASCADE-GRANDE or ICETOP findings, with a mixed composition having nearly the same contribution from protons and iron nuclei (Apel et al. 2009), is not in agreement with a proton dominated chemical composition that emerged from observations at the Pierre Auger Observatory (Abraham et al. 2010), HiRes (Abbasi et al. 2008, 2004) and Telescope Array (Tsunesada 2011; Jui & Telescope Array Collaboration 2012). This only shows the difficulty in estimating primary masses from air shower experiments that rest on comparisons of data with EAS simulations where the latter requires hadronic interaction models as input, which are still uncertain to a large extent at present. Moreover, the uniqueness of solutions of primary energy spectra in the knee region from EAS data is also questioned (Ter-Antonyan 2007). It is expected that the mass composition scenario predicted by the present model will motivate newer experiments, exploiting both muon to electron content ratio and optical techniques, to establish unambiguous cosmic ray mass composition in the knee region and in particular to confirm the KASCADE-Grande results including the Fe-knee.

An important question is to identify the sources, or more precisely identifying the gravitational explosions, that lead to formation of BHs. The viable galactic sources resulting in BH formation include Type 1b/1c SNe and hypernovae, whereas GRBs and AGNs seem to be possible extragalactic sources. The observed rate of Type 1b and 1c SNe is around $10^{-3}\ \mathrm{yr}^{-1}$ which is close to the rate of stars having mass greater than $20\ M_{\odot}$. Radio observations suggest that about 5% of Type 1b/1c SNe can be produced in GRBs (Berger et al. 2003). Earlier, Sveshnikova demonstrated that hypernovae can satisfy the power requirement for accelerating all galactic cosmic rays (Sveshnikova 2004) assuming the rate of hypernovae is about $10^{-4}\ \mathrm{yr}^{-1}$. The extragalactic origin of cosmic rays is usually considered to be unlikely on energetic grounds. However, such a problem can be circumvented by employing the flux trapping hypothesis as proposed in (Plaga 1998; Burbidge 1962). Hence the possibility of a GRB/AGN as the sole kind of dominant source of cosmic rays cannot be totally ruled out from an energetic consideration.

5 CONCLUSIONS

In summary, the proposed speculative BH based model of the origin of cosmic rays can account for all the major observed features of cosmic rays without any serious contradiction to observational results. The knee of the energy spectrum has been ascribed as a consequence of the mass distribution of the progenitor of the cosmic ray source. Such a philosophy seems applicable to the Cannonball model of cosmic ray origin, replacing the original proposal of second order Fermi acceleration of cosmic rays by Cannonballs of other SN explosions as the cause of spectral steepening above the knee (Dar & Plaga 1999; Plaga 2002; Dar 2005; de Rújula 2005). Precise measurement of the primary mass composition can be used to discriminate the proposed model from most of the standard prevailing models of the cosmic ray knee. No definite cosmic ray sources could be identified at this stage within the framework of the proposed model, which would be an important future task for further development of the proposed model.

Acknowledgements The authors are grateful to an anonymous reviewer for insightful comments and suggestions that helped us to improve the manuscript. AB thanks Professors C. L. Fryer and S. E. Woosley for helpful discussions. This work is partly supported by the Department of Science and Technology (Govt. of India) under the grant no. SR/S2/HEP-14/2007.

References

Aartsen, M. G., Abbasi, R., Abdou, Y., et al. 2013, Phys. Rev. D, 88, 042004

Abbasi, R. U., Abu-Zayyad, T., Amann, J. F., et al. 2004, Physical Review Letters, 92, 151101

Abbasi, R. U., Abu-Zayyad, T., Allen, M., et al. 2008, Physical Review Letters, 100, 101101

Abraham, J., Abreu, P., Aglietta, M., et al. 2010, Physical Review Letters, 104, 091101

Aglietta, M., Badino, G., Bologna, G., et al. 1990, Nuclear Physics B Proceedings Supplements, 14, 193

Ahlen, S., Ambrosio, M., Antolini, R., et al. 1992, Phys. Rev. D, 46, 4836

Aloisio, R., Berezinsky, V., & Gazizov, A. 2012, Astroparticle Physics, 39, 129

Amato, E. 2014, International Journal of Modern Physics D, 23, 30013

Apel, W. D., Arteaga, J. C., Badea, A. F., et al. 2009, Astroparticle Physics, 31, 86

Apel, W. D., Arteaga-Velázquez, J. C., Bekk, K., et al. 2011, Physical Review Letters, 107, 171104

Apel, W. D., Arteaga-Velázquez, J. C., Bekk, K., et al. 2012, Astroparticle Physics, 36, 183

Apel, W. D., Arteaga-Velàzquez, J. C., Bekk, K., et al. 2013, Phys. Rev. D, 87, 081101
Arqueros, F., HEGRA-Collaboration 2000, A&A, 359, 682
Bakatanov, V. N., Novosel'tsev, Y. F., & Novosel'tseva, R. V. 1999, Astroparticle Physics, 12, 19
Berezhko, E. G., & Ksenofontov, L. T. 1999, Soviet Journal of Experimental and Theoretical Physics, 89, 391
Berger, E., Kulkarni, S. R., Frail, D. A., & Soderberg, A. M. 2003, ApJ, 599, 408
Bhadra, A. 2005, International Cosmic Ray Conference, 3, 117
Bhadra, A., & Sanyal, S. 2005, International Cosmic Ray Conference, 6, 137
Biermann, P. L. 1993, A&A, 271, 649
Blake, P. R., & Nash, W. F. 1995, Journal of Physics G Nuclear Physics, 21, 1731
Blake, P. R., & Nash, W. F. 1998, Journal of Physics G Nuclear Physics, 24, 217
Blasi, P. 2014, Comptes Rendus Physique, 15, 329
Boothby, K., Chantell, M., Green, K. D., et al. 1997, ApJ, 491, L35
Burbidge, G. 1962, Progress of Theoretical Physics, 27, 999
Candia, J., Epele, L. N., & Roulet, E. 2002a, Astroparticle Physics, 17, 23
Candia, J., Roulet, E., & Epele, L. N. 2002b, Journal of High Energy Physics, 12, 33
Chernov, D. V., Korosteleva, E. E., Kuzmichev, L. A., et al. 2005, International Journal of Modern Physics A, 20, 6799
Christodoulou, D., & Ruffini, R. 1971, Phys. Rev. D, 4, 3552
Clausen, D., Piro, A. L., & Ott, C. D. 2015, ApJ, 799, 190
Danilova, E. V., Kabanova, N. V., Nikolsky, S. I., Romakhin, V. A., & Lebedev, P. N. 1995, 24th International Cosmic Ray Conference, 1, 285
Dar, A. 2005, Nuovo Cimento B Serie, 120, 767
Dar, A., & Plaga, R. 1999, A&A, 349, 259
de Rújula, A. 2005, International Journal of Modern Physics A, 20, 6562
Dickinson, J. E. 1999, International Cosmic Ray Conference, 3, 136
Efimov, N. N., & et al. 1991, in Astrophysical Aspects of the Most Energetic Cosmic Rays, ed. M. Nagano & F. Takahara, 20
Erlykin, A. D., & Wolfendale, A. W. 1997, Journal of Physics G Nuclear Physics, 23, 979
Erlykin, A. D., Martirosov, R., & Wolfendale, A. W. 2011, CERN Courier, 51, 21
Fichtel, C. E., & Linsley, J. 1986, ApJ, 300, 474
Fomin, Y. A., Kalmykov, N. N., Khristiansen, G. B., et al. 1996, Journal of Physics G Nuclear Physics, 22, 1839
Fowler, J. W., Fortson, L. F., Jui, C. C. H., et al. 2001, Astroparticle Physics, 15, 49
Fryer, C. L. 1999, ApJ, 522, 413
Fryer, C. L., & Heger, A. 2000, ApJ, 541, 1033
Fryer, C. L. 2003, Classical and Quantum Gravity, 20, 73
Giacinti, G., Kachelrieß, M., & Semikoz, D. V. 2014, Phys. Rev. D, 90, 041302
Ginzburg, V. L., & Syrovatskii, S. I. 1964, The Origin of Cosmic Rays (New York: Macmillan)
Glasmacher, M. A. K., Catanese, M. A., Chantell, M. C., et al. 1999, Astroparticle Physics, 12, 1
Haungs, A. 2011, Astrophysics and Space Sciences Transactions, 7, 295
Heger, A., Fryer, C. L., Woosley, S. E., Langer, N., & Hartmann, D. H. 2003, ApJ, 591, 288
Hillas, A. M. 1979, International Cosmic Ray Conference, 8, 7
Hillas, A. M. 1984, ARA&A, 22, 425
Hörandel, J. R. 2013, in American Institute of Physics Conference Series, 1516, ed. J. F. Ormes, 185
Hu, H.-B., Yuan, Q., Wang, B., et al. 2009, ApJ, 700, L170
Jokipii, J. R., & Morfill, G. 1987, ApJ, 312, 170
Jui, C. C. H., & Telescope Array Collaboration. 2012, Journal of Physics Conference Series, 404, 012037
Kachelrieß, M., & Semikoz, D. V. 2006, Physics Letters B, 634, 143
Karakula, S., & Tkaczyk, W. 1993, Astroparticle Physics, 1, 229
Karle, A., Merck, M., Plaga, R., et al. 1995, Astroparticle Physics, 3, 321
Kasahara, S. M., Allison, W. W., Alner, G. J., et al. 1997, Phys. Rev. D, 55, 5282
Kobayakawa, K., Honda, Y. S., & Samura, T. 2002, Phys. Rev. D, 66, 083004
Kroupa, P. 2002, Science, 295, 82
Kulikov, G. V., & Khristiansen, G. B. 1959, Soviet Physics JETP, 35, 441
Lithwick, Y., & Sari, R. 2001, ApJ, 555, 540
Longley, N. P., Bode, C. R., Border, P. M., et al. 1995, Phys. Rev. D, 52, 2760
Massey, P., Johnson, K. E., & Degioia-Eastwood, K. 1995, ApJ, 454, 151
Navarra, G. 1998, Nuclear Physics B Proceedings Supplements, 60, 105
Nikolsky, S. I., & Romachin, V. A. 2000, Physics of Atomic Nuclei, 63, 1799
Plaga, R. 1998, A&A, 330, 833
Plaga, R. 2002, New Astron., 7, 317
Ptuskin, V. S., Rogovaya, S. I., Zirakashvili, V. N., et al. 1993, A&A, 268, 726
Racusin, J. L., Oates, S. R., Schady, P., et al. 2011, ApJ, 738, 138
Ruffini, R., & Vitagliano, L. 2003, International Journal of Modern Physics D, 12, 121
Saha, G., Bhadra, A., Chakrabarti, C., Sarkar, S. K., & Chaudhuri, N. 1998, Nuovo Cimento C Geophysics Space Physics C, 21, 215
Salpeter, E. E. 1955, ApJ, 121, 161
Stanev, T., Biermann, P. L., & Gaisser, T. K. 1993, A&A, 274, 902

Stecker, F. W., Done, C., Salamon, M. H., & Sommers, P. 1991, Physical Review Letters, 66, 2697
Sveshnikova, L. G. 2003, A&A, 409, 799
Sveshnikova, L. G. 2004, Astronomy Letters, 30, 41
Swordy, S. P., & Kieda, D. B. 2000, Astroparticle Physics, 13, 137
Ter-Antonyan, S. 2014, Phys. Rev. D, 89, 123003
Ter-Antonyan, S. V. 2007, Astroparticle Physics, 28, 321
Tsunesada, Y. 2011, International Cosmic Ray Conference, 12, 67 (arXiv:1111.2507)
Wdowczyk, J., & Wolfendale, A. W. 1984, Journal of Physics G Nuclear Physics, 10, 1453
Woosley, S. E. 1993, ApJ, 405, 273
Zou, Y.-C., Fan, Y.-Z., & Piran, T. 2011, ApJ, 726, L2